Winter 2021

MOLECULAR ARCHITECTURE OF ROD PHOTORECEPTOR PHOSPHODIESTERASE IN ITS NONACTIVATED AND G-PROTEIN ACTIVATED STATES

Michael Irwin
University of New Hampshire

Follow this and additional works at: https://scholars.unh.edu/dissertation

MOLECULAR ARCHITECTURE OF ROD PHOTORECEPTOR PHOSPHODIESTERASE IN ITS NONACTIVATED AND G-PROTEIN ACTIVATED STATES

BY

MICHAEL J. IRWIN

B.S, University of Massachusetts at Dartmouth, 2012

DISSERTATION

Submitted to the University of New Hampshire

in Partial Fulfillment of

the Requirement for the Degree of

Doctor of Philosophy

in

Biochemistry

December, 2021

This dissertation was examined and approved in partial fulfillment of the requirements for the degree of Doctor of Philosophy in Biochemistry by

Dissertation Director, Rick H. Cote, Professor of MCBS

Feixia Chu, Associate Professor of MCBS

David Plachetzki, Associate Professor of MCBS

W. Kelley Thomas, Professor of MCBS

Harish Vashisth, Associate Professor of Chemical Engineering

On December 3, 2021

Original approval signatures are on file with the University of New Hampshire Graduate School.

DEDICATION

This dissertation is dedicated to my family, in particular to my wife, Joan, and my parents who showed never ending support throughout my graduate studies. Additionally, I must acknowledge my other friends and family who encouraged and supported me throughout this academic endeavor.

ACKNOWLEDGEMENTS

First, I would like to thank my advisor, Rick Cote. He has been a great mentor and was always willing to discuss the numerous problems encountered along the way. He was always encouraging of outside of the box thinking, while always making sure I was thinking and reasoning in a logical way. Under Rick's guidance I was able to productively implement my ideas and experimental designs and make great strides forward with my research projects.

I would also like to thank my committee members: Rick Cote, David Plachetzki, W. Kelley Thomas, Feixia Chu, and Harish Vashisth. Although I did not meet with them often, their guidance did not reflect that. They always had thoughtful suggestions for my research and always showed interest and enthusiasm for my projects.

Finally, I would like to thank the current and former members of the Cote lab, Sue Matte, Xin Wang, Xiong-Zhuo Gao, Richa Gupta, Kranti Galande, Karyn Cahill, and all the other undergraduate students we had in the lab. They made my time in the lab enjoyable and always made for a fun working environment in the lab.

Table of Contents

LIST OF TABLES

LIST OF FIGURES

ABSTRACT

The photoreceptor phosphodiesterase (PDE6) plays an important role in the G-protein coupled visual signaling pathway which uses cGMP as a second messenger to convert light stimuli into electrical signals. PDE6 is a tetrameric peripheral membrane protein consisting of two catalytic subunits and two inhibitory subunits and is localized to the outer segment membranes of rod and cone photoreceptors. Mutations in this enzyme are one cause of retinitis pigmentosa and other retinal degenerative diseases resulting in blindness or visual dysfunction that lack adequate therapeutic intervention due to inadequate knowledge of PDE6 structure and regulation PDE6 is tightly regulated in the nonactivated state, as well as during activation and deactivation of the visual signaling pathway. In the nonactivated state, the rod PDE6 catalytic dimer (consisting of the $P\alpha$ and $P\beta$ catalytic subunits) is inhibited by a pair of identical inhibitory subunits ($P\gamma$) to form the PDE6 holoenzyme ($P\alpha\beta\gamma\gamma$). Activation of PDE6 results from displacement of the $P\gamma$ subunit by the light-activated G protein alpha-subunit ($Gt\alpha$). Deactivation of PDE6 is the result of the GTPase activity of $Gt\alpha$ which is aided by a GTPase accelerating complex consisting of the Regulator of G Protein Signaling 9 (RGS9-1), the obligate dimer to RGS9-1, $G\beta 5L$, and the RGS9-1 anchoring protein (R9AP). Together this inactivation complex allows PDE6 to return to the nonactivated conformation. The hypotheses of my research are: (1) silica particles encased by large unilamellar phospholipid vesicles will mimic the photoreceptor membrane and provide a surface suitable for enhancing the interactions of PDE6 and $Gt\alpha$ as well as the proteins involved in the deactivation complex; (2) one $Gt\alpha$ molecule binds to each PDE6 catalytic domain and induces a large conformational change in the inhibitory $P\gamma$ subunit; (3) interaction of RGS9-1 with $Gt\alpha$ will induce changes in the interaction surface between activated $Gt\alpha$ and PDE6, allowing $P\gamma$ to resume the conformation which inhibits PDE6 activity.

The first aim of my research is to establish a methodology to study PDE6 and its associated complexes in a system that mimics the rod outer segment. In order to achieve this, a protocol for encasing silica particles in large unilamellar phospholipid vesicles (called "lipobeads") was developed. This methodology not only allowed for an increase in the extent of Gtα activation when compared to PDE6 in solution, but also allowed for study of membrane-attached PDE6 and Gtα at concentrations that more closely mimic those observed in the rod outer segment.

The second aim of my research is to characterize the structure of membrane-attached PDE6 in its nonactivated state and in the fully activated state upon binding of Gtα. This was achieved using chemical crosslinking and mass spectrometry in conjunction with a computational modeling program called the Integrative Modelling Platform. In the nonactivated state, it was observed the Pγ has significant interaction with the regulatory GAFa domain as well as the catalytic domain of Pαβ while displaying a less well defined structure in the central cationic region of Pγ. Upon activation, two Gtα are bound to specific docking sites on PDE6 resulting in the displacement of Pγ from both catalytic domains as well as a predicted shift of Pγ away from GAFa.

The third aim of my research is to understand the sequential activation mechanism of PDE6 by Gtα. Chemical crosslinking and mass spectrometry was again used in order to characterize the structures of PDE6 with a sub-stoichiometric amount of Gtα as well as a slight stoichiometric excess of Gtα (0.4:1 and 3:1 Gtα:PDE6, respectively). In the case of the stoichiometric excess, a high molecular weight cross-linked band on SDS-PAGE indicative of two Gtα bound to PDE6 was structurally analyzed; the sub-stoichiometric condition resulted in a single Gtα bound species which was also analyzed. Comparisons were also made between the inactive (Gtα-GDP) and activated (Gtα*-GDP-AlF$_4$⁻) states. This work showed that when two activated Gtα* molecules were bound to PDE6 both Gtα subunits were associated with the catalytic domains of

PDE6. When Gtα was present at sub-stoichiometric levels relative to PDE6, a single docking site was identified in proximity to the GAFb domains of PDE6. The inactive state of Gtα (Gtα-GDP) also was capable of binding PDE6 but bound only to the GAFb domains. Measurements of PDE catalytic activity established two Gtα-GDP-AlF$_4^-$ molecules were able to produce significant activation of PDE6, whereas the sub-stoichiometric condition (0.4 Gtα per PDE6) did not produce activity above basal levels. These results indicate that the binding of a single Gtα is not sufficient to stimulate activity of PDE6.

The final aim of my research is to establish a methodology for the study of the deactivation complex of PDE6. To achieve this aim, lipobeads were used in order to anchor the integral membrane protein R9AP to produce "proteolipobeads". This membrane-embedded R9AP preparation was then able to bind the RGS9-1/Gβ5L without affecting the ability of PDE6 and Gtα to also bind to the proteolipobeads. Chemical crosslinking and mass spectrometry analysis confirmed that all of the proteins were present on the membrane and in close enough proximity to allow future analysis of the PDE6 inactivation complex.

INTRODUCTION

1: Visual signal transduction

1.1 Visual Excitation

Both rods and cones contain outer segments where visual transduction takes place which is triggered when light enters the eye and stimulates the photoreceptor cells of the retina. Visual signaling is initiated by photopigments, consisting of a protein called opsin and a small, covalently attached chromophore (11-cis-retinal) (Nathans, 1999; Stenkamp et al., 2002). In mammals, rods only have one type of photopigment, rhodopsin whereas cones have up to four classes of visual pigments in mammalian cone photoreceptors: LWS, MWS, SWS1 and SWS2 (Hofmann and Palczewski, 2015). The wavelength sensitivity of the photopigment is determined by the amino acid composition of opsin in the vicinity of the chromophore binding site which has the effect of altering the spectral tuning of the visual pigment.

In both rods and cones, in the absence of light the visual signaling pathway proteins are inactive, the concentration of cGMP and calcium is relatively high and the plasma membrane is depolarized. Upon photon absorption by rhodopsin, isomerization of 11-*cis* retinal to all-*trans* retinal occurs which induces a conformational change in opsin allowing for interaction with the G-protein (transducin) on the disk membrane. This interaction results in the exchange of GDP for GTP in the α-subunit of transducin (Gtα). GTP-bound Gtα dissociates from the βγ subunits of transducin and is able to then activate PDE6. Activated PDE6 hydrolyzes cGMP to 5'-GMP, resulting in a decrease in cGMP concentration which in turn causes cGMP-gated ion channels to close. The closure of cGMP-gated ion channels prevents Na^+ and Ca^{+2} from entering the cell and thus causes hyperpolarization of rod outer segment plasma membrane, which is propagated

through the length of the photoreceptor cell to inhibit the release of neurotransmitter at the photoreceptor synaptic terminal (Zhang et al., 2005).

1.2. Inactivation of visual excitation

In order to recover to the dark-adapted state after light exposure, the visual signaling pathway needs to be shut off efficiently and reproducibly. To recover the dark-adapted state of the rod photoreceptor, three proteins in the visual signaling pathway need to be deactivated (rhodopsin, transducin, and PDE6) along with activation of guanylyl cyclase to restore cGMP levels.

1.2.1 Deactivation of rhodopsin

Deactivation of rhodopsin involves a photoreceptor-specific G-protein-coupled kinase, rhodopsin kinase (GRK1), which phosphorylates light-activated rhodopsin. This is followed by arrestin binding to the phosphorylated rhodopsin (Maeda et al., 2003). GRK1 has an "RH-kinase core" wherein a Ser/Thr kinase domain is inserted into a loop of a regulator of G protein signaling homology (RH) domain (Tesmer, 2009). Of note, the phosphorylation of the C-terminal serine and threonine initiate the uncoupling of rhodopsin from transducin (Zhang et al., 1997). An inactivating mutation of GRK1 was identified in Oguchi disease, a form of stationary night blindness, which supported a central role of GRK1 in vision (Dryja, 2000). Besides GRK1, most mammalian cone photoreceptors also express GRK7 which play an important role for deactivation of cone opsins. The presence of GRK7 in cones explains why patients with Oguchi disease have difficulty seeing in dim light but only exhibit relatively mild defects in cone-mediated vision (Chen et al., 2001; Wada et al., 2006; Weiss et al., 2001).

GRK1 activity is regulated by the Ca^{2+}-sensor protein, recoverin (Chen et al., 1995; Kawamura & Tachibanaki, 2008; Klenchin et al., 1995). Recoverin is a small calcium (Ca^{2+})-

binding protein which belongs to neuronal calcium sensor (NCS) family (Ames & Lim, 2012; Burgoyne & Haynes, 2012). Recoverin binds to and inhibits GRK1 in a calcium dependent manner, allowing for regulation of GRK1 activity (Chen et al., 1995). Besides regulation by rhodopsin and recoverin, GRK1 is also regulated by protein kinase A (PKA) phosphorylation. *In vitro* assays revealed that the sites in the amino terminus of GRK1 and GRK7 (Ser21 and Ser36, respectively) can be phosphorylated by PKA (Horner et al., 2005). GRKs phosphorylated by PKA showed decreased ability to phosphorylate rhodopsin. GRK phosphorylation by PKA is high in the dark and low in the light, consistent with the cAMP concentration change under different light conditions (Osawa et al., 2008). This provides another mechanism regulating the lifetime of activated rhodopsin.

Binding of arrestin to GRK1-phosphorylated rhodopsin is required for blocking transducin heterotrimer interaction with rhodopsin. Mammals have four types of arrestins. Arrestin-1 and -4 are specifically expressed in rod and cone photoreceptors, respectively. Arrestin-1 is the second most abundant signaling protein after opsin in photoreceptor cells (Hanson, Gurevich, et al., 2007; Nikonov et al., 2008; Song et al., 2011; Strissel et al., 2006). It has two all-β-strand domains (Granzin et al., 1998; Hirsch et al., 1999). Among all the signaling proteins in rods, only arrestin-1 self-associates at physiological concentration, forming dimers and tetramers (Hanson, et al., 2007; Imamoto et al., 2003; Schubert et al., 1999). Biochemical studies showed that only monomeric arrestin-1 binds rhodopsin while oligomers do not (Hanson, et al., 2007). Both *in vitro* (Vishnivetskiy et al., 2007) and *in vivo* (Mendez et al., 2000) experiments revealed that arrestin requires three phosphates on rhodopsin for high-affinity binding, but does not care which particular residues out of six (mouse) or seven (bovine) serines and threonines are phosphorylated. Site-directed mutagenesis identified multiple positively

charged arrestin-1 residues interacting with receptor-attached phosphates (Gurevich & Benovic, 1995, 1997; Sutton et al., 2005).

The specialized nature of the photoreceptor cell, with a light-harvesting outer segment connected by a connecting cilium to the inner segment (where most cellular organelles reside), requires regulated transport of proteins between these two compartments. For example, in the dark-adapted state, the concentration of arrestin in rod outer segment is low, and most arrestin resides in the inner segment in association with microtubules (Hanson, Cleghorn, et al., 2007; Nair et al., 2005). The fraction of total arrestin in the dark-adapted rod outer segment is estimated to be ~20% by immunohistochemistry (Hanson, Gurevich, et al., 2007; Nair et al., 2005). Upon illumination, visual arrestin translocates from photoreceptor cell bodies to outer segment where it quenches activated rhodopsin. However, both the mechanism and function of arrestin translocation are unresolved and controversial (Satoh et al., 2010).

1.2.2 Deactivation of transducin

Like all other G protein α-subunits, activated Gtα has an intrinsic GTPase activity so it can hydrolyze bound GTP to GDP, and then reassociate with the transducin βγ dimer to form the inactive, heterotrimeric G-protein. Since PDE6 activation is directly dependent on association with Gtα-GTP, the lifetime of PDE6 activation is dictated by the GTPase rate of Gtα. However, the intrinsic rate of GTP hydrolysis by transducin α-subunit is too slow by ~100-fold to control signal termination of a photoresponse (Arshavsky & Pugh, 1998), and this observation provided evidence for the existence of a GTPase accelerating protein (GAP) (Arshavsky et al., 1989; Arshavsky & Pugh, 1998)

The GAP responsible for transducin regulation during the visual signaling pathway consists of a complex of three proteins: RGS9-1, its obligate binding partner Gβ5L, and the

integral membrane anchoring protein, R9AP (Hu & Wensel, 2002). R9AP is a transmembrane

protein that enhances the ability of RGS9-1/Gβ5 to inactivate Gtα by increasing the rate of GTP

hydrolysis (Baker et al., 2006; Hu & Wensel, 2002; Lishko et al., 2002) and protects RGS9-

1/Gβ5L from intracellular proteolysis (Keresztes et al., 2004; Krispel et al., 2006).

In addition to deactivation by the RGS9 complex, Gtα also regulates the visual signaling

pathway by translocation between the inner and outer segments in rod cells. The triggering of

transducin translocation requires relatively bright light intensities (10,000 rhodopsin

photoactivated per rod per sec (Sokolov et al., 2002)), and occurs in what appears to be a

diffusion driven mechanism (Calvert et al., 2006). Transducin is membrane-associated due to

post-translational modifications on its γ-subunit (farnesylation) and its α-subunit (acylation).

Upon transducin activation upon illumination of the photoreceptor cell, transducin α-subunit

dissociates from the βγ subunits resulting in each subunit becoming more soluble because each

has only one lipid modification (Seitz et al., 1999), enabling them to diffuse to the inner segment

from the outer segment. Upon GTP hydrolysis by Gtα, it can reassociate with βγ subunits to form

the tightly membrane-bound trimer. It has been found that the translocation rates of transducin α-

and βγ-subunits are different, supporting the idea that transducin trimer dissociates before

translocation (Sokolov et al., 2002). Interaction of transducin βγ with an abundant photoreceptor-

specific protein, phosducin, further reduces its membrane affinity and enhances its translocation

(Sokolov et al., 2004; Yoshida et al., 1994).

1.2.3: Regeneration of Visual Pigment

Dark adaptation is the process of reversing the changes that occurred during light

excitation and preparing photoreceptors for the next photoactivation event. During

photoactivation, 11-*cis* retinal covalently bound to opsin undergoes photoisomerization to all-

trans-retinal, and this process need to be reversed during dark adaptation. The biochemical process to regenerate 11-*cis* retinal is called the retinoid cycle, which requires the participation of a monolayer of highly polarized epithelial cells adjacent to the retina, called the retinal pigment epithelium (RPE) (Smith et al., 2016).

The first step of the visual cycle is dissociation of all-*trans*-retinal from photo-activated rhodopsin and the release of all-*tran*-retinal into the disk membrane (Palczewski, 2006). The all-*trans*-retinal is flipped across the membrane by the retinal-specific ATP-binding cassette transporter (ABCA4) and then reduced to all-*trans*-retinol by all-*trans*-retinol dehydrogenases (all-*trans*-RDHs). The hydrophobic nature of retinoids limit their aqueous diffusion and hence transportation of all-*trans*-retinol from photoreceptors to RPE is facilitated by a soluble lipoglycoprotein in the interphotoreceptor matrix, called interphotoreceptor-binding protein (IRBP). In the RPE, all-*trans*-retinol is chaperoned by cellular retinol-binding protein (CRBP) and is esterified by lecithin-retinol acetyl transferase (LRAT) localized in the endoplasmic reticulum, where the all-*trans*-retinol is isomerized by retinoid isomerase (RPE65) to 11-*cis*-retinol. 11-cis-retinol is then oxidized to 11-*cis*-retinal and is then chaperoned by interphotoreceptor retinoid-binding protein (IRBP) where it can be conjugated to opsin to regenerate the visual pigment (Kiser et al., 2014; Kiser et al., 2012).

2. Biochemical insights into the mechanism of Gtα activation of PDE6

This section will summarize the biochemical evidence for the mechanism by which transducin binds to and activates rod PDE6 during phototransduction and then will apply that evidence to the structural studies of the Gtα-PDE6 activation complex to shed light on the sequence of steps progressing from nonactivated PDE6 to the fully activated enzyme.

2.1 Activation by transducin is enhanced when Gtα and PDE6 are membrane-associated

It is well established that Gtα activation of PDE6 occurs with greater efficiency when transducin and PDE6 are tethered to the rod outer segment membrane (or phospholipid bilayers) by their fatty acyl and prenyl groups, respectively (Malinski & Wensel, 1992; Melia et al., 2000). Gtα is acylated at its extreme N-terminal glycine residues which facilitates membrane attachment (Neubert et al., 1992). Gtα has heterogeneity in its acyl modification which may result in the observation that only a portion of Gtα exhibits high affinity binding to membranes (Gray-Keller et al., 1990; Wensel & Stryer, 1988). Co-localization of Gtα* and PDE6 on membranes potentially serves to optimize the activation mechanism, both by creating a high local concentration of protein as well as reducing the dimensionality of diffusional encounters.

2.2. Gtα-activated PDE6 can attain the same maximal extent of activation as the Pαβ catalytic dimer lacking Pγ

There have been a wide range of maximal extents of Gtα activation of PDE6 catalytic activity but the preponderance of evidence supports the idea that when both proteins are membrane-associated and a sufficient amount of Gtα is present, PDE6 can be activated by Gtα *in vitro* to a similar extent as Pαβ catalytic dimers devoid of Pγ (Bennett & Clerc, 1989; Liu et al., 2009; Melia et al., 2000). Whether full catalytic activation of PDE6 by transducin occurs *in vivo* is still a matter of debate.

2.3 Alteration in cGMP binding upon transducin activation

Two different mechanisms in which successive binding of two Gtα to PDE6 fully activates catalysis have been proposed. These mechanisms differ in whether the two binding events of Gtα occur with equal (Wensel & Stryer, 1990) or different (Bennett & Clerc, 1989; Liu et al., 2009; Min et al., 2000) affinities for PDE6. One such mechanism has been proposed

(Qureshi et al., 2018) which involves a two-stage process: (1) high-affinity binding of the first activated Gtα*-GTP to PDE6 but with little catalytic activation of PDE6; (2) low-affinity binding of a second Gtα*-GTP which results in full activation (i.e., equivalent to Pαβ lacking bound Pγ) at both active sites. This mechanism is not only consistent with the structural and functional asymmetry of the rod PDE6 catalytic heterodimer and its nonidentical binding interactions with its two Pγ subunits, but also is supported by computational simulations of the photoresponses of mammalian rod photoreceptors to dim and bright illumination (Lamb & Kraft, 2020; Lamb et al., 2018).

Binding of Gtα to PDE6 relieves Pγ inhibition of catalysis in the catalytic domain and also enhances the rate at which cGMP exchange occurs at the binding sites in GAFa (Zhang et al., 2012). Since the Pγ N-terminal region enhances cGMP binding affinity to the GAFa domains (Mou & Cote, 2001), this effect of Gtα has been attributed to Gtα binding to Pγ and disrupting the interactions of the N-terminal region of Pγ with the GAFa domain.

3. Structural studies of the Gtα*-PDE6   complex

Two recent structural determinations of the activation complex of Gtα with PDE6 (Gao et al., 2020; Irwin et al., 2019) provide two distinct mechanisms by which Gtα activates PDE6. The approach used by Irwin et al. employed chemical cross-linking and mass spectrometric analysis combined with integrative structural modeling that identified two distinct docking sites on each PDE6 catalytic subunit for Gtα, one interacting with the catalytic domain and the other site interacting with the GAFb domain (Irwin et al., 2019). Gao et al. utilized high-resolution cryo-EM analysis of the Gtα*-PDE6 complex which identified Gtα interacting only with the GAFb domains (Gao et al., 2020). A detailed discussion of these structural models is presented in later chapters.
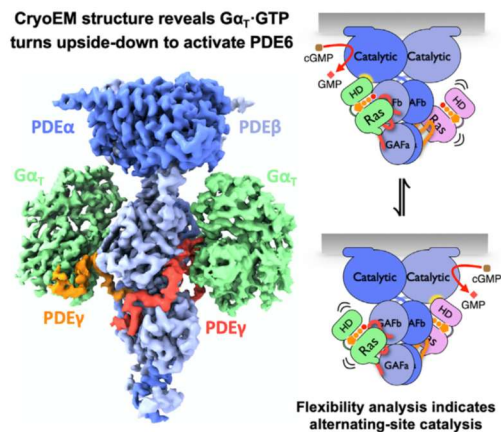
Figure 1-1. Graphical abstract presented in Gao et al. (2020) showing the binding of two Gtα to PDE6

3.1.1. Overview of the PDE6 holoenzyme

In order to elucidate the structure-function relationship of PDE6, there has been a significant effort to determine the structure of the PDE6 holoenzyme and its associated complexes. However, the inability to express rod PDE6 recombinantly has limited the study of the atomic-level structure of PDE6. Recently, there have been several high resolution cryo-EM structures published at 11 Å and 3.4 Å resolution (Zhang et al., 2015; Gulati et al., 2019). In one case, the cryo-EM resolution was sufficient to determine the position of the N- and C-terminal fragments of Pγ (Gulati et al., 2019).

In addition to cryo-EM, cross-linking with mass spectrometry (XL-MS) has been used to determine a homology model for the Pαβ structure of the holoenzyme (Zeng-Elmore et al., 2014). The homology model as well as the cryo-EM structure agree on the defining characteristics of PDE6; (1) there is an N-terminal "pony tail" region where Pα and Pβ seem to

wind together (2) the GAF domains of one subunit are located adjacent to the catalytic domain of the other subunit (3) there is significant disorder present in the GAFb domains of Pα and Pβ.

3.1.2 Structure and function of the inhibitor γ-subunit of PDE6

PDE6 is the only family of Class I phosphodiesterases whose catalytic activity is regulated by a distinct protein subunit, Pγ. Most of the sequence diversity between rod and cone Pγ isoforms is found in the N-terminal region of the protein, along with four highly conserved rod-cone differences at positions 21, 48, 74, and 84 of the rod Pγ sequence (Wang et al., 2019).

In non-activated PDE6, catalytic activity is suppressed by two Pγ subunits that physically prevent substrate access to the enzyme active site on each catalytic subunit (Barren et al., 2009; Granovsky et al., 1997). Upon photoactivation of the visual excitation pathway, Gtα*-GTP binds to Pγ, relieving its inhibitory constraint and activating PDE6 (Arshavsky et al., 2002). During photoresponse recovery, the Pγ subunit also interacts with the Regulator of G-protein Signaling9-1 (RGS9-1) to accelerate the intrinsic GTPase activity of Gtα*-GTP that leads to the restoration of PDE6 to its inhibited state (reviewed in (Arshavsky & Wensel, 2013)).

The ability of the Pγ subunit to carry out its many functions is a consequence of Pγ exhibiting the structural properties of an intrinsically disordered protein. The 87 amino acid sequence of rod Pγ is largely devoid of secondary structure (Uversky et al., 2002). The NMR solution structure of rod Pγ was determined to consist of an unfolded N-terminal region; similar results were observed for the N-terminal half of cone Pγ (Gupta et al., 2020) with only three small α-helical segments that interact with the catalytic domain (Song et al., 2008). The Pγ subunit assumes a linearly extended conformation upon binding to Pαβ (typical for intrinsically disordered protein) with its N-terminal region interacting with the GAFa domain, the central

polycationic region interacting with the GAFb domain, and the glycine-rich and C-terminal regions (containing α-helical content) binding to the catalytic domain.

4. Structural analysis of transducin and the transducin α-subunit

There have been several studies focused on the structural determination of transducin and the transducin α-subunit (Gtα). X-ray crystallography was used, and in each case the N-terminal α-helix (including the site of N-terminal acylation) was removed prior to structural determination. These studies found that there is minimal structural differences between the GDP-bound Gtα in a reconstituted heterotrimer, GDP-bound Gtα free in solution, and persistently activated Gtα (Lambright et al., 1994, 1996; Noel et al., 1993; Sondek et al., 1994). Additionally, a study by Slep et al. (2001) determined the structure of Gtα complexed with the RGS domain of RGS9 as well as a fragment of the PDE6 inhibitory subunit Pγ (Slep et al., 2001). In each of these studies, the overall conformation of Gtα did not vary significantly, indicating that Gtα likely posses a fairly static structure under crystallization conditions.

5. Structural studies of transducin-PDE6 activation complex

Gao et al. (Gao et al., 2020) provided the first high-resolution cryo-EM structure of the Gtα-PDE6 activation complex (PDBID: 7jsn), which shows the Gtα subunits located in the vicinity of the GAFb domains. The model was produced using a chimeric G protein α-subunit consisting of Gtα with substitutions of G_i α-subunit residues that enabled bacterial expression ($G_i\alpha$/Gtα). The Gao et al. structure identified interactions with the β5/β6 loops of both GAFa and GAFb of Pα and the GAFb α1/α2 helices and α11 of the catalytic domain of the Pβ subunit. The N-terminal half of Pγ retained a very similar conformation to that of nonactivated PDE6 holoenzyme, but the polycationic, glycine-rich, and C-terminal regions of Pγ show major displacement of Pγ from its sites of interaction in the nonactivated PDE6 holoenzyme (Gao et al.,

2020).The C-terminal residues of Pγ undergo an ~60 Å movement upon binding to Gtα, with the C-terminal region of Pγ interacting with the Switch II and Switch III elements of Gtα, similar to the conformation observed in the RGS9-1 inactivation complex (Slep et al., 2001).

From this model Gao et al. proposed an alternating-site activation mechanism where both Gtα subunits are associated with the GAFb domains in a complex with Pγ, inducing allosteric catalytic activation of one PDE6 subunit at a time. They proposed that binding of the Ras sub-domain of the first Gtα to Pγ removes the C-terminal region from the catalytic domain to form a stable interaction with the GAFb domain without inducing catalytic activation. Upon binding of the second Gtα, catalytic activation ensues in an alternating mechanism with one active site at a time. Gao et al. proposed that the GAFb domain of PDE6 and the helical sub-domain of Gtα allosterically regulate which PDE6 catalytic domain is active (for details, see Fig. 6 of Gao et al., 2020).

Limitations of the Gao et al. (Gao et al., 2020) structure of the Gtα-PDE6 activated complex include: (1) a chimeric G-protein consisting of 18 $G_i\alpha$ residues substituted into the transducin Gtα sequence which could change its interactions with PDE6; (2) tethering the two chimeric $G_i\alpha$/Gtα* subunits together with an antibody may have imposed steric restraints which restrict the number of orientations that Gtα could productively bind to PDE6; (3) use of vardenafil (a PDE5/6 inhibitor) likely weakened Pγ interactions with the catalytic domain (Barren et al., 2009; Gillespie et al., 1989; Granovsky et al., 1997; Zhang et al., 2005) and as a consequence may have enhanced the ability of Gtα to displace the C-terminal residues of Pγ from the active site in a non-physiological manner.

In chapters 3 and 4, I present an alternative hypothesis based on my own research. In brief, I will show that the initial docking site of Gtα resides on the GAFb domain, consistent with the work of Gao et al. However, this docking site only appears to be present when a single Gtα is bound and results in very little catalytic activation of PDE6. When two Gtα are bound to PDE6, the docking sites shift to the catalytic domain and PDE6 catalytic activation occurs. Our results support a sequential mechanism of activation upon Gtα binding to PDE6 resulting in both catalytic subunits being activated simultaneously.

6. Conclusion

The overall goal of my doctoral research is to elucidate the mechanism by which Gtα activates PDE6 to provide insights into the interactions occurring during phototransduction that may ultimately lead to developing therapeutic interventions for inherited retinal degenerative diseases. The central hypothesis of my work is that two Gtα interacting primarily with Pγ on PDE6 are required for full activation of PDE6. The specific aims of my project are to: (1) establish a methodology to study PDE6 and its associated complexes in a system that mimics the rod outer segment; (2) to characterize the structure of membrane-associated PDE6 in its nonactivated and in the fully activated complex of Gtα-PDE6; (3) elucidate activation mechanism of PDE6 by Gtα; and (4) establish a methodology for the future study of the deactivation complex of PDE6.

CHAPTER 2

RECONSTITUTION OF MEMBRANE-ASSOCIATED COMPONENTS OF A G-PROTEIN SIGNALING PATHWAY ON MEMBRANE-COATED NANOPARTICLES (LIPOBEADS)

Some of the content in this chapter is a manuscript in preparation.

Authors: Michael J. Irwin, Xin Wang, Rick H. Cote

Abstract

G-protein coupled signaling pathways are organized into multi-protein complexes called signalosomes that are organized within and on cellular membranes. We describe the use of silica nanoparticles coated with a unilamellar phospholipid bilayer (lipobeads) to reconstitute the activated photoreceptor G-protein α-subunit (Gtα*) with its cognate effector (phosphodiesterase-6; PDE6) for biochemical and structural studies of the activation mechanism of this GPCR signaling pathway. Lipobeads are prepared by resuspending dried-down phospholipid mixtures with monodisperse, 70 nM silica particles followed by extrusion through a 100 nm membrane filter. This uniform, supported liposomal preparation is easily sedimented, permitting separation of soluble from membrane-associated proteins. Upon loading lipobeads with Gtα* and PDE6, we find that activation of PDE6 catalysis by Gtα* occurs much more efficiently than in the absence of membranes. Chemical cross-linking of membrane-confined proteins allows detection of changes in protein-protein interactions resulting from G-protein activation of PDE6. The advantages of using lipobeads over traditional liposomal preparations are generally applicable to the study of other membrane-confined signal transduction pathways.

1. Introduction

1.1 Heterotrimeric G-protein coupled signaling pathways are organized in macromolecular complexes (signalosomes)

G-protein coupled receptor (GPCR) signaling pathways consist of protein complexes (signalosomes) associated with the cell membrane that form dynamic supramolecular structures. During signal transduction, these integral and peripheral membrane proteins undergo assembly/disassembly reactions and structural rearrangements that result in allosteric changes in protein-protein interactions, enzymatic activity and/or changes in membrane localization. Understanding the mechanistic processes underlying operation of GPCR signaling assemblies has been hampered by the difficulty of reconstituting these signalosomes with phospholipid bilayers in order to define the sequence of events occurring during receptor activation by its ligand(s), activation of G-proteins, binding to activated G-protein subunits to their effectors, and the subsequent reactions that terminate the activated state of the signalosome.

Whereas much progress has been recently been made in high-resolution structures of GPCRs complexed with their cognate G-proteins (for review, see ref. (Zhou et al., 2019)), there are few structural studies of the downstream signaling complexes resulting from interactions of activated G-protein subunits with their effectors on the membrane surface. For example, although phospholipase C-β3 and Gqα are normally associated with the cell membrane, the atomic-level structure was determined as a soluble complex (Lyon et al., 2013) whose molecular architecture may differ from the Gqα-PLC-β3 complex attached to the membrane. A more recent cryo-EM study of detergent-solubilized adenylyl cyclase-9 (AC9, an integral membrane protein) bound to activated Gsα revealed the interaction surface of this G-protein-effector complex, with the membrane-spanning helical bundle of AC9 embedded in detergent micelles (Qi et al., 2019).

Although cryo-EM is ideally suited to determine the structures of larger proteins and protein complexes, it remains challenging for numerous reasons to study integral and peripheral membrane proteins in their membrane-associated state with this approach (Akbar et al., 2020).

1.2 Most components of the visual transduction signalosome in vertebrate rod and cone photoreceptors are membrane-confined.

Visual transduction in vertebrate rod and cone photoreceptor cells is a prototypical G-protein coupled signaling pathway. The visual excitation pathway occurs upon photoactivation of the visual pigment, rhodopsin, which leads to the activation of the photoreceptor-specific G-protein (transducin) α-subunit (Gtα), and subsequent activation of its effector, cGMP phosphosdiesterase-6 (PDE6) (Cote, 2021). The signal-transducing outer segment of the rod photoreceptor cell consists of densely packed membranes that contain a high surface density of rhodopsin (to maximize photon capture), as well as Gtα and PDE6 (Molday & Moritz, 2015). The rate-limiting step in signal termination involves proteins that regulate the activated lifetime of Gtα, namely the Regulator of G-protein Signaling9-1 (RGS9-1), G-protein β-subunit5-L (Gβ5L), and the RGS9-1 anchoring protein (R9AP) which tethers this inactivation complex to the outer segment membrane (Arshavsky & Wensel, 2013). Proteomic profiling of highly purified rod outer segment disk membranes confirm that both the activation complex (Gtα-PDE6) and inactivation complex (RGS9-1-Gβ5L-R9AP) are membrane-confined, either as integral membrane proteins (rhodopsin, R9AP), lipidated peripheral membrane proteins (Gtα, PDE6), or as soluble proteins very tightly associated with R9AP (RGS9-1, Gβ5L) (Skiba et al., 2013).

Although detailed quantitative models of the visual transduction pathway have been developed that integrate electrophysiological and biochemical data (Lamb & Kraft, 2020), the

structural biology and conformational dynamics of the membrane-confined photoreceptor signalosome are poorly understood. Whereas atomic-level structures for rhodopsin (in various liganded states) and transducin have been available for some time, we still lack three-dimensional structures of the activated complex of rhodopsin with Gtα (although structures of rhodopsin complexed with the homologous Giα subunit (Kang et al., 2018) or with a chimeric Gtα/Giα subunit (Gao et al., 2019; Gao et al., 2017) have been reported). Likewise, the overall structure of the soluble form of the hetero-tetrameric rod PDE6 holoenzyme has been determined to near atomic-level resolution (Gulati et al., 2019; Qureshi et al., 2018; Zeng-Elmore et al., 2014); however, the molecular organization of the Gtα-PDE6 activated complex in its membrane-associated state has only recently been described (Gao et al., 2020; Irwin et al., 2019). Finally, the x-ray structure of two components of the inactivation complex of the visual transduction pathway (RGS9-1/Gβ5L) have been reported (Cheever et al., 2008), but studies of the related RGS7/Gβ5 complex (and the influence of the RGS7 binding protein (Patil et al., 2018)) suggest that binding of RGS9-1/Gβ5L to the homologous R9AP scaffolding protein may alter the molecular organization of this heterotrimeric inactivation complex. To summarize, while there is detailed information about the components that comprise the photoreceptor signalosome, there is a gap in our knowledge of the molecular architecture and structural rearrangements of these signaling complexes residing on the membrane surface.

1.3 Use of phospholipid bilayer-coated nanoparticles (lipobeads) to reconstitute the photoreceptor GPCR signaling pathway on membrane surfaces.

Supported phospholipid bilayers have been used for a variety of fundamental and applied applications, including membrane biophysics, biosensors, cell-cell interactions, screening assays of membrane proteins, and as drug-delivery vehicles (Chemburu et al., 2010; Crites et al., 2015;

Ng et al., 2004; Troutier & Ladavière, 2007). Microspheres consisting of silica or polymeric

materials (e.g., hydrogels) have been used as the typical solid support for

forming unilamellar phospholipid bilayers whose size, density, membrane

curvature, and other biophysical properties can be optimized for their intended applications.
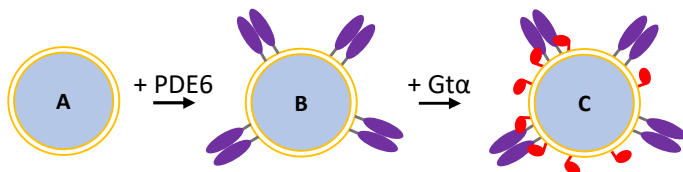
Figure 2-1. Reconstitution of the Gtα*-PDE6 activation complex on lipobeads. A. Lipobead composed of silica nanoparticle coated with a unilamellar phospholipid bilayer. B. PDE6 (purple) attached to lipobeads by their prenyl moieties. C. Addition of acylated Gtα* (red) to lipobeads with pre-bound PDE6 results Gtα* binding and the formation of the Gtα*-PDE6 activation complex.

We have utilized 70 nm diameter silica particles coated with a unilamellar lipid bilayer

(termed "lipobeads") in order to tightly bind Gtα and PDE6 (both peripheral membrane proteins

containing lipophilic post-translational modifications) suitable for enzymological and structural

studies of the Gtα-PDE6 activation complex in a membrane-confined environment. (Fig. 2-1).

The ability to reconstitute *in vitro* the proteins comprising GPCR signalosomes on well-

defined lipobeads enables the integration of biochemical, biophysical, and structural studies to

advance our mechanistic understanding of GPCR signaling pathways in the context of their

membrane environment.

2. Materials and Methods

Preparation of lipobeads.

Cationic phospholipids used for membrane attachment of PDE6 and Gtα were chosen

based on a previous study (Melia et al., 2000). 1,2-dioleoyl-sn-glycero-3-phosphocholine

(DOPC; Avanti Polar Lipids, Inc.) and 1,2-dioleoyl-3-trimethylammonium-propane (DOTAP;

Avanti Polar Lipids, Inc.) were dissolved in chloroform (molar ratio of 80:20) and evaporated. Silica nanoparticles (70 nm diameter, 2.0 g/cm^3; DiagNano) were initially prepared by resuspending 5 mg of beads (23 pmol) with HNM buffer (20 mM HEPES (pH 7.5), 100 mM NaCl, 2 mM MgCl$_2$) followed by centrifugation at 10,000 x g for 10 min, and resuspension in 1.0 ml of HNM buffer. The dried phospholipids were mixed with the lipobead suspension to a final phospholipid concentration of 5 mM. The mixture was gently vortexed for 2 min and allowed to settle for 1 min; this process was repeated four more times. Unilamellar vesicles coating the silica particles were formed by extruding the mixture fifteen times through a 0.1 μm polycarbonate membrane using a Mini-Extruder (Avanti Polar Lipids, Inc.). The unbound phospholipids were removed by several cycles of centrifugation and resuspension of the lipobeads with HNM buffer.

Given the surface area of a 100 nm liposome (0.03 μm^2), a lipid headgroup area of 0.7 nm^2 (Kučerka et al., 2006), and 5.0 nm for the thickness for the phospholipid bilayer (Marquardt et al., 2016), we calculate that each lipobead contains ~80,000 phospholipids. Thus, a lipobead concentration of 1 nM is equivalent to a total phospholipid concentration of 80 μM. Note that the surface-accessible phospholipid concentration (i.e., the outer monolayer) is about ~50% of the total phospholipid concentration, as previously determined experimentally for 100 nm unilamellar liposomes (Malinski & Wensel, 1992).

Isolation and purification of PDE6 and Gtα from bovine retina.

Bovine rod PDE6 holoenzyme was isolated from bovine retinas (W.L. Lawson Co.) and purified following standard procedures (Pentia et al., 2005). Gtα was extracted from PDE6-depleted photoreceptor membranes by addition of 100 μM GTP immediately prior to centrifugation (31,000 x g for 30 min); the process was repeated for a total of three extractions.

The recovered Gtα containing bound GDP was then purified by affinity chromatography in a HiTrap Blue HP column (GE Healthcare) as described previously (Ting et al., 1993), followed by Superdex 200 (GE Healthcare) gel filtration chromatography. Both proteins were purified to >95% homogeneity as judged by SDS-PAGE, stored in 50% glycerol at -20º C, and buffer-exchanged into the appropriate buffer before use.

 Analytical procedures.

Protein, phospholipid, and nanoparticle quantitation.

The PDE6 concentration was determined based on knowledge of the k_{cat} of the trypsin-activated enzyme (5600 cGMP hydrolyzed per PDE6 per s (H Mou et al., 1999)). Other protein concentrations were determined using the bicinchoninic colorimetric assay (Smith et al., 1985)with bovine γ-globulin as a standard. The phospholipid content of lipobeads preparations was quantified with a phospholipid assay kit (Millipore Sigma). Silica nanoparticle preparations were characterized by flow cytometry using a Sony SH800Z Cell Sorter to verify the accuracy of the manufacturer's stated concentration of particles.

Enzymatic assay of PDE6 activation by Gtα.

PDE6-catalyzed hydrolysis of cGMP was quantified using a coupled enzyme assay relying on colorimetric detection of inorganic phosphate (Cote, 2000). The extent of PDE6 activation by Gtα was referenced to the maximum activity of the same concentration of trypsin-activated PDE6 (Pentia et al., 2005).

Sodium dodecyl sulfate polyacrylamide gel electrophoresis (SDS-PAGE).

For characterization of protein purity, SDS-PAGE was performed using NuPAGE 4-12% Bis-Tris gels (Invitrogen) and Precision Plus molecular weight standards (BioRad). For characterization of chemically cross-linked samples that include high molecular weight

complexes not well resolved on Bis-Tris gels, we used 4-12% Tris-glycine gels (Invitrogen) and PAGERuler Plus protein ladder (Thermo Fisher). Excised protein bands were trypsin-digested and their identity determined by mass spectrometry (Zeng-Elmore et al., 2014).

3. Results and Discussion

3.1 Characterization of liposome-coated silica nanoparticles (lipobeads)

Consistent with previous reports (Ross et al., 2011)we found that vortexing a dried down mixture of DOPC and DOTAP (80:20) with an aqueous suspension of 70 nm silica spherical particles and subsequent extrusion through a 100 nm membrane allowed for the spontaneous formation of lipid bilayers coating the silica beads. Following sedimentation and resuspension in buffer to remove unbound phospholipids, measurements of the phospholipid content of the lipobead pellet showed that less than 10% of the silica particles lacked a surrounding phospholipid bilayer. Lipobead preparations were determined to be stable for at least three days after preparation, as judged by constant amounts of PDE6 and less than 20% loss of Gtα from the lipobeads over this time period. In summary, this preparation of unilamellar membranes coating spherical silica nanoparticles offers several advantages over liposomes, including a well-defined vesicle size (~100 nm diameter) and membrane curvature, high particle density for ease of sedimentation, and enhanced stability.

3.2 Reconstitution of the Gtα-PDE6 activation complex on lipobeads
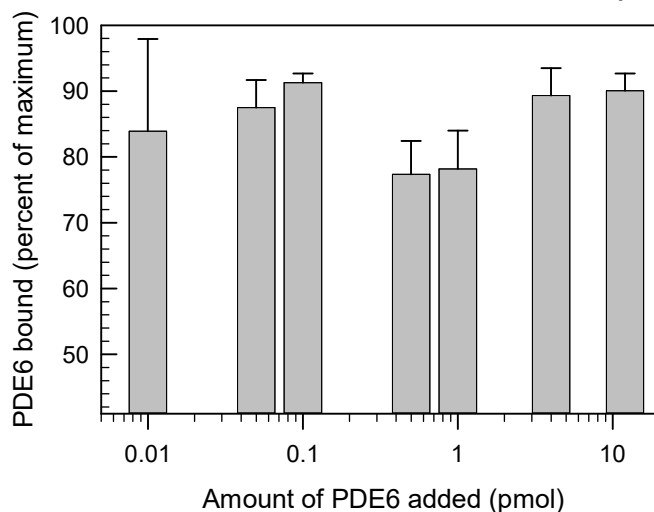
Figure 2-2. Binding of PDE6 to lipobeads. Lipobeads (0.46 pmol) are mixed with 40 µl of the indicated amount of PDE6 and incubated for 30 min. Following centrifugation, the supernatant fractions are assayed for PDE6 activity to calculate the percent of total PDE6 activity bound to the lipobeads. Data represent the mean ± S.D. (n = 3).

To examine the binding characteristics of lipobead preparations, we first quantified the ability of the purified rod PDE6 holoenzyme to bind to lipobeads. The PDE6 heterotetramer is composed of two catalytic subunits [PDE6A (Pα) and PDE6B (Pβ)] and two identical inhibitory subunits [PDE6G (Pγ)] (Cote, 2021). The affinity of PDE6 for membrane association is conferred by farnesyl (Pα) and geranylgeranyl (Pβ) groups at the C-terminus of each subunit (Anant et al., 1992). Fig. 2-2 shows that 80% or more of the total PDE6 added to lipobeads are pulled down when the protein-lipobead mixture is centrifuged. This result is consistent with the high affinity with which PDE6 binds to rod outer segment membranes (Baehr et al., 1979), and demonstrates that the binding capacity of lipobeads for PDE6 exceeds the highest concentration tested in Fig. 2-2. When referenced to the membrane surface area, 12 pmol PDE6 bound to lipobeads (~870 PDE6 per μm^2 of membrane) exceeds the surface

density estimated of PDE6 on rod outer segment disk membranes (500 PDE6 per μm^2 (Pugh & Lamb, 2000)). In addition to mimicking the *in vivo* density of PDE6 on the disk membrane, the tethering of PDE6 to the phospholipid bilayer of lipobeads likely provides a physiologically relevant conformation for the PDE6 holoenzyme to interact with its membrane-confined binding partners.

The efficacy with which PDE6 can be activated by activated Gtα *in vitro* is greatly enhanced when both proteins are tethered to either rod outer segment membranes (Fung, 1983) or liposomal preparations (Malinski & Wensel, 1992), especially those containing cationic phospholipids (Melia et al., 2000). To evaluate the effectiveness of our lipobead preparation to promote activation of PDE6 catalysis by activated Gtα, we incubated lipobeads (pre-incubated with PDE6 holoenzyme) with increasing concentrations of Gtα-GDP to which aluminum fluoride was added (to persistently activate Gtα by mimicking the terminal phosphate of GTP (Bigay et al., 1985)). As seen in Fig. 2-3, PDE6 holoenzyme confined to lipobeads was able to be fully activated by Gtα-GDP-AlF$_4^-$ in a concentration-dependent manner whereas incubation of PDE6 and Gtα in solution was much less effective. We were also able to show that increasing the PDE6 density 10-fold on the lipobeads allows for more efficient activation of PDE6 by Gtα.
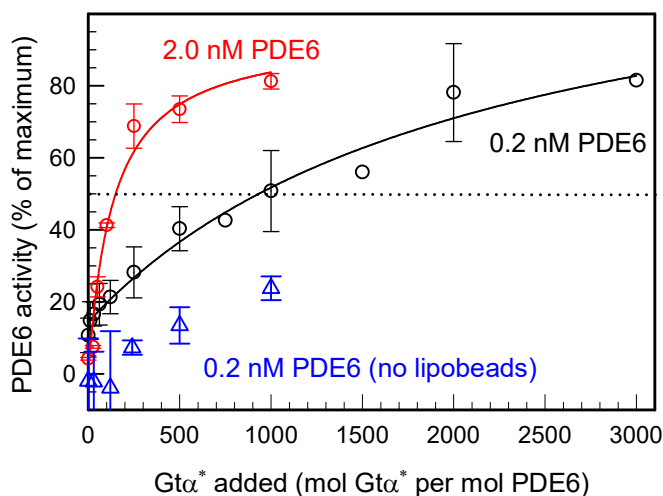
Figure 2-3. Concentration-dependent enhancement of G-protein activation of PDE6 when bound to lipobeads. PDE6 holoenzyme (either 0.2 nM or 2 nM) was incubated with 1.1 pmol of lipobeads for 30 min at room temperature prior to the addition of the indicated amounts of Gtα-GTPγS (Gtα*) for 45 min. Separate samples of PDE6 were mixed with Gtα* in the absence of lipobeads. Upon addition of cGMP (2 mM final concentration), the extent to which PDE6 was activated by Gtα* was determined by monitoring degradation of cGMP. The extent of activation by Gtα* is expressed as the percent of PDE6 activity measured when the inhibitory Pγ subunits of PDE6 are removed by limited trypsin proteolysis. Data represent the mean ± S.D. for 3 experiments (blue and black symbols; three black symbols without error bars are

In addition to providing a stable membrane environment for reconstituting the Gtα-PDE6 activation complex for biochemical studies, lipobead preparations can be used to investigate the molecular architecture and structural rearrangements occurring upon the interaction of activated G-protein α-subunits with their effectors at concentrations similar to those found *in vivo*. We have previously used lipobeads to carry out chemical cross-linking and integrative structural modeling to refine the x-ray structure of Gtα in its membrane-associated conformation as well as the Gtα-PDE6 activation complex (Irwin et al., 2019). To further

examine the stoichiometry of Gtα binding to PDE6 and the sequential mechanism of PDE6 activation (Qureshi et al., 2018), we conducted experiments at a low molar excess of Gtα to PDE6 on lipobeads at elevated PDE6 concentrations. The lipobead-associated proteins were chemically cross-linked with BS3, the protein complexes were subsequently resolved on a 4-12% Tris-glycine gel, and the identity of the proteins extracted from each band determined by MS (Figure 2-4). Less than 6-fold molar excess of activated Gtα relative to PDE6 was sufficient to observe cross-linked complexes of Gtα with individual PDE6 catalytic subunits (possibly also containing bound Pγ) at ~140 kDa, as well as one and two Gtα molecules cross-linked to the PDE6 holoenzyme that formed discrete bands at higher molecular weights.
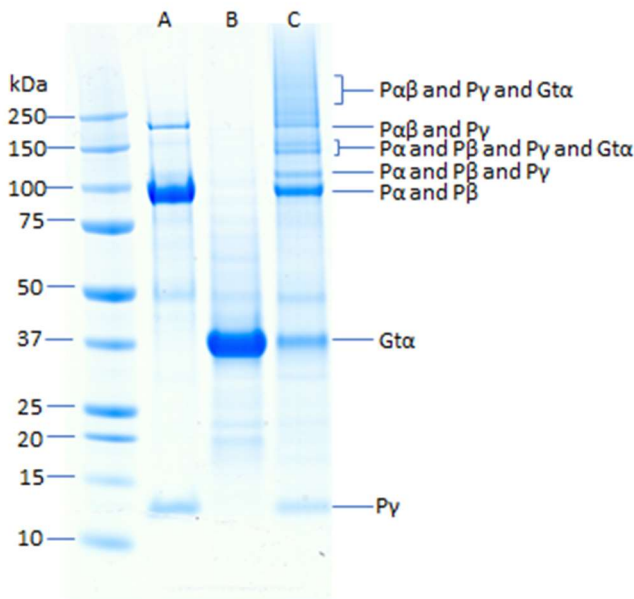
Figure 2-4. Chemical cross-linking of the activated complex of Gtα and PDE6. Cross-linking of PDE6 and Gtα* was performed by first binding 9 pmol of PDE6 to 0.46 pmol lipobeads for 20 min followed by centrifugation. The lipid pellet was resuspended with 115 pmol Gtα-GDP-ALF and incubated for 45 min followed by centrifugation. The pellet was resuspended in 20 μl HNM buffer containing 0.125 mM BS3 and crosslinking proceeded for 45 min. Lane A contains purified PDE6, lane B contains purified Gtα*, and lane C contains the crosslinked mixture.

4. Conclusions

Lipobeads provide many advantages over traditional liposomes. Similar to large unilamellar vesicles, lipobeads have a well-defined and uniform size. This property helps to control both membrane curvature as well as the ability to control the surface density of membrane proteins. Secondly, lipobeads have mechanical stability as well as increased density over traditional preparations of liposomes. This permits for the sedimentation of the lipobeads at relatively low g-forces allowing for easy control of lipobead concentration as well as the ability to remove unbound species from membrane bound-proteins.

In the context of visual transduction, we have shown that lipobeads present the same activity enhancement as traditional liposomes while still allowing for the many advantages mentioned above. The ability to increase PDE6 concentration on the membrane surface allowed us the illustrate that activation efficiency is enhanced with relation to PDE6 density on the membranes. This could allow for study of PDE6 activation at stoichiometric and substoichiometric levels in the future which could have significant implications in the understanding of the activation mechanism of PDE6.

Chapter 3

THE MOLECULAR ARCHITECTURE OF PHOTORECEPTOR PHOSPHODIESTERASE 6 (PDE6) WITH ACTIVATED G PROTEIN ELUCIDATES THE MECHANISM OF VISUAL EXCITATION

Some of the content in this chapter was published in Journal of Biological Chemistry (Irwin et al., 2019).

Authors: Michael J. Irwin, Richa Gupta, Xiong-Zhuo Gao, Karyn B. Cahill, Feixia Chu, Rick H. Cote

Abstract

Photoreceptor phosphodiesterase (PDE6) is the central effector of the visual excitation pathway in rod and cone photoreceptors, and mutations in PDE6 structure or regulation often result in a variety of human retinal diseases. The rod PDE6 holoenzyme consists of two catalytic subunits (Pαβ) whose activity is suppressed in the dark by binding of two inhibitory γ-subunits (Pγ). Upon photoactivation of rhodopsin, the heterotrimeric G-protein (transducin) is activated, resulting in binding of the activated transducin α-subunit (Gtα) to PDE6, displacement of Pγ from the PDE6 active site, and enzyme activation. Although the biochemical pathway is understood, the lack of detailed structural information about the PDE6 activation mechanism hampers efforts to develop therapeutic interventions for PDE6-associated retinal diseases. To address this, we used a cross-linking mass spectrometry approach to create a model of the entire interaction surface of Pγ with the regulatory and catalytic domains of Pαβ in its nonactivated state. Following reconstitution of PDE6 and activated Gtα with liposomes and identification of cross-links between Gtα and PDE6 subunits, the PDE6-Gtα protein complex was determined to consist of two Gtα binding sites bound per holoenzyme. Each Gtα interacts with the catalytic domains of both catalytic subunits, as well as inducing major changes in the sites of interaction of the Pγ subunit with the catalytic

subunits. These results provide a structural model for the activated state of the PDE6-Gtα* complex during visual excitation, thereby enhancing our understanding of the molecular etiology of inherited retinal diseases.

Introduction

The photoreceptor cGMP phosphodiesterase (PDE6) is the central effector enzyme of the G protein-coupled visual transduction pathway in vertebrate rod and cone photoreceptors. PDE6 is exquisitely regulated by a cascade of reactions beginning with photoactivation of the visual pigment, opsin, and subsequent activation of the heterotrimeric G-protein, transducin, in the signal-transducing outer segment of the photoreceptor cell. The activated transducin α-subunit (Gt_α) then binds to the membrane-associated PDE6 and accelerates its hydrolytic activity to transiently lower cGMP levels in the photoreceptor outer segment. This results in the closure of cGMP-gated ion channels and hyperpolarization of the membrane, leading to synaptic transmission to other retinal neurons (Cote et al., 2021).

PDE6 belongs to the eleven-member phosphodiesterase enzyme superfamily that shares a highly conserved catalytic domain responsible for the hydrolysis of the intracellular messengers cAMP and cGMP (Bender & Beavo, 2006; Francis et al., 2011). In addition to the C-terminal catalytic domain, the catalytic subunits of PDE6 consist of two N-terminal regulatory GAF domains (GAFa and GAFb) that are also present in four other PDE families (Zoraghi et al., 2004). However, PDE6 differs from the other ten PDE families in several important respects: (1) unlike the other ten homodimeric PDE families (as well as cone PDE6), rod PDE6 is composed of two different catalytic subunits, α and β, that form a heterodimer (Pαβ); (2) PDE6 catalysis is uniquely regulated by an intrinsically disordered, 9.7 kDa inhibitory γ-subunit (Pγ) that interacts with both the regulatory and catalytic domains of each catalytic subunit to form the nonactivated

rod PDE6 holoenzyme (stoichiometry αβγγ); (3) rod and cone PDE6 are the only PDEs whose activation directly results from binding of a G protein, specifically the activated Gt_α subunit; and (4) upon activation, PDE6 catalysis occurs at the diffusion-controlled limit, more than two orders of magnitude larger than the catalytic turnover rate of other PDE families [reviewed in (Cote, 2006)].

Numerous biochemical approaches have been undertaken to understand the molecular mechanism by which Gt_α binds to the nonactivated PDE6 holoenzyme and relieves the inhibitory constraint of Pγ on PDE6 catalysis. It has been conclusively demonstrated that in the nonactivated state of the PDE6 holoenzyme, the C-terminal portion of Pγ binds to the catalytic domain and blocks access of substrate to the enzyme active site (Barren et al., 2009; Granovsky et al., 1997; Zhang et al., 2010). Catalytic activation of PDE6 is believed to result from interactions of the switch II-α3-helix region of Gt_α with the C-terminal region of Pγ that displaces it from the catalytic pocket of PDE6 (Granovsky & Artemyev, 2001). This same region of Pγ also modulates the GTPase activity of Gtα (Slepak et al., 1995) by potentiating the activity of the regulator of G protein signaling-9 (RGS9) that binds to Gt_α and Pγ in this inactivation complex (Slep et al., 2001). Additional sites of interaction between the Gt_α and the N-terminal, polycationic, and glycine-rich regions of Pγ [reviewed in (Guo & Ruoho, 2008; Zhang et al., 2012)] have been implicated in regulating the efficacy with which Gt_α is able to activate PDE6 (Muradov et al., 2010; Wang et al., 2019; Zhang et al., 2010, 2012), as well as modulating the affinity of cGMP for noncatalytic binding sites in the GAFa domain of the PDE6 catalytic subunits (Cote et al., 1994; Mou & Cote, 2001; Norton et al., 2000).

Consistent with the demonstration of structural asymmetry in the binding interactions of the two Pγ subunits with the rod PDE6 Pαβ heterodimer (Guo et al., 2005; Zeng-Elmore et al.,

2014), complete activation of PDE6 by Gtα requires the binding of Gtα to two non-identical binding sites on PDE6 [(Qureshi et al., 2018) and references cited therein]. Due to the limited information on structure-function relationships of PDE6 holoenzyme in its nonactivated and Gtα-activated states, the molecular sequence of events by which Gtα binds to PDE6 to relieve the inhibition of catalysis by Pγ at two different sites is not known.

Building on recent advances to determine the molecular architecture of the PDE6 holoenzyme at the atomic level using integrative structural modeling (Zeng-Elmore et al., 2014) and cryo-EM (Gulati et al., 2019; Zhang et al., 2015), we present here a structural model for the nonactivated PDE6 holoenzyme that includes the complete interaction surface of its inhibitory Pγ subunits. We also provide a refined structural model for the membrane-associated structure of Gtα and its association with Pγ, as well as the complex of the activated G-protein α-subunit (Gtα-GDP-ALF$_4^-$) with PDE6. In addition to elucidating the mechanistic basis of the first steps in visual signaling, this work provides insights into the molecular etiology of retinal diseases associated with mutations in transducin and PDE6.

Materials and Methods

Materials.

Bovine retinas were purchased from W.L. Lawson, Inc. The Mono Q, HiTrap SP Sepharose FF, HiTrap Blue HP, and Superdex 200 columns were from GE Healthcare. The C18 reverse-phase column (Proto 300, 4.6 × 250 mm) was from Thermo-Fisher Scientific. The primers for Pγ mutagenesis and plasmid purification kits were from Invitrogen and Qiagen, respectively. The QuikChange II Site-Directed Mutagenesis Kit was from Agilent Technologies. Phospholipids and the Mini-Extruder were from Avanti Polar Lipids. Trypsin and Asp-N were purchased from Promega. Silica particles (70 nm diameter, plain) were obtained from Advance Scientific.

Chemical cross-linkers were from Thermo-Fisher, and all other reagents were from Millipore-Sigma, Thermo-Fisher, or VWR.

Preparation of purified PDE6.

Rod PDE6 holoenzyme (subunit composition, αβγγ) was isolated from bovine rod outer segments and purified by anion-exchange and gel filtration chromatography as described previously (Pentia et al., 2005). The Pαβ catalytic dimer was prepared from purified PDE6 holoenzyme by limited trypsin proteolysis to selectively degrade the Pγ subunits; the time course of proteolytic activation of PDE6 catalysis was empirically determined to ensure that > 90% of the Pγ subunit was degraded without altering the apparent molecular weight of the catalytic subunits on SDS-PAGE. Pαβ was then re-purified by Mono Q chromatography (Pentia et al., 2005). Purified PDE6 preparations were stored in 20 mM HEPES, pH 7.5, 100 mM NaCl, 2 mM MgCl$_2$ (HNM buffer) plus 50% glycerol at -20 °C until use. Just prior to an experiment, the protein was buffer exchanged and adjusted to the indicated concentration for the cross-linking reaction.

PDE6 catalysis of cGMP hydrolysis was quantified using a coupled-enzyme assay with colorimetric detection of inorganic phosphate (Cote, 2000). The PDE6 concentration was estimated based on the rate of cGMP hydrolysis of trypsin-activated PDE6 and knowledge of the k_{cat} of the enzyme [5600 mol cGMP hydrolyzed per mol Pαβ per second (Mou et al., 1999)].

Preparation of persistently activated transducin α-subunit.

Gtα was selectively extracted from PDE6-depleted rod outer segment membranes by adding either 50 µM GTPγS or 100 µM GTP to the ROS membranes and recovering the solubilized Gt$_α$ following centrifugation of the membranes. Gt$_α$ was subsequently purified by affinity chromatography on a HiTrap Blue HP column (Ting et al., 1993), followed by Superdex

200 gel filtration chromatography to remove residual PDE6. The concentration of Gt_α was determined by a colorimetric protein assay (Smith et al., 1985) using bovine γ-globulin as a standard. Purified Gtα was stored at -20 °C in 50% glycerol supplemented with 50 μM of GTPγS or GDP until use. Prior to a cross-linking experiment, the Gtα-GTPγS or Gtα-GDP was buffer exchanged into the appropriate cross-linking buffer. In the case of GDP-bound Gtα, the Gtα was incubated with 30 μM $AlCl_3$ and 10 mM NaF for 15 minutes on ice to form the activated Gtα-GDP-AlF_4^- complex (Deterre et al., 1986).

Expression and purification of Pγ mutants.

Pγ site-directed mutants were created with the codon-optimized wild-type bovine rod Pγ sequence as the template and the QuikChange II Site-Directed Mutagenesis Kit to introduce amino acid substitutions. The pET11a plasmids with the sequence-verified Pγ mutant sequences were transformed into *E. coli* BL21(DE3) cells and grown at 37 °C in 2-YT media to an OD_{600} of ~0.6. Then, 0.5 mM isopropyl β-D-1-thiogalactopyranoside was added and the cells incubated at 30 °C for 6 h. The recombinant Pγ protein was purified from the cell extract using a HiTrap SP column followed by C18 reverse-phase HPLC (Artemyev et al., 1998). The apparent molecular weight and purity (>95%) of the recombinant Pγ protein was verified by SDS-PAGE. Pγ cysteine mutants were prepared as described previously (Zeng-Elmore et al., 2014). All Pγ mutants were observed to inhibit Pαβ catalysis over the same concentration range as wild-type Pγ.

Preparation of liposomes and lipobeads to study interactions of transducin with PDE6.

Large unilamellar vesicles and sucrose-loaded vesicles (consisting of an 80:20 molar ratio of 1,2-dioleoyl-sn-glycero-3-phosphocholine and 1,2-dioleoyl-3-trimethylammonium-propane) were initially utilized to improve the efficiency of transducin activation of PDE6 (Melia et al., 2000), closely following established procedures (Wensel et al., 2005). To further improve the ability to

quantitatively sediment PDE6 and Gtα attached to the liposomes (and to eliminate soluble proteins), we adapted an existing method to prepare silica bead-supported liposomes [i.e., lipobeads; (Alkhammash et al., 2015)] for membrane association of PDE6 and Gtα. The ability to pull down PDE6 (~90% PDE bound) and the enhancement of PDE6 activation by Gtα (up to 95% of maximum activation) were equivalent for all of the above liposome preparations.

Lipobeads were prepared by first washing 5 mg of 70 nm silica beads several times with HNM buffer followed by centrifugation for 3 min at 15,000 x g. The bead pellet was then resuspended in HNM buffer. 1,2-dioleoyl-sn-glycero-3-phosphocholine and 1,2-dioleoyl-3-trimethylammonium-propane were mixed at a molar ratio of 80:20 in chloroform, evaporated, and resuspended in HNM buffer containing the lipobeads to a final phospholipid concentration of 500 µM. Unilamellar vesicles coating the silica particles were formed by extruding the mixture fifteen times through a 0.1 µm polycarbonate membrane using a Mini-Extruder.

Chemical cross-linking, in-gel digestion, and MS analysis.

Chemical cross-linking reactions were carried out following the manufacturer's protocols for each cross-linker. For cross-linking reactions with BS3, DSS, Sulfo-SDA, or Sulfo-MBS, proteins were cross-linked in HNM buffer; for EDC cross-linking reactions, 100 mM MES buffer, pH 6.5 was used. After the cross-linking reaction was quenched, proteins were precipitated with trichloroacetic acid, separated by SDS-PAGE and visualized with Coomassie Brilliant Blue G-250. For the case of the nonactivated PDE6 holoenzyme, a 50-fold molar excess of the cross-linker was used, closely following the protocol of our previous study (Zeng-Elmore et al., 2014).

To carry out cross-linking reactions with the complex of activated Gt_α and PDE6 holoenzyme, PDE6 holoenzyme (10-50 pmol) was mixed with a 500-fold molar excess of Gtα-

GDP-AlF$_4^-$ or Gtα-GTPγS along with 0.6 mg lipobeads. The mixture was incubated at room temperature for 1 h and then spun at 10,000 x g for 1.5 min. Unbound proteins in the supernatant fraction (~10% of the total PDE6 and ~50% of the Gtα) were discarded, and the lipobead-associated proteins were resuspended and cross-linked for 1 h with the following molar excess of cross-linker relative to PDE6: BS3 or DSS (500-fold), Sulfo-MBS (100-fold), Sulfo-SDA (100-fold), or EDC (1000-fold). Following quenching of the cross-linking reaction with 20 mM Tris, pH 7.5, the samples were spun at 5,000 x g for 1.5 min, resuspended in SDS-PAGE sample buffer and loaded onto NuPAGE 4-12% Bis-Tris gels. Protein bands on the gel were visualized with Coomassie Brilliant Blue G-250.

Cross-linked products were in-gel digested and analyzed by LC-MS and LC-MS/MS as described previously (Zeng-Elmore et al., 2014), except that we also used Asp-N to generate peptide fragments. For Asp-N digestions, 3 ng Asp-N were added to the gel pieces and incubated for 18 h at 37 ºC. For proteolytic digestions with both enzymes, 300 ng trypsin was added to the gel pieces for 4 h, then 3 ng of Asp-N was added and samples incubated for an additional 18 h. The tryptic peptides were extracted as described (Zeng-Elmore et al., 2014), and Asp-N or double digested peptide samples were extracted using 50% acetonitrile and 7% formic acid.

One microliter aliquots of the concentrated peptides were injected into the Dionex Ultimate 3000 RSLC nano UHPLC system (Dionex Corporation, Sunnyvale, CA) and separated by a PepMap RSLC column (75 μm × 25 cm, 100 Å, 2 μm) at a flow rate of 450 nl/min (mobile phase A: 0.1% formic acid in H$_2$O, mobile phase B: 0.1% formic acid in 80% acetonitrile). The eluant was directed into the nano-electrospray ionization source of an LTQ Orbitrap XL mass spectrometer (Thermo Scientific, Waltham, MA). LC-MS data were acquired in an information-dependent acquisition mode. Full MS spectra were acquired in the Orbitrap (m/z 315–2000). The

five most intense ions were selected for collision-induced dissociation in the linear ion trap for MS/MS data acquisition.

Identification of cross-linked peptides.

Cross-linked peptides were identified using an integrated module in Protein Prospector, using a previously described strategy (Chu et al., 2010; Zeng-Elmore et al., 2014). Cross-linked peptide scores were based on the number and types of fragment ions identified, in conjunction with the sequence and charge state of the peptide. Only results where the score difference confirmed that the cross-linked peptide match was better than a single peptide match alone were considered. Expectation values were calculated based on matches to single peptides and thus were treated as another score, rather than as a statistical measure of reliability.

Integrative structural modeling of PDE6, Gt_α, and the Gt_α-PDE6 activated complex.

Integral structural modeling was performed using the open-source Integrated Modeling Platform (Webb et al., 2018) and Modeller (Sali & Blundell, 1993) in an iterative manner. To perform rigid body docking of protein subunits, IMP was carried out in $2x10^4$ Metropolis Monte-Carlo sampling steps with a high temperature of 2.0, a low temperature of 0.5, and with a new system configuration following each step. The top 100 scoring models were generated and saved, and IMP was then used to perform clustering on the top 100 models in order to aid in model selection. The best fitting model was run in Modeller using the same cross-linking restraints in order to further refine the model, evaluate stereochemical quality, and fill in the missing atoms. Secondary structure identification was initially determined by Pymol version 2.3 (Schrodinger) and further refined and validated with Coot (Emsley et al., 2010).

The Pαβ catalytic dimer refinement was performed using the PDE6 cryo-electron microscopic (EM) structure (Gulati et al., 2019) as the template (PDB ID: 6MZB). Structural

model refinements used the spatial restraints imposed by cross-linked peptides we identified in samples of native and reconstituted PDE6 catalytic subunits, as described previously (Zeng-Elmore et al., 2014). Analysis of the root mean square deviations of our structural model with other available structures was carried out using Visual Molecular Dynamics (VMD) software version 1.9.3 (Humphrey et al., 1996).

To model the PDE6 holoenzyme (Fig. 3-1), the refined Pαβ model was used as a single, unchanging rigid body and each Pγ subunit was treated as eight separate rigid bodies consisting of residues 2-30, 31, 38-41, 44-45, 52-53, 58-62, 68, 70-87. This approach circumvented the lack of uniform cross-linking data for the entire Pγ subunit. Two of the rigid bodies (residues 2-30 and 70-87) were based on the Pγ structure and topology obtained from the PDE6 cryo-EM structure (Gulati et al., 2019). The remaining Pγ peptide fragments were generated *in-silico* (http://www.arguslab.com/arguslab.com/ArgusLab.html) assuming a linearly extended conformation. IMP was then used to dock the Pγ fragments. Subsequently, Modeller was used with the same cross-linking constraints to fill in the missing portions of Pγ as well as to add the missing atoms to each subunit.

The structure of membrane-associated Gtα-GDP-AlF$_4^-$ was obtained using the x-ray crystal structure of Gtα-GDP-AlF$_4^-$ [1TAD; (Sondek et al., 1994)] as the primary template and imposing distance restraints from cross-linked peptides we identified, as described above. Because the cross-linking data of purified Gt$_α$ included cross-links from the N-terminal α-helix of Gt$_α$ that is not included in the 1TAD crystal structure, the Gt$_α$ structure was refined by including the N-terminal helix (amino acids 1-27) obtained from the transducin heterotrimer structure (PDB ID: 1GOT) with the 1TAD structure as two rigid bodies for conducting integrative modeling.

36

The structure of Pγ docked to Gtα-GDP-AlF$_4^-$ (Fig. 2) was performed by treating Gtα-GDP-AlF$_4^-$ as a rigid body and dividing the central region of Pγ into 3 rigid bodies consisting of residues 25, 39-41, and 45 in IMP. Modeller was used to refine the structure and add missing atoms to the model.

The structure of the activated complex of Gtα and the Pαβ catalytic dimer (Fig. 3-3) was docked using the previously described structures as templates. Pαβ was treated as a single rigid body and two Gtα-GDP-AlF$_4^-$ structures were included in the modeling in IMP, followed by refinement with Modeller.

The input data files, modeling scripts and output models can be accessed at https://github.com/rcotelab/Irwin-et-al-2019.

Results

Solution structure of the PDE6 catalytic heterodimer.

Upon comparing the 3.4 Å cryo-EM structure of the PDE6 holoenzyme (Gulati et al., 2019) with our previous solution structure of PDE6 catalytic dimer determined by chemical cross-linking, identification of cross-linked peptides by mass spectrometric analysis, and integrative structural modeling (Zeng-Elmore et al., 2014), we observed that a number of distance restraints defined by our cross-linking results were inconsistent with the cryo-EM structure (e.g., cross-links in the β-subunit between residues 675 and 813, and between 675 and 815; Table 3-1). In addition, neither of the above-mentioned studies resolved the entire structure of the Pγ subunits that are tightly bound to the PDE6 catalytic dimer in its nonactivated state. We therefore performed integrative structural modeling of the bovine rod PDE6 holoenzyme using the Gulati et al. cryo-EM structure as a template [PDB ID: 6MZB; (Gulati et al., 2019)] and the previously reported (Zeng-Elmore et al., 2014) and new cross-linking data for the PDE6

holoenzyme (Table 3-1) as inputs into the Integrated Modeling Platform (IMP) and Modeller

(see *Materials and Methods*) to determine the complete structure for the tetrameric PDE6.

Exp. m/z	z	Δ (ppm)	pep1	aa1	pep2	aa2	crosslinker
658.9788	3	7.4	Pβ	471	Pβ	475	EDC
431.8966	3	-3.5	Pβ	675	Pβ	813	EDC
431.8969	3	-2.8	Pβ	675	Pβ	815	EDC
405.4728	4	2.9	Pβ	823	Pβ	832	EDC
540.2943	3	2.3	Pβ	824	Pβ	832	EDC
606.6677	3	1.7	Pβ	825	Pβ	827	Sulfo-SDA
540.2935	3	0.81	Pβ	826	Pβ	828	EDC
530.9468	3	2.4	Pβ	826	Pβ	829	Sulfo-SDA
530.9463	3	1.4	Pβ	826	Pβ	831	Sulfo-SDA
567.6403	3	-6.7	Pβ	826	Pα/Pβ	445/444	Sulfo-SDA
425.9827	4	-5.2	Pβ	826	Pα/Pβ	442/441	Sulfo-SDA
606.6667	3	0.034	Pβ	826	Pβ	828	Sulfo-SDA
524.9417	3	-7.8	Pβ	826	Pα/Pβ	444/443	Sulfo-SDA
573.6439	3	0.044	Pβ	826	Pβ	832	Sulfo-SDA
578.0868	4	-6.9	Pγ	1[b]	Pβ	78	BS3
479.7	4	-18	Pγ	C2[c]	Pβ	92	BMH
474.8	2	-18	Pγ	C2[c]	Pα	77	BMH
678.3601	3	-9.4	Pγ	4[a]	Pβ	146	EDC
1034.308	4	2.5	Pγ	7[d]	Pβ	184	BS(PEG)9
926.715	4	0.73	Pγ	C18[e]	Pα	383	Sulfo-MBS
1134.087	4	15	Pγ	C18[e]	Pβ	84	BMH
860.94	2	-3.6	Pγ	C22[f]	Pα	77	BMH
795.87	2	-12	Pγ	C22[f]	Pα	272	BMH
653.051	4	-1.6	Pγ	31[e]	Pβ	200	Sulfo-MBS
596.0509	4	-15	Pγ	41[a,g]	Pα	469	Sulfo-SDA
1063.227	3	-17	Pγ	44	Pα/Pβ	613/611	BS3
800.656	4	-8.8	Pγ	44	Pβ	475	BS3
498.4935	4	-17	Pγ	52[a,g]	Pα/Pβ	328/326	EDC
911.4194	3	-15	Pγ	K62[a,g]	Pβ	450	EDC
911.4185	3	-4.8	Pγ	K62[a,g]	Pβ	446	EDC
660.0972	4	-1.3	Pγ	K62[a,d]	Pα/Pβ	394	EDC
879.7957	3	0.78	Pγ	K62[a,d]	Pα/Pβ	393	EDC
478.512	4	0.34	Pγ	K63[a,h]	Pα	767	EDC
670.0686	4	-13	Pγ	K64[g]	Pβ	839	BMOE
545.0488	4	-7.6	Pγ	K65[g]	Pα/Pβ	677/675	BS3

Table 3-1. PDE6 holoenzyme intra- and inter-molecular crosslinked peptides. Cross-linked peptides were identified following chemical cross-linking of 10-50 pmol purified rod PDE6 holoenzyme as described in Materials and Methods. Except where indicated with superscripts, samples consisted of native PDE6 holoenzyme and were digested with trypsin prior to mass spectrometric analysis: [a]trypsin/asp-N double digest; [b]Sample consisted of Pαβ reconstituted with recombinant, wild-type rod Pγ; [c]Pαβ reconstituted with Pγ2C/68S; [d]Pαβ reconstituted with Pγ58K/62K/65K/73K; [e]Pαβ reconstituted with Pγ18C/68S; [f]Pαβ reconstituted with Pγ 22C/68S; [g]Pαβ reconstituted with Pγ62K/65K/73K/79K, [h]Pαβ reconstituted with Pγ53K/62K/65K/73K. Exp. m/z is the experimentally measured mass-to-charge ratio, z is the charge state of the peptide, and Δ is the accuracy measured in parts per million. The crosslinked peptides are defined as the protein subunit (pep1, pep2) and amino acid residue number (aa1, aa2) identified using the indicated crosslinker. In the "aa1" column, the presence of a single letter amino acid residue preceding the residue number indicates an amino acid substitution of the wild-type Pγ sequence at the site of cross-linking. In addition to the cross-links in this table, the PDE6 structural model included spatial constraints from cross-links reported previously for the PDE6 holoenzyme (Zeng-Elmore, 2014).

As shown in Fig. 3-1A, the cross-link-refined solution structure of the PDE6 holoenzyme fits well within the cryo-EM envelope (Gulati et al., 2019), with the spatial restraints imposed by the cross-linking results generating a more compact arrangement of structural elements as well as providing predicted structures for missing elements in the cryo-EM structure. Comparisons at the level of individual domains of our cross-link-refined PDE6 solution structure with the cryo-EM structure (Gulati et al., 2019) identified several significant differences in conformation: (1) the N-terminal region preceding the GAFa domain in our structural model contains additional α-helical elements (Fig. S2B), consistent with the hypothesis (Gulati et al., 2019) that this region may contribute to dimerization of the catalytic subunits. (2) Whereas the GAFa domains showed relatively small differences in secondary structure when compared to the cryo-EM structure, the GAFb domains of the PDE6 solution structure exhibited greater dissimilarity. Our cross-linking restraints identified conformational differences in several loop structures of GAFb, including the β1/β2 loop that contains a novel α2/α3 helix *(data not shown);* this loop is in close proximity to the catalytic domain, and as previously suggested may play a role in inter-subunit allosteric communication (Chu et al., 2019; Gulati et al., 2019). (3) The catalytic domains of our structural model also exhibited significant differences in comparison with the cryo-EM structure, particularly in the flexible H-loop and M-loop regions near the enzyme active site and in the α16 helix. Cross-links in the C-terminal region (Table 3-1 and ref. (Zeng-Elmore et al., 2014)) imposed spatial restraints to the conformation of the α15 and α16 helices in our model that displaced these two helices toward the center of the catalytic domain (and are likely to contribute to the observed conformation of the H- and M-loops), as well as defining additional α-helical segments (Cα1 and Cα2) in the C-terminal region. The fact that the C-termini of the PDE6

catalytic subunits are prenylated (Anant et al., 1992)and membrane-associated under our

experimental conditions likely account for the structural differences we observe in the catalytic

domain and C-terminus. Together, these observations emphasize the importance of chemical

cross-linking to define both
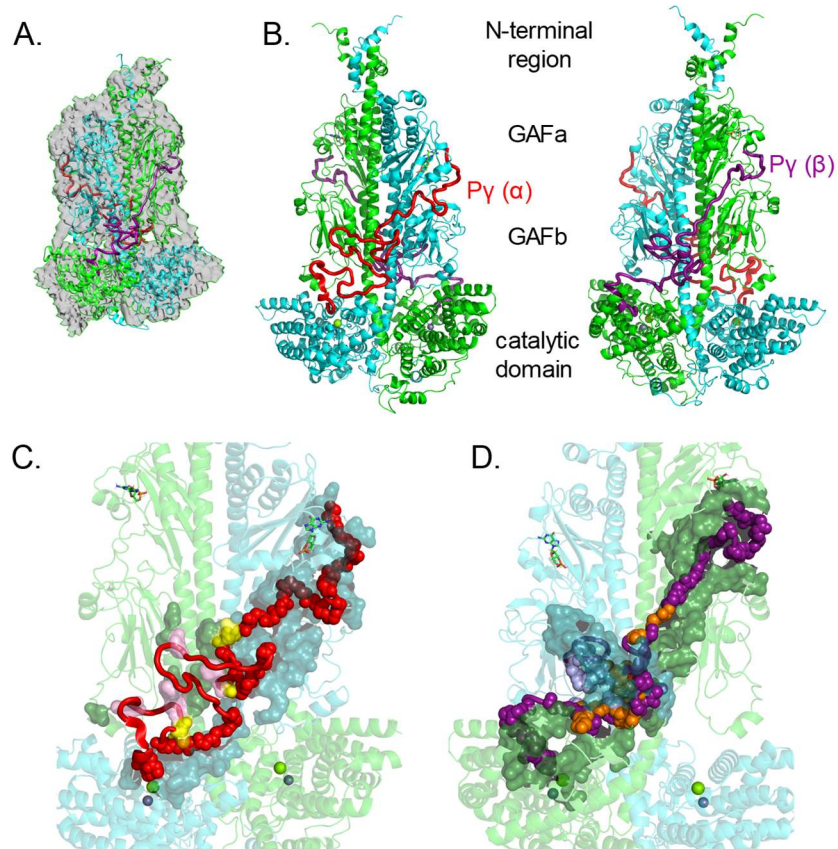
Fig 3-1. Integrative structural model of the PDE6 holoenzyme. The structural model of rod PDE6 holoenzyme (αβγγ) was determined by using the cryoEM structure 6MZB (Gulati, 2019) as a template and applying spatial restraints determined by chemical cross-linking of purified bovine rod PDE6 (Table 3-1 and (Zeng-Elmore, 2014)). In the model, PDE6 subunits are colored as follows: α-subunit, cyan; β-subunit, green; Pγ subunit primarily associated with α-subunit (Pγ(α); red) and β-subunit (Pγ(β); deep purple). **A.** Superimposition of the template cryoEM map (EMD-9297) with the cross-link refined structural model of nonactivated PDE6 holoenzyme. **B.** Asymmetric interactions of Pγ with the Pαβ catalytic dimer extending from the cGMP-binding GAFa domain to the GAFb domain and then crossing over to the catalytic domain to the site of inhibition of catalysis. Each Pγ subunit primarily interacts with one catalytic subunit. The two images are rotated 180 degrees. **C.** Interaction surface of the Pγ(α) subunit with the PDE6 catalytic dimer. Pγ(α) residues interacting with the catalytic dimer are shown as main chain atom spheres: red, residues interacting with the α-subunit; pink, residues interacting with the β-subunit; and yellow, Pγ residues that interact with both catalytic subunits; non-interacting Pγ(α) residues are shown as red loops and α-helix. The catalytic subunit interacting residues are shown as a surface representation (α-subunit, dark cyan; β-subunit, dark green). **D.** Interaction surface of the Pγ(β) subunit with Pαβ. The interaction surface of the Pγ(β) subunit (180 degree rotation of panel C) is depicted in which the deep purple, light purple, and orange spheres represent interactions with the β-subunit, α-subunit, or both catalytic subunits, respectively.

flexible structural elements (e.g., loops) and protein conformations unique to the membrane-associated state that are often challenging to resolve by more traditional structural methods.

Each intrinsically disordered Pγ subunit forms multiple interactions with both PDE6 catalytic subunits.

In order to map the entire interaction surface of Pγ with the PDE6 catalytic dimer, we performed cross-linking experiments with a variety of chemical cross-linkers as well as using several site-directed mutants of Pγ that were reconstituted with Pαβ. The 21 new intermolecular cross-links between Pγ and the α- or β-subunits (Table 3-1) along with previously reported cross-links (Zeng-Elmore et al., 2014)) and the cryo-EM structure of two fragments of Pγ (Gulati et al., 2019) permitted visualization for the first time of the molecular architecture of the entire PDE6 holoenzyme. Fig. 3-1B shows that the overall topology of the each Pγ subunit is similar, originating at the noncatalytic cGMP binding pocket in the GAFa domain of one catalytic subunit and terminating at the enzyme active site of the same catalytic subunit. While the N-and C-terminal regions of Pγ assume a predominantly linearly extended conformation, the mid-region of Pγ exists in a random coil conformation.

Analysis of the interaction surface of Pγ with the catalytic subunits (Figs. 3-1C-D) reveals marked differences in the number and types of interactions of each Pγ with the two catalytic subunits. One Pγ subunit (designated Pγ(Pα)) follows the trajectory of the α-subunit (Fig. 3-1C), with approximately one-half of its 87 residues forming an interaction surface in the GAFa, GAFb and catalytic domains, ending at the active site of the α-subunit. Nine Pγ(Pα) residues interact with the β-subunit in its GAFa and GABb domains, with four of the nine being in close proximity to both catalytic subunits. The second Pγ subunit (Pγ(Pβ)) has an even greater interaction surface with the catalytic dimer (Fig. 3-1D), with 89% of its residues interacting with

Pαβ. Pγ(Pβ) interactions with Pαβ include 62 residues of the β-subunit and 30 residues of the α-subunit, with 15 of these residues being in close proximity to both catalytic subunits. The large number of Pγ(Pβ) interactions with the α-subunit is most evident in the GAFb domain where the Pγ(Pβ) subunit comes into contact with the α-subunit GAFb domain (leftward projection in Fig. 3-1D), as well as multiple interactions of Pγ(Pβ) with the central α-helical "backbone" of both catalytic subunits. This complex network of interactions of both Pγ subunits with both catalytic subunits localized predominantly in the GAFb domains of the catalytic dimer may represent the structural basis for allosteric communication between the α- and β-subunits during transducin activation of PDE6 (see Discussion).

Structure of membrane-associated Gt_α and its interactions with soluble Pγ.

We first carried out cross-linking experiments with activated Gtα attached to liposomes to determine the solution structure of membrane-associated Gtα. Experiments were carried out with Gtα-GDP-AlF$_4^-$ for which a crystal structure is available (PDB ID:1TAD). For the N-terminal α-helix (αN) which is missing from this crystal structure [and proposed to have conformational flexibility; (Zhang et al., 2004)], we used as a template the structure of the αN helix that was determined for the inactive transducin heterotrimer (PDB ID:1GOT). With the αN helix and the Gtα-GDP-AlF$_4^-$ structures as templates and the intramolecular Gtα cross-links that we identified (Table 3-2), a model of the membrane-associated, activated Gtα-GDP-AlF$_4^-$ subunit of transducin was created (Fig. 3-2A). Intramolecular cross-links (K18 to K267 and E21 to K275; Table 3-2) between the αN helix and the Ras-like GTPase sub-domain of Gtα imposed spatial constraints that are reflected in a major shift of the αN helix toward the αF/β2 loop region

Exp. m/z	z	Δ (ppm)	pep1	aa1	pep2	aa2	crosslinker
451.2427	4	9.2	Gtα	16	Gtα	20	EDC
451.2424	4	-9.8	Gtα	16	Gtα	25	EDC
539.2929	3	-9.1	Gtα	17	Gtα	20	BS3
451.2498	4	6.6	Gtα	17	Gtα	21	EDC
487.267	3	-9.4	Gtα	17	Gtα	22	EDC
723.7675	3	6.4	Gtα	17	Gtα	31	BS3
434.9019	3	-7.8	Gtα	18	Gtα	26	EDC
434.9022	3	-7.1	Gtα	18	Gtα	26	EDC
637.7287	3	-9	Gtα	18	Gtα	31	BS3
565.9201	5	-9.4	Gtα	18	Gtα	31	BS3
345.2063	4	3.3	Gtα	18	Gtα	267	BS3
899.8458	3	7.3	Gtα	20	Gtα	31	BS3
415.5742	3	-1.3	Gtα	20	Gtα	205	BS3
468.2516	3	-9.5	Gtα	21	Gtα	275	Sulfo-SDA
733.7522	3	-8	Gtα	24	Gtα	31	EDC
899.8322	3	-7.9	Gtα	25	Gtα	31	BS3
455.7341	4	-8.3	Gtα	25	Gtα	189	EDC
576.6672	3	-8.3	Gtα	26	Gtα	31	EDC
330.5199	3	-3.6	Gtα	26	Gtα	205	EDC
658.381	3	-9.1	Gtα	39	Gtα	47	EDC
817.4389	4	-10	Gtα	169	Gtα	176	EDC
459.9397	3	4.2	Gtα	267	Gtα	275	DSS
446.2453	3	8	Gtα	267	Gtα	342	EDC
504.2656	2	-3	Gtα	98	Pγ	39	BS3
975.9864	2	-10	Gtα	129	Pγ	25	BS3
469.5794	3	7.2	Gtα	203	Pγ	39	BS3
440.913	3	-10	Gtα	203	Pγ	45	BS3

Table 3-2. Intra- and inter-molecular crosslinked peptides of membrane-associated Gtα-GDP-AlF₄⁻ and Pγ. Cross-linked peptides were identified following chemical cross-linking of either lipobead-associated Gtα-GDP-AlF^{4-} or Gtα-GDP-AlF$_4^-$ incubated with a 2-fold stoichiometric excess of purified Pγ and analyzed as described in Materials and Methods. Abbreviations are defined in the legend to Table 3-1. All Gtα intramolecular crosslinks were detected in both the absence and presence of Pγ.

that is part of the interface between the GTPase sub-domain and the helical insertion sub-domain. This shift brings the αN helix in proximity with the nucleotide binding site. We

conclude that the structural model shown in Fig. 3-2A better represents the membrane-associated, solution structure of Gtα in that it takes into account the N-terminal acylation of Gtα responsible for its association with rod outer segment membranes *in vivo*.

Previous biochemical studies have identified two major regions of Pγ that bind to activated Gtα, namely the polycationic central region of Pγ and the C-terminal half of Pγ (Artemyev et al., 1993; Artemyev & Hamm, 1992; Guo & Ruoho, 2008; Slep et al., 2001; Zhang et al., 2012; Zhang & Artemyev, 2010). To determine the topological relationship of Gtα with Pγ, we incubated liposome-associated Gtα-GDP-AlF$_4^-$ (see *Materials and Methods*) with purified Pγ and conducted cross-linking analyses of the protein band migrating at the apparent molecular weight expected for a 1:1 complex of Pγ and Gtα (~50 kDa). We identified five intermolecular, cross-linked peptides spanning residues 25 to 45 of the central region of the Pγ molecule (Table 3-2) which interact with both the helical sub-domain and the Switch II region of the GTPase sub-domain of Gtα (Fig. 3-2A). This 20 amino acid segment of Pγ interacts on the opposite face of the Gtα subunit from the interface of Gtα with the PDE6 catalytic domain (*see below*). As seen in Fig. 3-2B, Pγ assumes a highly extended linear structure when bound to Gtα compared with the conformation of the same region of Pγ bound to the PDE6 α- or β-subunits. [Although there is structural evidence that the C-terminal half of Pγ binds to the PDE6-facing side of Gtα (Grant et al., 2006; Slep et al., 2001), our inability to observe cross-linked peptides between Gt$_α$ and this region of Pγ arises from the absence of amino acid residues in the C-terminal half of Pγ capable of generating cross-linked peptides for mass spectrometric detection (Zeng-Elmore et al., 2014).] No significant changes in the tertiary structure of Gtα were detected upon Pγ binding.
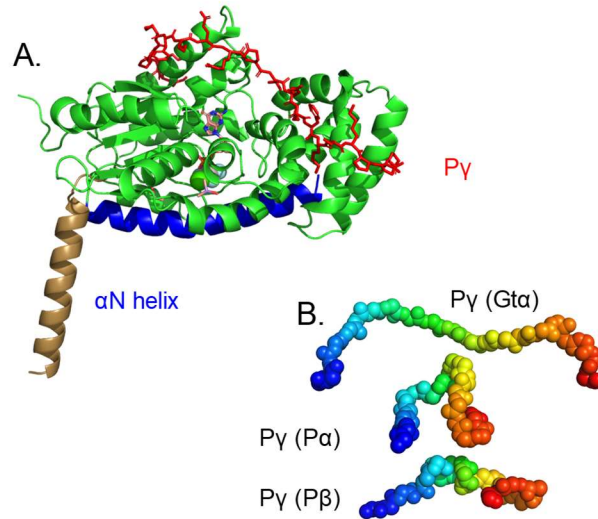
Fig 3-2. Structural model of Gtα-GDP-AlF$_4^-$ and its interaction with Pγ in solution. A. The structural model of Gtα was determined using the 1TAD crystal structure as the template (Sondek, 1994) and refined with spatial restraints imposed from cross-linking results in the absence or presence of Pγ (Table 3-2). Structural elements that were unchanged in the cross-link refined model are represented in green, with the conformational change of the αN helix shown in brown (for the crystal structure) and blue (for the cross-link modified solution structure). Also shown is the docked structure of Pγ (red) with Gtα-GDP-AlF$_4^-$ based on the observed cross-linking results when Gtα associated with lipobeads was incubated with a 2-fold molar excess of Pγ. Note that no significant changes in Gtα conformation were observed upon Pγ binding. **B.** A comparison of the conformation of the central region of Pγ (residues 24 to 44, depicted as a gradient from blue to red spheres) when bound to Gtα or to the PDE6 catalytic subunits.

Molecular architecture of the G protein-effector activation complex.

Full activation of PDE6 by Gtα is greatly enhanced when both proteins are associated with either rod outer segment membranes or are reconstituted with phospholipid bilayers (Malinski & Wensel, 1992). In order to determine the structure of the transducin-PDE6 complex in its membrane-associated state, we therefore pre-incubated purified proteins with cationic phospholipid vesicles that have been shown to enhance PDE6 activation by Gtα (Melia et al., 2000). To restrict our analysis to only membrane-associated Gtα and PDE6, we prepared liposome-coated silica beads ("lipobeads;" see *Materials and Methods*) that allowed for sedimentation of membrane-associated proteins for further analysis. Using this method, ~90% of

the PDE6 holoenzyme was pulled down in the lipobead pellet, and under these conditions we

observed at least 80% of maximal activation of PDE6 catalysis by transducin (*data not shown*).

Exp. m/z	z	Δ (ppm)	pep1	aa1	pep2	aa2	crosslinker
947.4468	2	3.7	Gtα	9	Pα/Pβ	442/440[a]	EDC
673.5722	4	-4.1	Gtα	10	Pβ	826[b]	BS(PEG)$_5$
447.0946	8	7.8	Gtα	10	Pα	854[b]	BS3
684.3533	3	-3.1	Gtα	17	Pα	551[b]	BS3
545.3019	2	2.4	Gtα	17	Pα/Pβ	808/806	EDC
674.0325	3	-1	Gtα	17	Pβ	817[b]	Sulfo-SDA
558.3024	4	-8.9	Gtα	20	Pα/Pβ	807/805	BS3
1360.241	2	4.3	Gtα	20	Pα/Pβ	620/618	BS3
812.4367	3	5.7	Gtα	24	Pα/Pβ	326/328[a]	Sulfo-SDA
752.024	3	-7.6	Gtα	25	Pα	309[c]	BS3
775.0531	3	-3.9	Gtα	128	Pα/Pβ	807/805	BS3
569.994	3	-7.8	Gtα	275	Pβ	307[c]	BS3
381.2	3	-9.3	Gtα	98	Pγ	41	EDC
332.469	4	1.7	Gtα	275	Pγ	29	BS3
337.8635	3	-7.3	Pα/Pβ	328/326	Pγ	25	EDC
413.2165	5	-14	Pα	551	Pγ	29	BS3

Table 3-3. Intermolecular crosslinked peptides of the activated complex of Gt$_α$-GDP-AlF^{4-} with PDE6 holoenzyme. Cross-linked peptides were identified following chemical cross-linking of a mixture of Gtα-GDP-AlF$_4^-$ and PDE6 holoenzyme attached to lipobeads and analyzed as described in *Materials and Methods*. Abbreviations are defined in the legend to Table 1. Superscripts indicate cross-links that were omitted from specific structural models: [a]omitted during docking of Gt$_α$ to catalytic domain; [b]omitted during docking Gtα to GAFb domain; [c]omitted from computational modeling due to loop flexibility. All identified intra- and inter-molecular cross-links involving PDE6 catalytic subunits were identical to those observed in the holoenzyme structure [Table 3-1 and (Zeng-Elmore, 2014)] and omitted here.

We first assessed whether all of the cross-linked peptides we observed between Gt$_α$ and

the PDE6 catalytic subunits could be accounted for by a single Gtα binding site per Pαβ. Table 3

shows that three PDE6 α-subunit-specific and three β-subunit-specific cross-links with Gt$_α$ ruled

out a single binding site per Pαβ, consistent with biochemical studies (Qureshi et al., 2018).

When 10 cross-linked peptides between Gt$_α$ and the α- or β-subunit of PDE6 in Table 3-3 were

used as distance restraints for input into the IMP workflow, we found no single structural model

that was able to accommodate all of the cross-link restraints. Instead, we observed two major

classes of structural models with different cross-links that violated the distance restraints. The

predominant set of structural models was generated by omitting the two cross-links between Gt_α

and the GAFb domains (Gtα9-Pα442/Pβ440 and Gtα24-Pα330/Pβ328; Table 3-3); the remaining

eight cross-links permitted docking of Gtα to two similar—but not identical—sites on the α- and

β-subunit catalytic domains (Fig. 3-3A).

Closer examination of the interface of Gtα with the PDE6 α-subunit catalytic domain

(Fig. 3-3B) revealed that the GTPase sub-domain of this Gtα molecule (including the Switch II

region and the αN helix) interacts with the α14 helix, the M-loop region [implicated in regulating

Pγ occlusion of the active site (Barren et al., 2009)] and the α15 and α16 helices of the α-subunit

catalytic domain, in excellent agreement with previous mutagenesis studies (Natochin et al.,

1998). Interestingly, the αB helix of this Gt_α molecule interacts with the adjacent PDE6 β-subunit

in the linker region between the GAFb and β-subunit catalytic domain (Fig. 3-3B). The
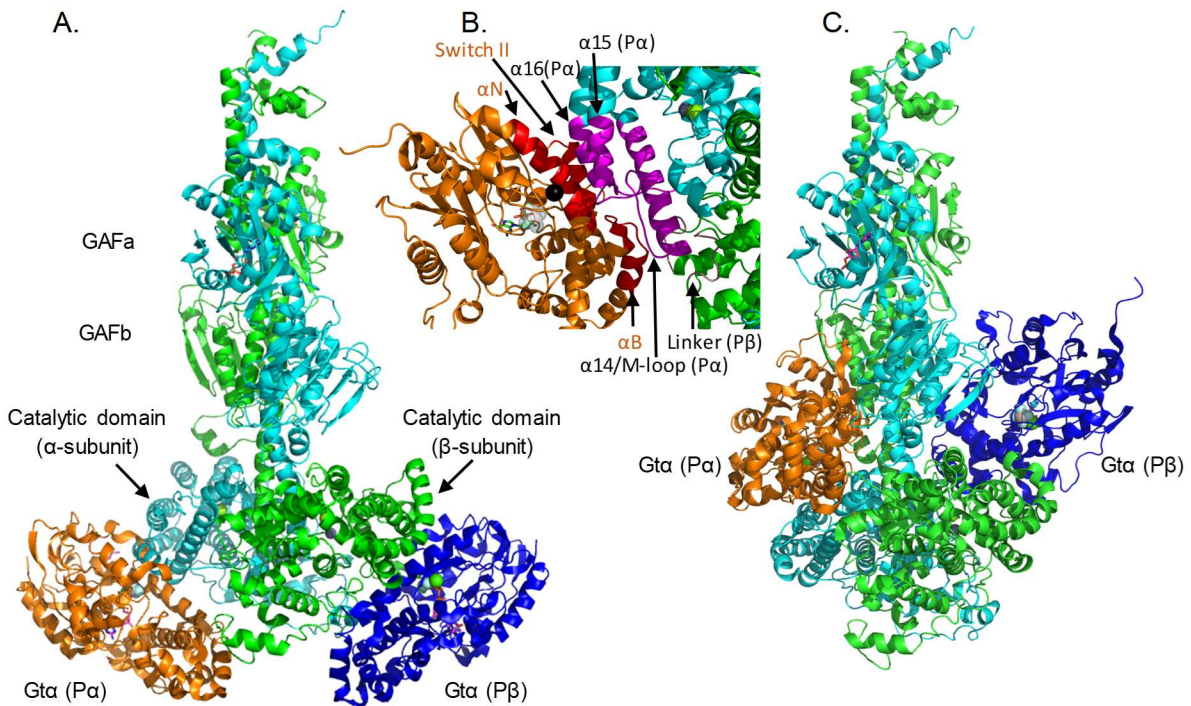
Fig 3-3. Model of Gtα-GDP-AlF₄⁻ docked to the Pαβ catalytic dimer. PDE6 holoenzyme and Gtα-GDP-AlF₄⁻ bound to lipobeads (see *Materials and Methods*) were exposed to chemical cross-linkers, and the identified cross-linked peptides between Gtα and PDE6 subunits (Table 3) were then used as spatial restraints for integrative structural modeling. Two predominant clusters of models of the Gt$_α$-Pαβ complex were generated, one with Gtα docked to the two catalytic domains (with distance violations for Gtα24-Pα330/Pβ328, Gtα9-Pα442, and Gtα9-Pβ440), the other with Gtα docked to the GAFb domains (with distance violations for Gtα10-Pα854, Gtα17-Pα551, and Gtα128-Pα807/Pβ817). Due to insufficient cross-links for Pγ in the activated complex, the inhibitory subunit is not shown. **A.** Structural model of association of Gtα-GDP-AlF₄⁻ to the α-subunit [(Gtα(Pα), orange] and to the β-subunit [(Gt$_α$(Pβ), blue] catalytic domains. **B.** Detailed view of the Gtα GTPase sub-domain interface with the α-subunit catalytic domain, with the interaction surface of Gt$_α$ colored red and the α- and β-subunit interacting residues colored magenta and brown, respectively. Black sphere indicates Gt$_α$ Q200. **C.** Alternate docking of Gtα to the GAFb domains of the Pαβ catalytic dimer (with the same orientation as in Panel A).

interaction surface of the second Gtα with the β-subunit was generally similar to the α-subunit, but with a greater surface of interaction reflecting additional interactions with the region of the β-subunit linking the GAFb and catalytic domains. For both Gtα subunits, the N-terminal α-helix has significant surface interactions with the catalytic domains. With the cross-links in Table 3-3, we were unable to observe any significant changes in Gtα-GDP-AlF₄⁻ conformation upon

interaction with Pαβ. The same was true for the PDE6 catalytic dimer where the overall RMSD for each catalytic subunit was ~1.0 A when comparing the nonactivated and transducin-activated conformations of each PDE catalytic subunit (*data not shown*). Interestingly, the interaction surface of Gtα with PDE6 catalytic subunits is similar to that observed for the complex of a membrane-bound adenylyl cyclase with the G_s α-subunit, particularly in the Switch II and α3 helix regions of the GTPase domain (Qi et al., 2019).

A second cluster of structural models of Gtα-activated PDE6 docking with the GAFb domain (Fig. 3-3C) was identified when three different cross-links at the bottom of the Pαβ catalytic domains (Gtα10-Pα854, Gtα17-Pα551, and Gtα128-Pα807/Pβ805) were omitted during the structural modeling (Table 3-3). Although insufficient cross-linking data for the Pγ subunit precluded structural modeling of Pγ in the transducin-activated PDE6 complex, the same central region of Pγ that binds to purified Gtα in an extended conformation (Fig. 3-2A) is associated with the GAFb domain of nonactivated PDE6 (Fig. 3-1C-D) and likely promotes Gtα binding to the GAFb domain shown in Fig. 3-3C. This second binding site for Gtα is supported by biochemical studies indicating a role for the central region of Pγ in facilitating Gtα activation of PDE6 catalysis (Zhang et al., 2010) as well as enhancing the dissociation of cGMP from GAFa noncatalytic binding sites (Zhang et al., 2012).

Discussion

This paper reports the first complete structural models for the PDE6 holoenzyme (Fig. 3-1), the activated α-subunit of transducin in a complex with the inhibitory γ-subunit of PDE6 (Fig. 3-2), as well as the fully activated state of PDE6 in a complex with two transducin α-subunits (Fig. 3-3)—all in their membrane-associated state that mimics the localization of the transducin-PDE6 protein complex on photoreceptor outer segment disk membranes. Together, these

structural models advance our understanding of the mechanism of visual excitation in rod photoreceptors by revealing the asymmetric surface of interaction between each Pγ subunit and the Pαβ catalytic dimer, as well as the different sites of interaction of Gtα with PDE6 and the major conformational changes that the Pγ subunits must undergo upon transducin activation of PDE6 in the phototransduction pathway.

Chemical cross-linking combined with mass spectrometric analysis (Chu et al., 2018) has enabled us to refine the secondary, tertiary, and quaternary structure of PDE6 in its nonactivated and transducin-activated states. The distance restraints imposed by cross-linked residues within and between proteins comprising the nonactivated and activated states of PDE6 permitted us to dock Gtα subunits to each catalytic subunit of PDE6, thereby providing a structural basis for the allosteric mechanism for G-protein-coupled activation of PDE6 during visual excitation—including the functional asymmetry of the PDE6 holoenzyme that underlies the requirement for successive binding of two Gtα molecules for full enzyme activation (Lamb et al., 2018; Qureshi et al., 2018) and references cited therein.] This cross-linking/mass spectrometric approach also permitted visualization of flexible regions of the catalytic and inhibitory subunits that were poorly resolved by cryo-EM (Gulati et al., 2019).

Our integrative structural modeling of PDE6 reveals the multiple inter-subunit interactions that underlie the multi-faceted allosteric regulation of this G protein-activated enzyme: (1) each Pγ subunit interacts with both PDE6 catalytic subunits, with lateral, cross-subunit communication likely transmitted through the GAFb domains where a number of Pγ residues are in close proximity to both catalytic subunits (Fig. 3-1C-D); (2) the β-subunit exhibits greater interactions with Pγ than the α-subunit, consistent with two classes of binding sites for Pγ with Pαβ (Mou & Cote, 2001); (3) in addition to the extensive Pαβ dimerization surface, direct

allosteric communication may occur between the β1/β2 loop in the GAFb domain of one

catalytic subunit and the catalytic domain of the other subunit (Gulati et al., 2019), as well as

between the catalytic domains and C-terminal regions of the two subunits (Fig. 3-1B).

Defining the molecular architecture of the transducin-PDE6 activated complex permitted

structural verification of the stoichiometry of two Gtα subunits bound to the PDE6 catalytic

subunits in its fully activated state, as well as unexpectedly revealing two distinct sites of

interaction of Gt_α with the GAFb (Fig. 3-3C) and catalytic domains (Fig. 3-3A-B) of the PDE6

catalytic subunits. The observation that each Gtα subunit has sites of interaction with both the α-

and β-subunits of PDE6 is consistent with a cooperative activation mechanism in which the

binding of the first Gtα induces conformational changes in Pαβ that alter the ability of the

second Gtα subunit to bind to and trigger full enzyme activation (Lamb et al., 2018; Qureshi et

al., 2018).

Model for G protein activation of the central effector enzyme of the visual signaling pathway.

Fig. 3-4 presents a model consistent with our experimental results for the light-induced

activation of PDE6 holoenzyme by transducin that involves the sequential binding of two Gtα

subunits that results in both Gtα subunits releasing the inhibitory constraint of Pγ from its
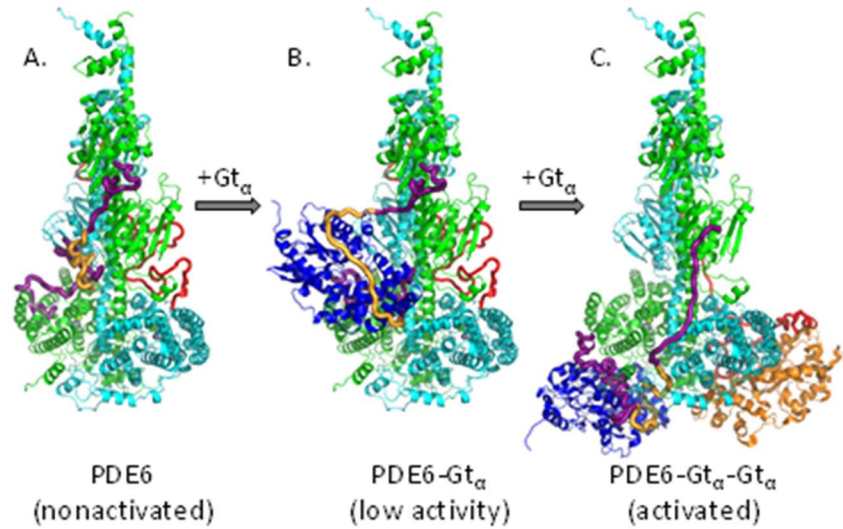
Fig 4. Proposed model for the activation of PDE6 by transducin during visual excitation. A. In the dark-adapted condition, the PDE6 holoenzyme is inhibited by its Pγ subunits occluding the enzyme active site (Fig. 3-1, rotated 90º). **B**. The first light-activated Gtα subunit is proposed to initially bind to the GAFb docking site (Fig. 3-3C) without causing significant catalytic activation of PDE6 (Qureshi, 2018). The Pγ subunit was docked to this complex using the following information: (1) the central region of Pγ (gold) was docked using the cross-links obtained for the Gtα-Pγ complex (Table 3-2) in conjunction with the cross-links used to dock Gtα to the GAFb domain (Table 3-3); (2) lacking cross-linking data for the N-terminal region of Pγ in the activated complex, this region of Pγ (purple) relied on PDE6 holoenzyme cross-links and thus its topology differs from Fig. 3-1 only to the extent needed to accommodate cross-link spatial restraints imposed by the Pγ central region; (3) in the absence of Pγ cross-links for its C-terminal region in the activated complex, we modeled this region of Pγ (purple) interacting with Gtα using the crystal structure of Pγ (residues 50-87) bound to a chimeric G-protein [PDB: 1FQJ; (Slep, 2001)]. **C**. Upon binding of a second Gtα, PDE6 becomes fully activated as both Gtα subunits dock to the catalytic domains and displace the C-terminal region of Pγ from the enzyme active sites. In order to accommodate the binding of the central region of Pγ to the helical face (Table 3-2) and the C-terminal region of Pγ to the GTPase face of Gtα [Table 3-3 and (Slep, 2001)], a major displacement of the N-terminal Pγ residues from the GAFa domains must occur.

interactions with each PDE6 catalytic domain to cause full activation of PDE6 (Lamb et al., 2018).

Upon light activation of the phototransduction cascade, nonactivated PDE6 holoenzyme (Fig. 3-4A) is proposed to form initial interactions between the central region of Pγ (associated

with the GAFb domains) and an activated Gt_α subunit (Fig. 3-3C) resulting in the central region of $P\gamma$ becoming significantly more extended (Fig. 3-4B). In this model, the binding of $Gt\alpha$ to this central region of $P\gamma$ does not require major displacement of either the N- or C-terminal regions of $P\gamma$ from its holoenzyme conformation. Upon binding of a second $Gt\alpha$, Fig. 3-4C depicts a relocation of the first $Gt\alpha$ from the GAFb to the catalytic domain, along with binding of the second $Gt\alpha$ to the catalytic domain of the other catalytic subunit (Fig. 3-4C)—resulting in full enzyme activation. As a consequence of $Gt\alpha$ binding to the central and C-terminal regions of $P\gamma$ when docked to the catalytic domains, our model requires that the N-terminal region of $P\gamma$ dissociate from its interactions with the GAFa domain (Fig. 3-4C). This structural model for sequential activation of PDE6 is supported by prior biochemical and structural studies of $Gt\alpha$ interactions with PDE6 subunits in the activated complex (Liu et al., 1999; Milano et al., 2018; Natochin et al., 1998; Skiba et al., 1996; Slep et al., 2001). The required displacement of $P\gamma$ from the GAFa domains is also consistent with a lowered affinity of cGMP to its GAFa binding sites upon transducin activation of rod PDE6 (Norton et al., 2000; Zhang et al., 2012; Zhang & Artemyev, 2010), as well as offering insights into differences in how rod and cone PDE6 may be activated by transducin (Wang et al., 2019). Experimental support for the model in Fig. 3-4 is currently under investigation, including validating the GAFb domain as an initial docking site for one or both $Gt\alpha$ subunits, identifying whether the α- or β-subunit preferentially binds the first $Gt\alpha$, the allosteric communication pathway leading to binding of the second Gt_α subunit, and the significance of cGMP occupancy of the GAFa binding sites for the activation, recovery, and light adaptation stages of visual transduction.

Summary.

In addition to advancing a structural basis for understanding the initial events in the visual signaling pathway, structural elucidation of PDE6 in its nonactivated and transducin-activated states offers insights into the molecular etiology of pathogenic mutations in these proteins and possible therapeutic interventions. For example, having characterized the interaction surface of Gtα-PDE6, it is now evident that the missense mutation (Q200E; black sphere in Fig. 3B) resulting in autosomal dominant congenital stationary night blindness (Szabo et al., 2007) is located at the interface between the Gtα Switch II region and the PDE6 catalytic domain where Pγ regulation of catalytic activation occurs. Since somatic mutations in PDE6 catalytic subunit genes have been implicated in various cancers [(Maryam et al., 2019) and references cited therein], understanding the atomic-level structure of PDE6 is also relevant to non-retinal diseases. Given that abnormal accumulation of cGMP is believed to be the causative factor in many retinal degenerative diseases (Power et al., 2020), understanding the structural organization of PDE6 and the protein-protein interactions that regulate its activity may provide insights into development of allosteric activators of PDE6 analogous to those being developed for other members of the PDE family of enzymes (Baillie et al., 2019; Omar et al., 2019).

Chapter 4

DETERMINATION OF THE SEQUENTIAL ACTIVATION OF PDE6 BY G-PROTEIN α-SUBUNIT

Abstract

Photoreceptor phosphodiesterase is the central enzyme in the phototransduction pathway in rod and cone photoreceptors. PDE6 is a heterotetramer, consisting of two catalytic subunits (Pαβ) and two identical inhibitory subunits (Pγ). Upon light stimulation, an activation cascade results in the binding of the activated G-protein transducin alpha subunit (Gtα*) to PDE6, displacement of Pγ from the PDE6 active site, and enzyme activation. The biochemical pathway has been well studied, however the structural basis for the activation mechanism has yet to be elucidated. To address this gap, we used lipobeads to reconstitute PDE6 and Gtα* and performed chemical crosslinking and mass spectrometric analysis of PDE6 interactions with Gtα* at near physiological concentrations and at near stoichiometric and sub-stoichiometric amounts of Gtα* to PDE6. This allowed for isolation of crosslinked species containing a single Gtα* bound with very low activation, and two Gtα* bound to PDE6 with significant activation. A single Gtα* is found to interact primarily with the regulatory GAF domains of PDE6. The addition of a second Gtα* results in a shift in Gtα* binding, with both Gtα* now primarily interacting with the two catalytic domains of Pαβ. These results support an activation mechanism for PDE6, with Gtα* first interacting with the regulatory domains of PDE6 followed by a shift to the catalytic domains and full activation of PDE6.

Introduction

The photoreceptor cGMP phosphodiesterase (PDE6) is the central effector enzyme of the G protein-coupled visual transduction pathway in vertebrate rod and cone photoreceptors. PDE6

is regulated by a cascade of reactions. Photoactivation of the visual pigment, opsin, is followed by activation of the heterotrimeric G-protein, transducin, in the signal-transducing outer segment of the photoreceptor cell. The activated transducin α-subunit (Gtα*-GTP) then binds to PDE6 and accelerates its hydrolytic activity to transiently lower cGMP levels in the photoreceptor outer segment. This results in the closure of cGMP-gated ion channels and hyperpolarization of the membrane, leading to synaptic transmission to other retinal neurons (Arshavsky & Burns, 2012).

PDE6 belongs to the eleven-member phosphodiesterase enzyme superfamily that shares a highly conserved catalytic domain responsible for the hydrolysis of the intracellular messengers cAMP and cGMP (Bender & Beavo, 2006; Francis et al., 2011). In addition to the C-terminal catalytic domain, the catalytic subunits of PDE6 consist of two N-terminal regulatory GAF domains (GAFa and GAFb) that are also present in four other PDE families (Zoraghi et al., 2004). However, PDE6 differs from the other ten PDE families in several respects. Rod PDE6 is composed of two different catalytic subunits, α and β, that form a heterodimer (Pαβ) and is inhibited by a separate protein, Pγ. Additionally, upon activation, PDE6 catalysis occurs at the diffusion-controlled limit, more than two orders of magnitude larger than the catalytic turnover rate of other PDE families [reviewed in (Cote, 2021)].

Many biochemical studies have aimed to understand the molecular mechanism by which Gtα* binds to the nonactivated PDE6 holoenzyme and relieves the inhibitory constraint of Pγ. It has been conclusively demonstrated that in the nonactivated state of the PDE6 holoenzyme, the C-terminal portion of Pγ binds to the catalytic domain and blocks access of substrate to the enzyme active site (Barren et al., 2009; Granovsky et al., 1997; Zhang et al., 2010). Catalytic activation of PDE6 is believed to result from interactions of the switch II-α3-helix region of $Gt_α$ with the C-terminal region of Pγ that displaces it from the catalytic pocket of PDE6 (Granovsky

& Artemyev, 2001). This same region of Pγ also modulates the GTPase activity of Gt_α (Slepak et al., 1995) by potentiating the activity of the regulator of G protein signaling-9 (RGS9) that binds to Gtα and Pγ in this inactivation complex (Slep et al., 2001). Additional sites of interaction between the Gtα and the N-terminal, polycationic, and glycine-rich regions of Pγ [reviewed in (Cote et al., 2021)] have been implicated in regulating the efficacy with which Gtα is able to activate PDE6 (Muradov et al., 2010; Wang et al., 2019; Zhang et al., 2010, 2012), as well as modulating the affinity of cGMP for noncatalytic binding sites in the GAFa domain of the PDE6 catalytic subunits (Cote et al., 1994; Mou & Cote, 2001; Norton et al., 2000).

Building on recent advances to determine the molecular architecture of the PDE6 holoenzyme at the atomic level using integrative structural modeling (Irwin et al., 2019; Zeng-Elmore et al., 2014) and cryo-EM (Gulati et al., 2019; Zhang et al., 2015), we present here a structural model for the mechanism of activation of PDE6. This mechanism was elucidated through the construction of homology models based on stoichiometric and sub-stoichiometric crosslinking data, allowing for determination of the initial binding site of Gtα. In addition to elucidating the mechanistic basis of the first steps in visual signaling, this work provides insights into the molecular etiology of retinal diseases associated with mutations in transducin and PDE6.

Materials and Methods

Materials.

Bovine retinas were purchased from W.L. Lawson, Inc. The Mono Q, HiTrap SP Sepharose FF, HiTrap Blue HP, and Superdex 200 columns were from GE Healthcare. The C18 reverse-phase column (Proto 300, 4.6 × 250 mm) was from Thermo-Fisher Scientific. Phospholipids and the Mini-Extruder were from Avanti Polar Lipids. Trypsin and Asp-N were purchased from Promega. Silica particles (70 nm diameter, plain) were obtained from Advance

Scientific. Chemical cross-linkers were from Thermo-Fisher, and all other reagents were from Millipore-Sigma, Thermo-Fisher, or VWR.

Preparation of purified PDE6.

Rod PDE6 holoenzyme (subunit composition, αβγγ) was isolated from bovine rod outer segments and purified by anion-exchange and gel filtration chromatography as described previously (Pentia et al., 2005). Purified PDE6 preparations were stored at -20 ºC in HNM buffer consisting of 20 mM HEPES, pH 7.5, 100 NaCl, 2 mM $MgCl_2$ supplemented with 50% glycerol. Just prior to an experiment, the protein was buffer exchanged and adjusted to the indicated concentration for cross-linking or for activity measurements.

Preparation of persistently activated transducin α-subunit.

Gtα was selectively extracted from PDE6-depleted rod outer segment membranes by adding either 50 µM GTPγS or 100 µM GTP to the ROS membranes and recovering the solubilized Gtα following centrifugation of the membranes. Gtα was subsequently purified by affinity chromatography on a HiTrap Blue HP column (Ting et al., 1993), followed by Superdex 200 gel filtration chromatography to remove residual PDE6. The concentration of Gtα was determined by a colorimetric protein assay (Smith et al., 1985) using bovine γ-globulin as a standard. Purified Gtα was stored at -20 °C in 50% glycerol supplemented with 50 µM of GTPγS or GDP until use. Prior to a cross-linking experiment, the Gtα-GTPγS or Gtα-GDP was buffer exchanged into the appropriate cross-linking buffer. In the case of AlF-activated Gtα, the Gtα was incubated with 30 µM $AlCl_3$ and 10 mM NaF for 15 minutes on ice to form the activated Gtα-GDP-AlF_4^- complex (Deterre et al., 1986).

Preparation of liposomes and lipobeads to study interactions of transducin with PDE6.

The detailed procedure for preparing lipobeads is described in Chapter 5 (Irwin et al., 2022). Briefly, lipobeads were prepared by first washing 5 mg of 70 nm silica beads several times with HNM buffer followed by centrifugation for 3 min at 15,000 x g. The bead pellet was then resuspended in HNM buffer. 1,2-dioleoyl-sn-glycero-3-phosphocholine and 1,2-dioleoyl-3-trimethylammonium-propane were mixed at a molar ratio of 80:20 in chloroform, evaporated, and resuspended in HNM buffer containing the lipobeads to a final phospholipid concentration of 500 µM. Unilamellar vesicles coating the silica particles were formed by extruding the mixture fifteen times through a 0.1 µm polycarbonate membrane using a Mini-Extruder.

Chemical cross-linking, in-gel digestion, and MS analysis.

Chemical cross-linking reactions were carried out following the manufacturer's protocols for the cross-linker BS3. Proteins were cross-linked in HNM buffer after which the cross-linking reaction was quenched, proteins were precipitated with trichloroacetic acid, separated by SDS-PAGE and visualized with Coomassie Brilliant Blue G-250. For the case of the nonactivated PDE6 holoenzyme, a 50-fold molar excess of the cross-linker was used, closely following the protocol of our previous study (Zeng-Elmore et al., 2014).

To carry out cross-linking reactions with the complex of activated Gtα and PDE6 holoenzyme, PDE6 holoenzyme (10-50 pmol) was mixed with lipobeads (0.46 pmol) followed by centrifugation. Pellets were resuspended with a 0.4 or 3-fold molar excess of Gtα-GDP-AlF^{4-} (for cross-linking) or Gtα-GTPγS (for activity assays) The mixture was incubated at room temperature for 1 h and then spun at 10,000 x g for 1.5 min. Unbound proteins in the supernatant fraction (~10% of the total PDE6 and ~50% of the Gtα) were discarded, and the lipobead-associated proteins were resuspended and cross-linked for 1 h with the following 50 molar

excess of cross-linker relative to PDE6 or BS3. Samples were quenched with sample loading buffer and run of Tris-glycine gels. Protein bands on the gel were visualized with Coomassie Brilliant Blue G-250 and excised.

Cross-linked products were in-gel digested with trypsin and analyzed by LC-MS and LC-MS/MS as described previously (Zeng-Elmore et al., 2014). Tryptic peptides were extracted as described (Zeng-Elmore et al., 2014).

One microliter aliquots of the concentrated peptides were injected into the Dionex Ultimate 3000 RSLC nano UHPLC system (Dionex Corporation, Sunnyvale, CA) and separated by a PepMap RSLC column (75 µm × 25 cm, 100 Å, 2 µm) at a flow rate of 450 nl/min (mobile phase A: 0.1% formic acid in H_2O, mobile phase B: 0.1% formic acid in 80% acetonitrile). The eluant was directed into the nano-electrospray ionization source of an LTQ Orbitrap XL mass spectrometer (Thermo Scientific, Waltham, MA). LC-MS data were acquired in an information-dependent acquisition mode. Full MS spectra were acquired in the Orbitrap (m/z 315–2000). The five most intense ions were selected for collision-induced dissociation in the linear ion trap for MS/MS data acquisition.

Identification of cross-linked peptides.

Cross-linked peptides were identified using an integrated module in Protein Prospector, using a previously described strategy (Chu et al., 2010; Zeng-Elmore et al., 2014). Cross-linked peptide scores were based on the number and types of fragment ions identified, in conjunction with the sequence and charge state of the peptide. Only results where the score difference confirmed that the cross-linked peptide match was better than a single peptide match alone were considered. Expectation values were calculated based on matches to single peptides and thus were treated as another score, rather than as a statistical measure of reliability.

Integrative structural modeling of PDE6, Gtα, and the Gtα-PDE6 activated complex.

Integrative structural modeling was performed using the open-source Integrated

Modeling Platform (Webb et al., 2018) and Modeller (Sali & Blundell, 1993) in an iterative

manner. To perform rigid body docking of protein subunits, IMP was carried out in $2x10^4$

Metropolis Monte-Carlo sampling steps with a high temperature of 2.0, a low temperature of 0.5,

and with a new system configuration following each step. The top 100 scoring models were

generated and saved, and IMP was then used to perform clustering on the top 100 models in

order to aid in model selection. The best fitting model was run in Modeller using the same cross-

linking restraints in order to further refine the model, evaluate stereochemical quality, and fill in

the missing atoms. Secondary structure identification was initially determined by Pymol version

2.3 (Schrodinger) and further refined and validated with Coot (Emsley et al., 2010).

PDE activity assays

PDE6 catalysis of cGMP hydrolysis was quantified using a coupled-enzyme assay with

colorimetric detection of inorganic phosphate (Cote, 2000). The PDE6 concentration was

estimated based on the rate of cGMP hydrolysis of trypsin-activated PDE6 and knowledge of the

k_{cat} of the enzyme [5600 mol cGMP hydrolyzed per mol Pαβ per second (Mou et al., 1999)].

To determine the enzyme activity at high concentrations of PDE6, 10µL of lipobeads

were mixed with the desired amount of PDE6 in HNM buffer. The PDE6 and lipobeads were

incubated at room temperature for 1 hour, followed by centrifugation at 10,000 x g for 10

minutes. The PDE6-containing pellets were resuspended in the desired molar excess of Gtα

(either -GDP or -GTPγS) in 40 µL HNM containing 2 µM vardenafil and incubated at room

temperature for 1 hour. Trypsinized and basal control samples were treated similarly, but did not

contain Gtα in the resuspension buffer. Following incubation, 40 µL of 4 mM cGMP was added

to each sample. In order to quench the reaction, 25 µL was transferred to a 96 well plate containing 50 µL of 0.1 M HCl. The remainder of the assay was performed as described previously (Cote, 2000).

Results

Reconstitution of the membrane-confined Gtα*-PDE6 activation complex at near physiological concentrations

To determine the efficiency of transducin activation of PDE6 at concentrations approaching those found in the rod outer segment, we first measured cGMP hydrolytic rates at several PDE6 concentrations when reconstituted on lipobeads with approximately stoichiometric amounts of either Gtα-GDP and Gtα-GTPγS. Fig. 4-1B shows that sub-stoichiometric levels of Gtα-GTPγS do not activate PDE6 to a significant extent above basal levels even at the highest concentration tested. However, with a 3-fold excess of Gtα*-GTPγS to PDE6, we observed significant catalytic activation of PDE6 at the two highest PDE concentrations.
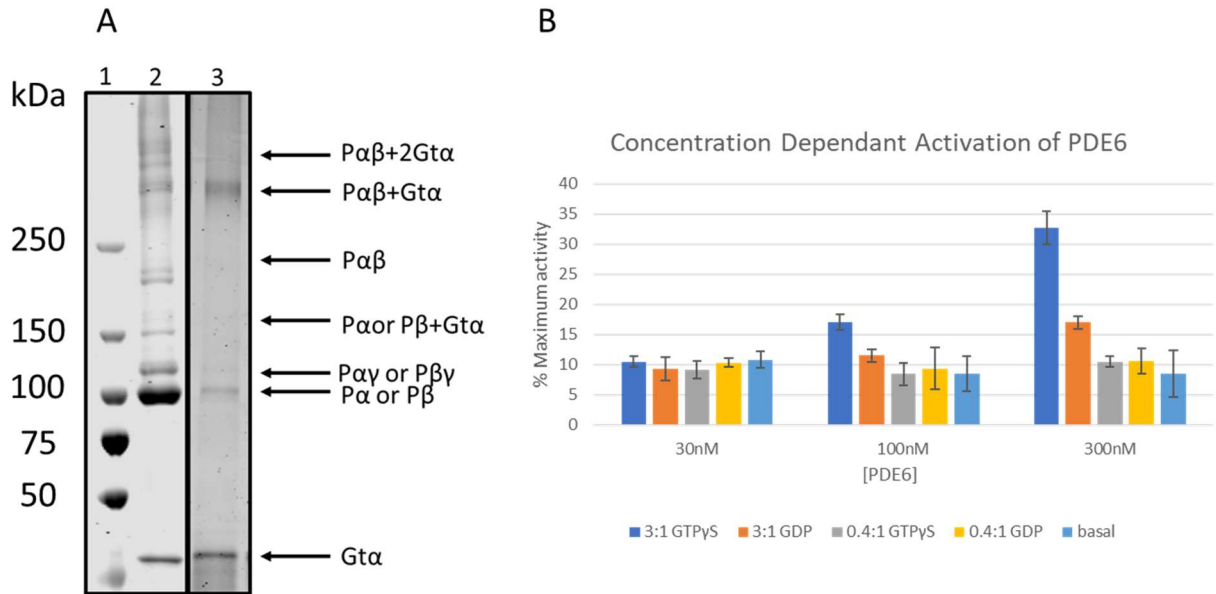
Figure 4-1. **Cross-linking and activity of PDE6 at near stoichiometric and sub-stoichiometric concentrations of Gtα.** Cross-linking and activity assays were performed as described in Materials and Methods. A. Chemical crosslinking of 3:1 and 0.4:1 molar ratios of Gtα*-GDP-AlF$_4^-$ (75 and 60 pmol, respectively) to PDE6 (25 and 150 pmol, respectively). Lane 1: Molecular weight ladder. Lane 2: 3:1 Gtα*:PDE6. Lane 3: 0.4:1 Gtα*:PDE6. B Activation of PDE6 at set stoichiometric ratios of Gtα*-GTPγS or Gtα-GDP to PDE6 over a range of 30-300 nM PDE6 .

In contrast, PDE6 activation was not observed when incubated with Gtα-GDP at either 0.4:1 or 3:1 ratios of Gtα:PDE6 except at the highest PDE6 concentration tested (Fig. 4-1B). At 300 nM PDE6, we did observe a small increase in activation induced by a 3-fold molar excess of Gtα-GDP, consistent with earlier studies (Kroll et al., 1989). These results demonstrate that the efficacy of Gtα* activation of PDE6 is greatly enhanced as the density of PDE6 and Gtα* on the lipobead membrane approaches that of the rod outer segment membrane.

Sub-stoichiometric amounts of activated Gtα-GDP-AlF4- relative to PDE6 results in binding of one Gtα to either the Pα or Pβ GAFb domain*

The ability to reconstitute high concentrations of PDE6 and Gtα at defined molar ratios on lipobead membranes in conjunction with separation of discrete Gtα-PDE6 complexes by SDS-PAGE permitted us to determine whether sub-stoichiometric amounts of Gtα*-GDP-AlF$_4^-$ were able to bind to the PDE6 holoenzyme (in the absence of catalytic activation). As seen in Fig. 4-1A, lane 3, reconstitution of 0.4 Gtα*-GDP-AlF$_4^-$ per PDE6 holoenzyme on lipobeads and chemical cross-linking led to the formation of a single cross-linked, high molecular weight species migrating at a position indicative of a single Gtα bound to the PDE6 holoenzyme. This band was isolated from the gel and processed for LC-MS analysis in order to identify cross-linked peptides. Using previously published structural models of Pαβ and Gtα as templates, the two cross-linked peptides between Gtα*-GDP-AlF$_4$- and Pα and Pβ (Table 4-1) were used as spatial restraints for integrative structural modeling of the interface of interaction between Gtα*-

z	m/z	pep1	aa1	pep2	aa2
2	897.9128	Gtα^B	10	Pβ	195
3	912.0898	Gtα^B	313	Pβ	438
3	824.1034	Gtα	42	Pα/Pβ	390/391
3	915.4214	Gtα^A	25	Pβ	440
3	917.0972	Gtα^A	117	Pβ	440
4	731.8498	Gtα	102	Pα/Pβ	393/391

Table 4-1. Intermolecular cross-links of the sub-stoichiometric complex of Gtα-GDP-AlF$_4^-$ with PDE6. Cross-linked peptides were identified as described in Materials and Methods. The crosslinked peptides are described using the protein subunit (pep1, pep2) and the amino acid residue number (aa1, aa2). m/z is the measured mass to charge ratio and z is the charge state of the peptide. The superscripts signify cross-links that provide specificity to either the Pα ("A") or Pβ ("B") catalytic face.

GDP-AlF4- and the Pαβ catalytic dimer. [Unfortunately, Pγ-containing cross-linked peptides were present at levels below the detection limit.]
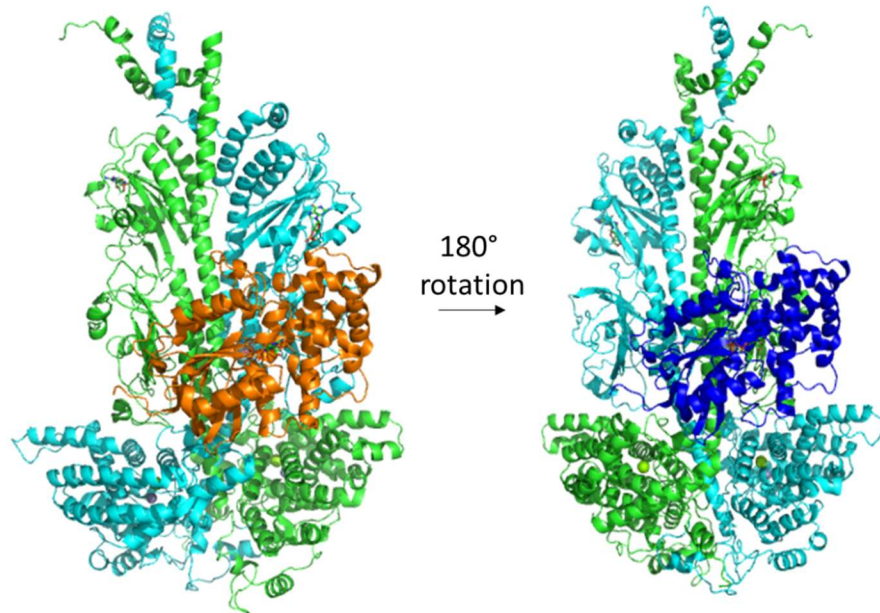
Figure 4-2. Homology model of a single Gtα-GDP-AlF4- bound to Pαβ. Pα is depicted in cyan, Pβ is depicted in green, the Gtα interacting with the Pα catalytic face is depicted in orange and the Gtα interacting with the Pβ catalytic face is depicted in blue. Homology modeling was performed as described in the Materials and Methods. A 180° rotation is used in order to show the docking site of Gtα on the opposite catalytic face.

As shown in Fig. 4-2, the Pα-specific and Pβ-specific cross-links with Gtα* revealed that a single Gtα*-GDP-AlF4- had two similar but non-identical binding sites on opposite faces of Pαβ, each one centered on the GAFb domains. The Gtα* subunits were oriented such that the α-helical sub-domain was in proximity to the GAFa and GAFb domains while the ras sub-domain of Gtα* was oriented with the Switch 2 element pointing toward the catalytic domain H-loop that regulates PDE6 catalysis. Although not resolved in this study, the polycationic, disordered central region of Pγ subunit that traverses the GAFb domain is likely to be responsible for stabilizing the binding of Gtα* to the GAFb region of the PDE6 catalytic dimer (see Fig. 4-6 in Discussion). Since the PDE6 catalytic activity was not significantly different from its basal rate

when sub-stoichiometric amounts of Gtα are present, we infer that the GAFb binding sites for

Gtα* do not interact with the C-terminal region of Pγ that is responsible for inhibition of

catalysis. In summary, under conditions where only a single Gtα*-GDP-AlF$_4^-$ binds to the PDE6,

the activity measurements and structural modeling both support a model in which the initial

binding event of transducin with PDE6 occurs at one of the two GAFb binding sites without

causing catalytic activation of PDE6.

When Gtα* is in molar excess to PDE6, Gtα localizes to the catalytic domains of Pα and Pβ and

is accompanied by activation of PDE6 catalysis

Analysis of the band corresponding to two Gtα*-GDP-AlF4- crosslinked to PDE6 (Fig.

4-1A, lane 2) resulted in a set of crosslinks (Table 4-2) consistent with docking of Gtα* to the

catalytic domains. Structural homology modeling using the crosslinks as spatial restraints

identified two distinct docking sites, one on each of the catalytic faces. All of the most likely

z	m/z	pep1	aa1	pep2	aa2
3	574.2477	Gtα^A	10	Pβ	579
3	600.6728	Gtα^A	300	Pα	554
3	912.0983	Gtα^B	238	Pβ	437
3	844.3485	Gtα^B	25	Pβ	784
3	916.0959	Gtα^A	117	Pβ	578

Table 4-2 Chemical cross-links of the complex observed with an excess of Gtα-GDP-AlF$_4^-$ and PDE6. Cross-links were identified in the protocol detailed in the Materials and Methods. Abbreviations are defined in Table 4-1.

homology models generated by clustering analysis identified docking sites only at the catalytic

domains, not to the GAFb domains (Fig. 4-3).
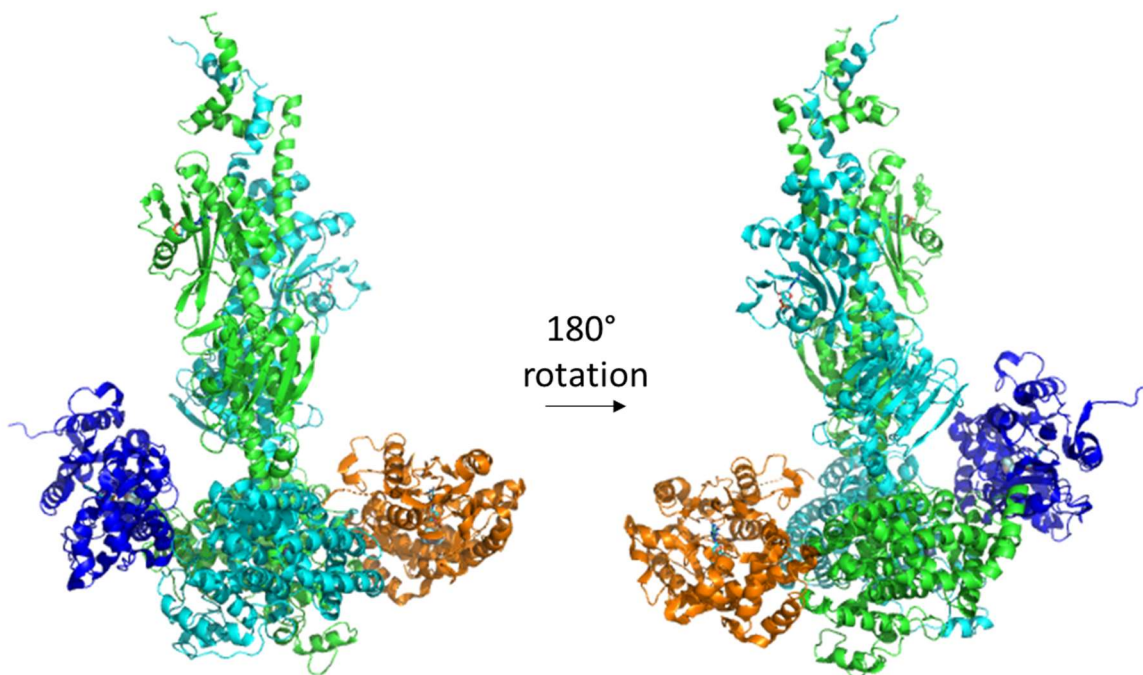
Figure 4-3. Homology model of a 3:1 molar excess of Gtα-GDP-AlF$_4^-$ cross-linked to PDE6. Subunit colors are defined in Fig. 4-2. Homology modeling was performed as described in the Materials and Methods.

Similar to the homology models presented in Irwin et al. (2019), each Gtα has an

interface surface with each of the catalytic subunits (Irwin et al., 2019). Unlike the other

structural models described in this study, the homology models with a molar excess of Gtα-GDP-

AlF$_4^-$ show asymmetry in the two docking sites. The Gtα* on the catalytic face of Pα shows

primary interactions with α12, α14 and the M-loop on the primary catalytic subunit, with

secondary interactions with several α-helical segments on the other catalytic subunit. The Gtα*

that primarily interacts with Pβ also interacts with α14 and the M-loop, but lacks interaction with

α12 and has an additional set of interaction with the Cα1 of Pβ. Additionally, this Gtα* molecule

has secondary interaction with the Pα GAFb domain as well as the helix in the Pα catalytic

domain. A comparison to the model presented in Irwin et al. (2019) shows very similar docking of Gtα* to Pα but significant difference in the docking site of Gtα* to the Pβ catalytic domain (*not shown*).

Gtα-GDP binding to PDE6 interacts primarily with the GAFb domains but with reduced ability to stimulate PDE6 activation

Because we (Fig. 4-1B) and others (Kroll et al., 1989) observed limited activation of PDE6 when Gtα-GDP was present, we investigated the binding sites when sub-stoichiometric amounts of Gtα-GDP were incubated with PDE6.

z	m/z	pep1	aa1	pep2	aa2
4	523.512	Gtα[B]	188	Pα	357
3	915.4196	Gtα[B]	25	Pβ	436
3	916.4271	Gtα[B]	341	Pβ	397
3	832.7147	Gtα[B]	128	Pα	455

Table 4-3. Chemical cross-links of the complex observed between sub-stoichiometric Gtα-GDP and PDE6. Cross-links were identified using the protocol detailed in the Materials and Methods. Abbreviations are defined in Table 4-1.

Cross-links identified under these conditions (Table 4-3) were used to create a homology model, using the previously published structures for Pαβ and Gtα.as initial templates (Irwin et al., 2019). All of the cross-links were consistent with a single binding site located on the Pβ catalytic face of PDE6.
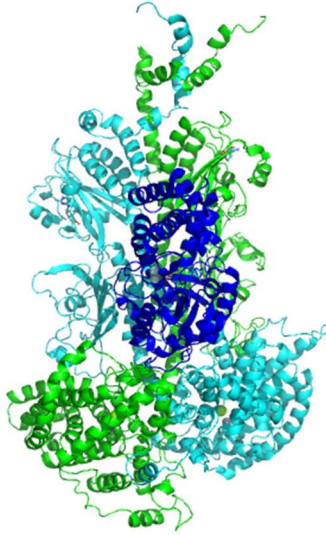
Figure 4-4. Homology model of Gtα-PDE6 interactions with sub-stoichiometric (0.4:1) amounts of Gtα-GDP relative to PDE6. Modeling was performed as described in the Materials and Methods. Subunit colors are as defined in Fig. 4-2.

The cross-linking data for sub-stoichiometric amounts of Gtα-GDP relative to PDE6 resulted in a structural model (Fig. 4-4) in which Gtα is localized to the mid-region of the catalytic dimer on the same surface that interacts with the Pγ subunit associated with Pβ, referred to as the "Pβ catalytic face"). Unlike the situation with activated Gtα*-GDP-AlF$_4^-$, there was no experimental support from the cross-linking data for a second docking site for Gα-GDP on the Pα catalytic face under these sub-stoichiometric conditions. The complex of Gtα-GDP with the Pβ catalytic face has the helical sub-domain of Gtα extending to the GAFa domain of the Pβ subunit, while the ras sub-domain of Gtα is inserted between the Pα GAFb and catalytic domains, with the switch II region of Gtα forming close interactions with the H- and M-loops of the Pβ catalytic domain. This model shows the αN helix of Gtα as the primary site of interaction with sites on both Pα and Pβ (Fig. 4-4). Gtα is in close proximity to GAFb on Pα, with potential interaction sites on the α1 and α2 helices as well as theβ2 strand and the β2/3 loop. The absence of catalytic activation of sub-stoichiometric amounts of Gtα-GDP relative to PDE6 (Fig. 4-1B) suggests that

the Pγ C-terminal region responsible for blocking access to the active site is not being displaced when a single Gtα-GDP binds in this conformation.

When we prepared samples containing a 3-fold excess of Gtα-GDP, we observed a high molecular weight band consistent with two Gtα bound. Analysis of the crosslinks (Table 4-4) led to a structural model for Gtα-GDP binding to both catalytic faces. The structural models for two

z	m/z	pep1	aa1	pep2	aa2
3	601.2801	Gtα	10	Pα/Pβ	636/634
3	611.0082	Gtα	157	Pα/Pβ	726/724
3	915.7612	Gtα^A	102	Pα	442
3	857.442	Gtα^B	206	Pβ	381

Table 4-4. Cross-links identified from the complex consisting of a 3:1 molar excess of Gtα-GDP to PDE6. Cross-links were identified using the protocol detailed in Materials and Methods. Abbreviations are defined in Table 1.

Gtα-GDP bound to Pαβ show nearly symmetrical docking sites on each catalytic face (Fig. 4-5). Both Gtα docking sites show primary interactions with GAFb for both subunits as well as interaction with the catalytic domain with αN of Gtα as the primary interacting region. The primary catalytic subunit has potential interaction at α2 and α5 as well as β5 on GAFb. In addition, there is potentially significant interaction with the long helix (LH2) between GAFb and the catalytic domains. Finally, interactions are predicted between Gtα helical sub-domain and the H-loop as wells as α14, α15 and M-loop on the catalytic domain.

Each Gtα also has multiple interactions with the other catalytic subunit. This interaction surface occurs at α2 and β2, β3, and the β2/3 loop on GAFb. Additionally, there is also potential interaction with α11 on the catalytic domain. In a comparison with previously published structures, this model shows significant similarity to the GAF docked structure published previously [(Irwin et al., 2019); *data not shown*].
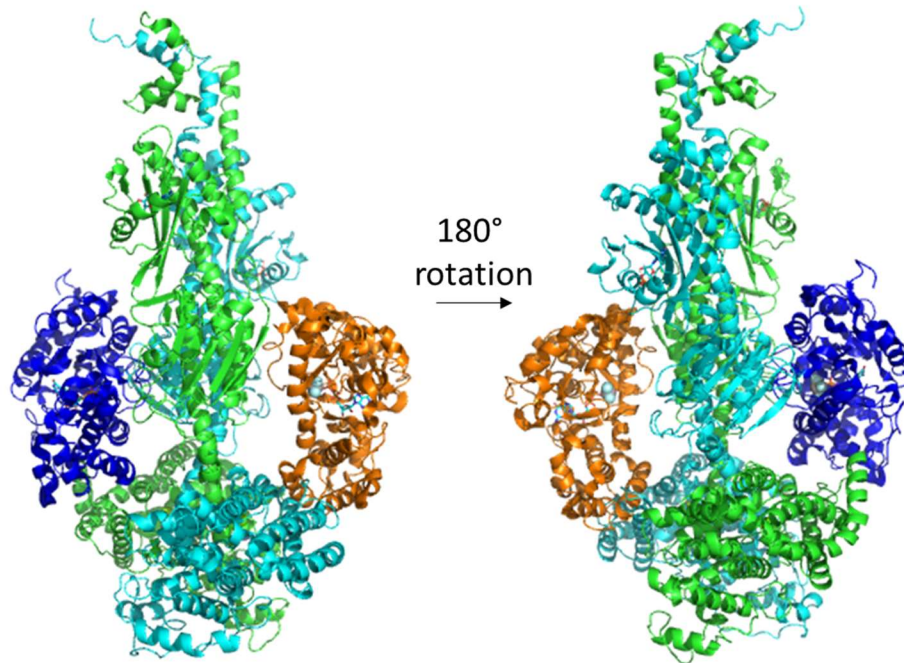
Figure 4-5. Homology model produced from cross-links obtained from a structure containing a 3:1 excess of Gtα-GDP to PDE6. Integrative modeling was performed as described in the materials and methods. Colors of protein subunits are defined in Fig. 4-2.

Discussion

This work provides the first structural models for the Gtα*-PDE6 activation complex in which a stoichiometry of one or two bound Gtα in both its inactive and activated states have been characterized structurally and biochemically. These structural models advance our understanding of the activation mechanism of PDE6 by elucidating the initial interaction site(s) between Gtα* and PDE6 GAFb domains, as well as the interaction sites of activated Gtα* with the PDE6 catalytic domains in its activated state.

The combination of activity measurements along with homology models from crosslinking experiments performed at high, membrane-confined protein concentration represents a significant advance in the mechanism by which Gtα binding to PDE6 leads to its

activation. This work also poses interesting questions with regards to the subsequent mechanism

of deactivation of PDE6. Combining the crosslinking measurements with activity measurements

demonstrates that binding of a single Gtα* to the PDE6 GAFb domains does not lead to

significant catalytic activation. Under conditions where two Gtα* are bound to PDE6,
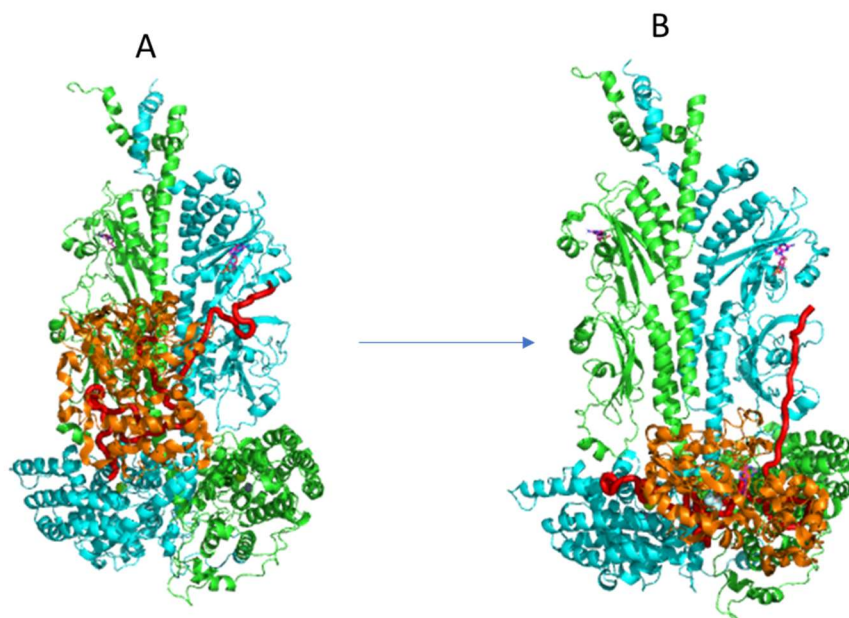
Figure 4-6. Proposed activation mechanism of PDE6 activation by Gtα based on homology models produced by cross-links for complexes with single and doubly bound Gtα*. A single Gtα binds at the GAFb domain but does not relieve Pγ inhibition. Upon the binding of a second Gtα, both migrate to the catalytic domains relieving the inhibition of both Pγ simultaneously. A. The structure of Pγ was placed on the Gtα-GDP-AlF$_4^-$ sub-stoichiometric structure using Figure 2 and the position of the non-activated state (Irwin et al., 2019) and the cross-links between Gtα and Pγ for positions 25-45 (Irwin, 2019). B. The structure of Pγ was placed on the Gtα-GDP-AlF$_4^-$ structure using Figure 3 and the position of the activated state (Irwin et al., 2019) and the cross-links between Gtα and Pγ for positions 25-45 (Irwin et al., 2019).

significant activation of catalysis correlates with both Gtα* molecules being docked with the

catalytic domains of Pαβ.

From these results, we propose an activation model in which the initial site of interaction

of Gtα* is at the GAF domains (Fig. 4-6A). Upon the binding of a second Gtα*, both Gtα*

localize to the catalytic domains resulting in removal of the C-terminus of Pγ and activation of PDE6 catalysis (Fig. 4-6B). The shift in Pγ crosslinking observed in Irwin et al. (2019) suggests that both Gtα* initially interact with PDE6 at the GAF domains and the resulting migration of Gtα* results in the dislocation of Pγ from its interaction sites with the GAFa domain. This proposed displacement of Pγ from GAFa is supported by biochemical studies showing that the affinity of noncatalytic cGMP binding to GAFa is reduced upon Gtα activation of PDE6 (Zhang et al., 2012).

Comparison of the structural model of two Gtα-GDP bound to the GAFb domains (Fig. 4-5), with the limited catalytic activation of PDE6 (Fig. 4-1B) also provides structural insights into the previously observed ability of high concentration of Gtα-GDP to induce limited activation of PDE6 catalysis (Kroll et al, 1989). The limited interaction of Gtα-GDP with the catalytic domains that we observed may be sufficient to weaken the interactions of the Pγ C-terminus with the PDE6 active site without completely displacing Pγ occlusion of substrate access to the active site.

This model also raises interesting questions with regards to the role of the RGS9-1 inactivation complex in accelerating transducin's GTPases activity and leading to the dissociation of Gtα-GDP from its PDE6 binding sites. The ability of Gtα-GDP to bind PDE6 at sub-stoichiometric and stoichiometric amounts of Gtα relative to PDE6 suggests that the deactivation mechanism of PDE6 likely requires active displacement of the Gtα-GDP following hydrolysis of GDP.

In addition, understanding visual signaling on a structural level is essential to understanding disease causing mutations. Irwin et al (2019) reported on sites at the interaction of

PDE6 and Gtα which have been implicated in congenital stationary night blindness, and that

interaction surface was also seen in this work. Being able to distinguish mutations that are likely

interfering at different stages of the activation mechanism will be essential to developing

pharmaceutical regulators of PDE6 aimed at treating retinal diseases.

Chapter 5

ASSEMBLY OF THE PDE6 INACTIVATION COMPLEX ON LIPOSOME-ENCASED SILICA PARTICLE ("LIPOBEAD") SURFACE

Abstract

The deactivation of PDE6 involves binding to a protein complex containing Regulator of G-protein Signaling 9 (RGS9-1) and G-protein β subunit-5 (Gβ5L) anchored to the membrane with the RGS-9 anchoring protein (R9AP). The C-terminal region of Pγ is essential for the interaction of RGS9-1 with the transducin α-subunit (Gtα), the result of which is the inactivation of Gtα and thus PDE6.(Slep et al., 2001; Slepak et al., 1995) To study this inactivation complex, I developed a protocol that integrates R9AP into lipobeads (called "proteolipobeads") which allows for the study of the deactivation complex bound to membranes. My preliminary data demonstrates that proteolipobeads bind to purified RGS9/Gβ5 and are able to bind PDE6 and Gtα. I have also optimized separation of proteins by sodium dodecyl sulfate polyacrylamide gel electrophoresis (SDS-PAGE) to resolve all of the individual proteins and their cross-linked complexes for future determination of the molecular architecture of the PDE inactivation complex.

Introduction

Like all other heterotrimeric G protein α-subunits, the activated Gtα has an intrinsic GTPase activity that hydrolyzes bound GTP to GDP, leading to reassociation with the transducin βγ dimer to re-form the inactive, heterotrimeric G-protein. Since PDE6 activation is directly dependent on association with Gtα-GTP, the lifetime of PDE6 activation is dictated by the GTPase rate of Gtα. However, the intrinsic rate of GTP hydrolysis by transducin α-subunit is too slow by ~100-fold to control signal termination of the photoresponse (Arshavsky & Pugh, 1998),

and this observation led to evidence for the existence of a GTPase accelerating protein (GAP) (Arshavsky et al., 1989; Arshavsky & Pugh, 1998)

The GAP responsible for transducin regulation during the visual signaling pathway consists of a complex of three proteins, RGS9-1, its obligate binding partner Gβ5L, and the integral membrane anchoring protein R9AP (Hu & Wensel, 2002). R9AP is a transmembrane protein that enhances the ability of RGS9-1/Gβ5 to inactivate Gtα by increasing the rate of GTP hydrolysis (Baker et al., 2006; Hu & Wensel, 2002; Lishko et al., 2002) and also protects RGS9-1/ Gβ5L from intracellular proteolysis [Figure 5-1 (Cote, 2021) (Keresztes et al., 2004; Krispel et al., 2006)].
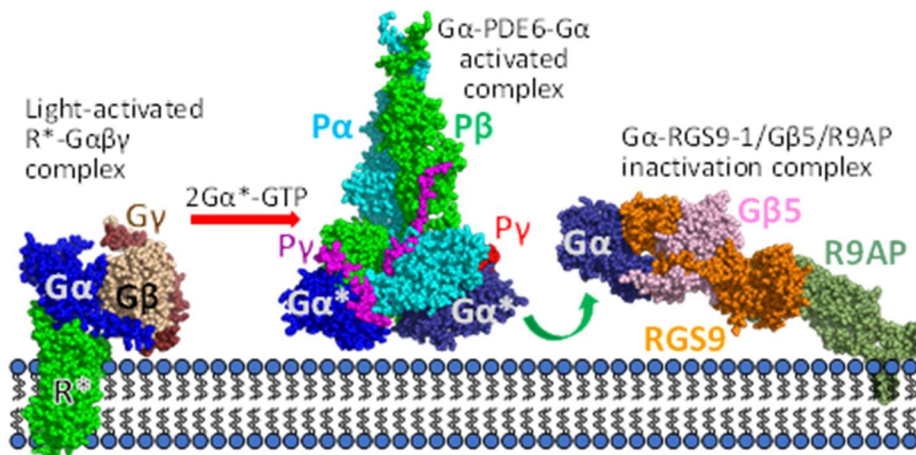
Figure 5-1. Model of the inactivation mechanism presented in Cote 2021.

Under most conditions, the rate-limiting step for recovery of the photoresponse in rod and cone photoreceptors is the inactivation of the Gα-PDE activated state that is regulated by RGS9-1 and its binding partners. RGS9-1 is a photoreceptor-specific splice variant of the R7 subfamily of RGS proteins(Anderson et al., 2009) . The RGS9-1 domain organization (Fig. 5-1) consists of an RGS catalytic domain (responsible for its GAP activity), a G protein γ-like (GGL) domain

that interacts with the Gβ5L protein (a member of the G protein β-subunit family), and the N-terminal DEP (Dishevelled, Egl10, Pleckstrin) and DEP helical extension (DHEX) domains(Cheever et al., 2008). The DEP domain is believed to interact with R9AP. The PDE6 Pγ subunit is known to potentiate the intrinsic GAP activity of RGS9-1, with enhancement of GAP activity occurring when Gα is reconstituted with the entire RGS9-1/Gβ5 heterodimer (Cheever et al., 2008). Binding of R9AP to RGS9-1/Gβ5 is reported to further enhance GAP activity by a distinct mechanism (Cheever et al., 2008). In addition, reversible phosphorylation of RGS9-1 near its C-terminus and/or other light-dependent reactions have been suggested to influence R9AP binding affinity and/or potentiation of GAP (Patil et al., 2018).

The molecular architecture of the RGS9-1 heterotrimer has not been reported, and little is known about the conformational changes that regulate the GAP activity of RGS9-1 upon binding to the activated Gα-PDE6 complex. The fact that the maximum GAP activity of the RGS9-1 heterotrimer is greatly enhanced when R9AP is membrane anchored suggests that the structural model of the lipobeads-attached RGS9-1 heterotrimer complexed with activated Gα-Pγ will provide novel insights when compared to previously reported solution structures (Slep et al., 2001).

Materials and Methods

Recombinant protein expression and purification of RGS9-1, Gβ5L, and R9AP.

Mouse RGS9-1 and Gβ5L were co-expressed in the baculovirus expression system as described by Skiba et al. (Skiba et al., 2001).Briefly, SF9 cells were grown to a density of 1-2 x 10^6 cells/mL in SF900 II SFM media (Thermo Fisher) containing 0.1% Pluronic, 2% fetal bovine serum, and 50 µg/mL gentamicin at 27°C. Cells were co-infected with recombinant baculovirus for RGS9-1 and Gβ5L (a gift from Dr. Kirill Martemyanov) at a multiplicity of infection of 3,

harvested after 72 h and the cell pellet stored at -80°C until use. Cell pellets were resuspended in

20 mM Tris-HCl (pH. 8.0), 150 mM NaCl, and mammalian protease inhibitor cocktail (Millipore

Sigma) and sonicated for 10 sec followed by 40 sec of incubation on ice for a total of 5 cycles.

Following centrifugation (100,000 x g for 1 h) the supernatants were loaded onto a 1 mL Ni^{2+}-

NTA affinity column. After washing the column with the isolation buffer containing 20 mM

imidazole, the RGS9-1/Gβ5L dimer was eluted with a linear gradient of 20 to 500 mM

imidazole. The pooled protein was buffer-exchanged and then added to a Mono S column

(Cytiva) and eluted with a 0.1 to 0.4 M NaCl gradient. The purified RGS9-1/Gβ5L dimer was

stored at -20° C in the isolation buffer containing 40% glycerol (Fig. 5-2).
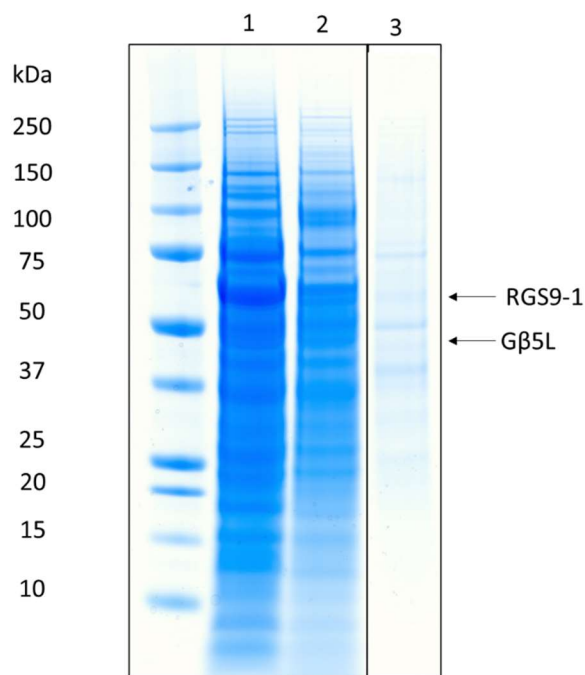
Figure 5-2. Purification of RGS-1/Gβ5L. Purification performed as described in Materials and Methods. Lane 1 pooled NiNTA purified RGS9-1/Gβ5L. Lane 2 pooled MonoS purified

The coding sequence for mouse R9AP was subcloned into the pET47b vector containing

a 6-histidine tag and transformed into *Escherichia coli* BL21/DE3 cells. Expression and affinity

purification of R9AP closely followed Hu and Wensel (Hu & Wensel, 2004). Affinity-purified

R9AP was further purified by Superdex 200 chromatography with the mobile phase consisting of

300 mM NaCl, 25 mM Tris (pH 8.0), 2 mM dithiothreitol, and 4% sodium cholate (Fig. 5-3).
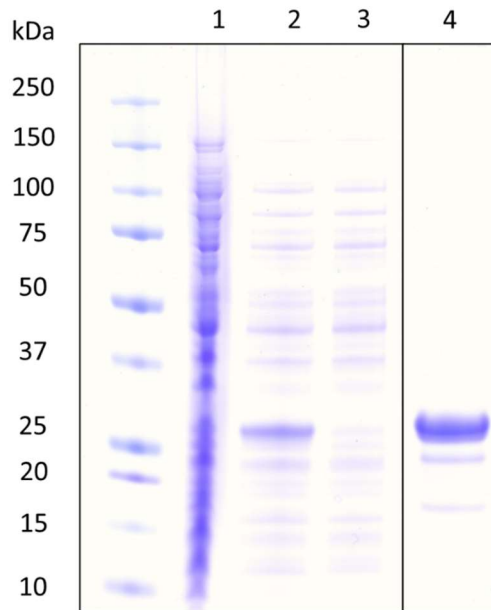
Figure 5-3. Purification of R9AP. Purification performed as described in Materials and Methods. Lane 1 detergent extracted R9AP. Lane 2 Ni-NTA elution sample. Lane 3 Ni-NTA unbound sample. Lane 4 Superdex 200 gel filtration chromatography peak (pooled and

Preparation of R9AP-containing proteolipobeads.

To incorporate R9AP into the phospholipid bilayer of lipobeads,

22 pmol of lipobeads were resuspended in 200 µl of 40 µM R9AP in the buffer used for R9AP

isolation. The mixture of R9AP and lipobeads were incubated with gentle mixing for 4 h at 4° C,

and then diluted to 1 ml with R9AP isolation buffer lacking sodium cholate. Following overnight

incubation with gentle mixing, the proteolipobeads were centrifuged at 10,000 x g for 10 min.

The R9AP-containing proteolipobead pellet was then stored at -80° C until use.

Protein binding to lipobeads and proteolipobeads.

R9AP proteolipobeads were resuspended in HMN buffer containing equimolar amounts of the RGS9-1/Gβ5L obligate dimer and incubated for 15 min prior to centrifugation. Unbound protein was discarded and the proteolipobead pellet containing the R9AP/RGS9-1/Gβ5L heterotrimer was resuspended in HMN buffer.

To reconstitute the entire inactivation complex, the inactivation timer was prepared as described above. PDE6 and Gtα were then bound as described previously (Irwin et al., 2019). Briefly, PDE6 was incubated with the proteolipobeads for 30 minutes followed by centrifugation at 10,000 x g for 10 minutes. The protein containing pellets were then resuspended in 40μL of HNM buffer containing the relevant concentration of Gtα.

Evaluation of protein-protein interactions on lipobeads by chemical cross-linking and SDS-PAGE.

For chemical cross-linking experiments with proteolipobeads, we minimized the sample volume by incubating 10 µl of lipobeads (1.1 pmol) with RGS9-1/Gβ5L for 30 min prior to centrifugation. The proteolipobead pellet was then resuspended in 25μL HNM buffer containing a 25-fold molar excess of bis(sulfosuccinimidyl)suberate (BS3) to R9AP. The reaction was allowed to proceed for 1 hour at room temperature and quenched by the addition of 1x gel sample buffer.

Results and Discussion

Proteolipobeads containing the anchoring protein R9AP permit reconstitution of the RGS9-1 inactivation complex

To enable studies of the proteins that form the RGS9-1 inactivation complex on outer segment membranes, we first incubated detergent-solubilized R9AP (an integral membrane

protein) with lipobeads to incorporate R9AP into the phospholipid bilayer to

form proteolipobeads (see Materials and Methods). Unlike standard liposomal preparations

where incorporation of integral membrane proteins into lipid bilayers can result a portion of

the proteins incorrectly oriented in the membrane, the characteristics of

our lipobead preparations (70 nm silica core, ~100 nm total diameter of the bilayer) enhanced the

likelihood that R9AP would insert into the lipobeads with its cytoplasmic domain facing outward

on the exterior of the proteolipobead. The difference between the inner diameter of the liposome

and the outer diameter of the silica particle does not allow for sufficient space within the

proteolipobead to accommodate inverse R9AP anchoring. Additionally, the liposomes are not

fully solubilized, and thus only the transmembrane segment of R9AP is likely to pass through the

semi-permeable membrane.

Fig. 5-4 shows that R9AP can be incorporated into lipobeads (lane A), and that the

resulting proteolipobeads can pull-down the obligate dimer of RGS9-1 and Gβ5L (lane B). Note

that a minor fraction of R9AP running at a MW consistent with dimer formation is also

observed. Lane C shows both PDE6 and Gtα can also be pulled down in the presence of the

RGS9-1/Gβ5L/R9AP heterotrimer.
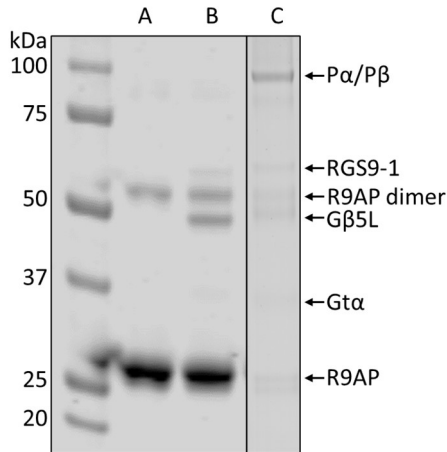
Figure 5-4. R9AP proteolipobeads pulldown assay with RGS9-1/Gβ5L, Gtα, and PDE6.
A. R9AP proteolipobeads. B. R9AP proteolipobeads incubated with RGS9-1/Gβ5L. C. R9AP proteolipobeasds with RGS9-1/Gβ5L, PDE6, and Gtα.

Upon incubation of the proteolipobead inactivation complex with the bifunctional cross-

linker BS3, higher MW species are observed (Fig. 5-5) consistent with the formation of the

RGS9-1/Gβ5L dimer and the heterotrimer that also contains R9AP. Excision

and proteomic analysis of the indicated Coosmassie-stained bands confirmed the composition of

each protein band on the gel.
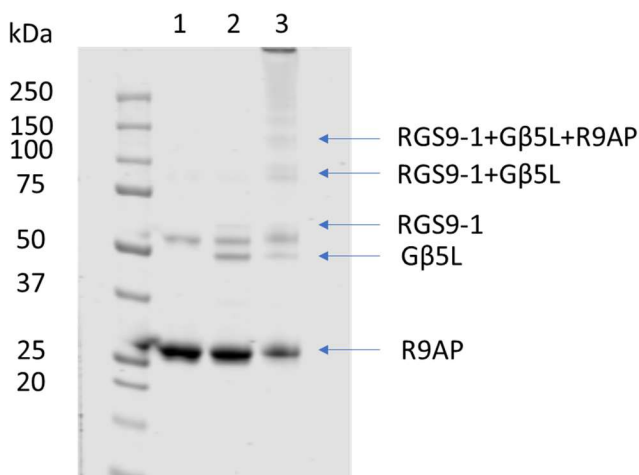
Figure 5-5. Crosslinking of the inactivation complex. Lane 1: R9AP proteolipobeads. Lane 2: R9AP, RGS9-1/Gβ5L pulldown. Lane 3 Crosslinking of R9AP with RGS9-1/Gβ5L with a 25-fold molar excess of BS3 to R9AP.

Conclusions

This work provides the foundation and proof-of-principle for use of XL-MS to study the PDE6 inactivation complex. We have determined that the existing lipobead protocol (see Chapter 2) can be adapted to create stable R9AP-containing proteolipobeads. Theses proteolipobeads have been shown to anchor RGS9-1/Gβ5L, as well as binding the peripheral membrane proteins PDE6 and Gtα. Our preliminary cross-linking results also demonstrates that the inactivation complex is forming on the proteolipobeads, with upper molecular weight bands identified consistent with the sizes of crosslinked complexes expected from the inactivation complex. Future work will be required to optimize the protocols as well as to ensure the proteolipobeads are not having unexpected effects on the established protein-protein interactions on lipobeads.

Chapter 6

Conclusions and Future Work

Conclusions

Chemical cross-linking and mass spectrometry analysis of PDE6 has allowed the structure of the PDE6 holoenzyme bound to lipobeads to be determined. Of particular note, this methodology enabled docking of the full-length Pγ structure which was not completely resolved by other structural models. The structure of the PDE6 heterotrimer shows the expected interaction of Pγ with the GAFa as well as the catalytic domain, but also showed the central region of Pγ to be very disordered and loosely associated with the GAFb and catalytic domains of rod PDE6 catalytic dimer. This structure was then used as the basis for docking of the activated G-protein α-subunit (Gtα). Our original model showed two distinct sets of docking sites, one to GAFb and a second set to the catalytic domains. Our proposed sequential docking mechanism involves Gtα first binding to the central region of Pγ located in proximity to the GAFb domain, followed by binding of the original as well as a second Gtα subunit to the catalytic domains, thereby relieving Pγ inhibition at both catalytic sites (Irwin et al., 2019).

This model was further strengthened by analysis of PDE6 with Gtα at near stoichiometric and substiochiometric levels (3:1 and 0.4:1 respectively). Cross-links produced from the sub-stoichiometric condition using Gtα-GDP-AlF$_4^-$ identified a Gtα binding to either GAFb docking sites of PDE6; activity measurements under similar conditions to the cross-linking experiments indicated very little PDE6 activity with sub-stoichiometric amounts of Gtα per PDE6. Upon addition of a slight excess of Gtα relative to PDE6, two Gtα were found to bind to the catalytic domains accompanied by PDE6 catalytic activation. This work represents the most detailed

analysis to date of the sequential mechanism for transducin activation of PDE6 (Chapter 3, manuscript in preparation).

The lipobead preparation detailed in chapter 2 has allowed for the completion of cross-linking and PDE6 activity experiments at near physiological concentrations, allowing for use of stoichiometric and sub-stoichiometric amounts of Gtα PDE6 where previously a large excess was required. Additionally, the ability to prepare R9AP embedded in lipobeads ("proteolipobeads") provides a strong foundation for future studies of the molecular architecture and sequential mechanism of the RGS9 inactivation complex. R9AP-containing proteolipobeads have been shown to bind RGS9-1/Gβ5L to form the trimeric complex, as confirmed by preliminary chemical cross-linking experiments. The R9AP proteolipobeads were also able to bind PDE6 and Gtα, thus demonstrating "proof of principle" for future studies of the protein complex that controls the rate of recovery of the photoresponse in rod photoreceptors.

Future Work

Future work for the analysis of the activation complex will require new techniques in order to understand the dynamic movement of proteins (especially the intrinsically disorder Pγ subunit) during formation of the PDE6 activation and inactivation complexes. For example, hydrogen deuterium exchange with mass spectrometry analysis (HDX-MS) will allow analysis of the protein dynamics occurring during the activation of PDE6, which will elucidate the movements of Pγ upon Gtα binding and catalytic activation of PDE6. Elucidation of the movement of Pγ and the orientation of Pγ during each of the states previously developed is essential to enhancing our understanding of the PDE6 activation mechanism.

In order to determine the structure of the inactivation complex, our current chemical cross-linking coupled with LC-MS (XL-MS) will provide the first structural analysis of this assemblage of PDE6, Gtα, and the heterotrimeric RGS9-1/Gβ5L/R9AP. This experimental approach will provide a strong framework for follow-up studies of the protein dynamics and subunit rearrangements that accompanies the inactivation of Gtα and the subsequent re-inhibition of PDE6 catalysis.

LIST OF REFERENCES

Akbar, S., Mozumder, S., & Sengupta, J. (2020). Retrospect and Prospect of Single Particle Cryo-Electron Microscopy: The Class of Integral Membrane Proteins as an Example. *Journal of Chemical Information and Modeling*, *60*(5), 2448–2457. https://doi.org/10.1021/acs.jcim.9b01015

Alkhammash, H. I., Li, N., Berthier, R., & De Planque, M. R. R. (2015). Native silica nanoparticles are powerful membrane disruptors. *Physical Chemistry Chemical Physics*, *17*(24), 15547–15560. https://doi.org/10.1039/c4cp05882h

Ames, J. B., & Lim, S. (2012). Molecular structure and target recognition of neuronal calcium sensor proteins. *Biochimica et Biophysica Acta*, *1820*, 1205–1213. https://doi.org/doi: 10.1016/j.bbagen.2011.10.003

Anant, J. S., Ong, O. C., Xie, H. Y., Clarke, S., O'Brien, P. J., & Fung, B. K. (1992). In vivo differential prenylation of retinal cyclic GMP phosphodiesterase catalytic subunits. *Journal of Biological Chemistry*, *267*, 687–690. https://doi.org/https://doi.org/10.1016/S0021-9258(18)48336-6

Anderson, G. R., Posokhova, E., & Martemyanov, K. a. (2009). The R7 RGS protein family: Multi-subunit regulators of neuronal G protein signaling. *Cell Biochemistry and Biophysics*, *54*(1–3), 33–46. https://doi.org/10.1007/s12013-009-9052-9

Arshavsky, V Y, Lamb, T. D., & Pugh, E. N. (2002). G proteins and phototransduction. *Annual Review Physiology*, *64*, 153–187. https://doi.org/10.1146/annurev.physiol.64.082701.102229

Arshavsky, V Y, & Wensel, T. G. (2013). Timing is everything: GTPase regulation in

phototransduction. *Investigative Ophthalmology & Visual Science*, *54*(12), 7725–7733.

https://doi.org/10.1167/iovs.13-13281

Arshavsky, Vadim Y., Antoch, M. P., Lukjanov, K. A., & Philippov, P. P. (1989). Transducin

GTPase provides for rapid quenching of the cGMP cascade in rod outer segments. *FEBS

Letters*, *250*, 353–356.

Arshavsky, Vadim Y., & Burns, M. E. (2012). Photoreceptor signaling: Supporting vision across

a wide range of light intensities. *Journal of Biological Chemistry*, *287*(3), 1620–1626.

https://doi.org/10.1074/jbc.R111.305243

Arshavsky, Vadim Y., & Pugh, E. N. (1998). Lifetime regulation of G protein-effector complex:

Emerging importance of RGS proteins. *Neuron*, *20*(1), 11–14.

https://doi.org/10.1016/S0896-6273(00)80430-4

Artemyev, N O, & Hamm, H. E. (1992). Two-site high-affinity interaction between inhibitory

and catalytic subunits of rod cyclic GMP phosphodiesterase. *Biochemical Journal*, *283*,

273–279. https://doi.org/10.1042/bj2830273

Artemyev, N O, Mills, J. S., Thornburg, K. R., Knapp, D. R., Schey, K. L., & Hamm, H. E.

(1993). A site on transducin alpha-subunit of interaction with the polycationic region of

cGMP phosphodiesterase inhibitory subunit. *Journal of Biological Chemistry*, *268*, 23611–

23615.

Artemyev, Nikolai O., Arshavsky, V. Y., & Cote, R. H. (1998). Photoreceptor

phosphodiesterase: Interaction of inhibitory γ subunit and cyclic GMP with specific binding

sites on catalytic subunits. *Methods: A Companion to Methods in Enzymology*, *14*(1), 93–104. https://doi.org/10.1006/meth.1997.0568

Baehr, W., Devlin, M. J., & Applebury, M. L. (1979). Isolation and characterization of cGMP phosphodiesterase from bovine rod outer segments. *Journal of Biological Chemistry*, *254*(22), 11669–11677. https://doi.org/10.1016/s0021-9258(19)86536-5

Baillie, G. S., Tejeda, G. S., & Kelly, M. P. (2019). Therapeutic targeting of 3′,5′-cyclic nucleotide phosphodiesterases: inhibition and beyond. *Nature Reviews Drug Discovery*, *18*(10), 770–796. https://doi.org/10.1038/s41573-019-0033-4

Baker, S. A., Martemyanov, K. A., Shavkunov, A. S., & Arshavsky, V. Y. (2006). Kinetic mechanism of RGS9-1 potentiation by R9AP. *Biochemistry*, *45*, 10690–10697. https://doi.org/https://doi.org/10.1021/bi060376a

Barren, B, Gakhar, L., Muradov, H., Boyd, K. K., Ramaswamy, S., & Artemyev, N. O. (2009). Structural basis of phosphodiesterase 6 inhibition by the C-terminal region of the gamma-subunit. *The EMBO Journal*, *28*, 3613–3622. https://doi.org/10.1038/emboj.2009.284

Barren, Brandy, Gakhar, L., Muradov, H., Boyd, K. K., Ramaswamy, S., & Artemyev, N. O. (2009). Structural basis of phosphodiesterase 6 inhibition by the C-terminal region of the γ-subunit. *EMBO Journal*, *28*(22), 3613–3622. https://doi.org/10.1038/emboj.2009.284

Bender, A. T., & Beavo, J. A. (2006). Cyclic nucleotide phosphodiesterases: Molecular regulation to clinical use. *Pharmacological Reviews*, *58*(3), 488–520. https://doi.org/10.1124/pr.58.3.5

Bennett, N., & Clerc, A. (1989). Activation of cGMP phosphodiesterase in retinal rods:

mechanism of interaction with the GTP-binding protein (transducin). *Biochemistry*, *28*, 7418–7424.

Bigay, J., Deterre, P., Pfister, C., & Chabre, M. (1985). Fluoroaluminates activate transducin-GDP by mimicking the γ-phosphate of GTP in its binding site. *FEBS Letters*, *191*(2), 181–185. https://doi.org/10.1016/0014-5793(85)80004-1

Burgoyne, R. D., & Haynes, L. P. (2012). Understanding the physiological roles of the neuronal calcium sensor proteins. *Molecular Brain*, *5*, 2.

Calvert, P. D., Strissel, K. J., Schiesser, W. E., Pugh, E. N., & Arshavsky, V. Y. (2006). Light-driven translocation of signaling proteins in vertebrate photoreceptors. *Trends in Cell Biology*, *16*(11), 560–568. https://doi.org/10.1016/j.tcb.2006.09.001

Cheever, M. L., Snyder, J. T., Gershburg, S., Siderovski, D. P., Harden, T. K., & Sondek, J. (2008a). Crystal structure of the multifunctional Gbeta5-RGS9 complex. *Nature Structure & Molecular Biolology*, *15*(2), 155–162. https://doi.org/10.1038/nsmb.1377

Cheever, M. L., Snyder, J. T., Gershburg, S., Siderovski, D. P., Harden, T. K., & Sondek, J. (2008b). Crystal structure of the multifunctional Gβ5-RGS9 complex. *Nature Structural and Molecular Biology*, *15*(2), 155–162. https://doi.org/10.1038/nsmb.1377

Chemburu, S., Fenton, K., Lopez, G. P., & Zeineldin, R. (2010). Biomimetic silica microspheres in biosensing. *Molecules*, *15*(3), 1932–1957. https://doi.org/10.3390/molecules15031932

Chen, C. K., Inglese, J., Lefkowitz, R. J., & Hurley, J. B. (1995). Ca(2+)-dependent interaction of recoverin with rhodopsin kinase. *Journal of Biological Chemistry*, *270*, 18060–18066.

Chen, C. K., Zhang, K., Church-Kopish, J., Huang, W., Zhang, H., Chen, Y. J., Frederick, J. M.,

& Baehr, W. (2001). Characterization of human GRK7 as a potential cone opsin kinase. *Molecular Vision*, *7*, 305–313.

Chu, F, Hogan, D., Gupta, R., Gao, X. Z., Nguyen, H. T., & Cote, R. H. (2019). Allosteric regulation of rod photoreceptor phosphodiesterase 6 (PDE6) elucidated by chemical cross-linking and quantitative mass spectrometry. *Journal of Mo*, *243*(19), 3677–3689. https://doi.org/10.1016/j.jmb.2019.07.035

Chu, Feixia, Baker, P. R., Burlingame, A. L., & Chalkley, R. J. (2010). Finding chimeras: A bioinformatics strategy for identification of cross-linked peptides. *Molecular and Cellular Proteomics*, *9*(1), 25–31. https://doi.org/10.1074/mcp.M800555-MCP200

Chu, Feixia, Thornton, D. T., & Nguyen, H. T. (2018). Chemical cross-linking in the structural analysis of protein assemblies. *Methods*, *144*(March), 53–63. https://doi.org/10.1016/j.ymeth.2018.05.023

Cote, R H. (2000). Kinetics and regulation of cGMP binding to noncatalytic binding sites on photoreceptor phosphodiesterase. *Methods in Enzymology*, *315*, 646–672. https://doi.org/10.1016/s0076-6879(00)15873-2

Cote, R H. (2006). Photoreceptor Phosphodiesterase (PDE6): A G-Protein-Activated PDE Regulating Visual Excitation in Rod and Cone Photoreceptor Cells. In J. A. Beavo, S. H. Francis, & M. D. Houslay (Eds.), *Cyclic Nucleotide Phosphodiesterases in Health and Disease* (pp. 165–193). CRC Press.

Cote, Rick H. (2021). Photoreceptor phosphodiesterase (PDE6): activation and inactivation mechanisms during visual transduction in rods and cones. *Pflugers Archiv European*

Journal of Physiology, *473*(9), 1377–1391. https://doi.org/10.1007/s00424-021-02562-x

Cote, Rick H., Bownds, M. D., & Arshavsky, V. Y. (1994). cGMP binding sites on photoreceptor phosphodiesterase: Role in feedback regulation of visual transduction. *Proceedings of the National Academy of Sciences of the United States of America*, *91*(11), 4845–4849. https://doi.org/10.1073/pnas.91.11.4845

Cote, Rick H. (2006). Regulating Visual Excitation. *Cyclic Nucleotide Phosphodiesterases in Health and Disease*, *2*, 165–194.

Cote, Rick H, Gupta, R., Irwin, M. J., & Wang, X. (2021). Photoreceptor Phosphodiesterase (PDE6): Structure , Regulatory Mechanisms , and Implications for Treatment of Retinal Diseases. *Advances in Experimental Medicine and Biology*. https://doi.org/10.1007/5584_2021_649

Crites, T. J., Maddox, M., Padhan, K., Muller, J., Eigsti, C., & Varma, R. (2015). Supported Lipid Bilayer Technology for the Study of Cellular Interfaces. In *Current Protocols in Cell Biology* (Vol. 68, Issue 1). https://doi.org/10.1002/0471143030.cb2405s68

Deterre, P., Bigay, J., Robert, M., Pfister, C., Kühn, H., & Chabre, M. (1986). Activation of retinal rod cyclic GMP-phosphodiesterase by transducin: Characterization of the complex formed by phosphodiesterase inhibitor and transducin α-subunit. *Proteins: Structure, Function, and Bioinformatics*, *1*(2), 188–193. https://doi.org/10.1002/prot.340010210

Dryja, T. P. (2000). Molecular genetics of Oguchi disease, fundus albipunctatus, and other forms of stationary night blindness: LVII Edward Jackson Memorial Lecture. *American Journal Ophthalmology*, *130*, 547–563. https://doi.org/https://doi.org/10.1016/S0002-

9394(00)00737-6

Edward Zhou, X., Melcher, K., & Eric Xu, H. (2019). Structural biology of G protein-coupled receptor signaling complexes. *Protein Science*, *28*(3), 487–501. https://doi.org/10.1002/pro.3526

Emsley, P., Lohkamp, B., Scott, W. G., & Cowtan, K. (2010). Features and development of Coot. *Acta Crystallographica Section D: Biological Crystallography*, *66*(4), 486–501. https://doi.org/10.1107/S0907444910007493

Francis, S. H., Blount, M. A., & Corbin, J. D. (2011). Mammalian cyclic nucleotide phosphodiesterases: Molecular mechanisms and physiological functions. *Physiological Reviews*, *91*(2), 651–690. https://doi.org/10.1152/physrev.00030.2010

Fung, B. K. K. (1983). Characterization of transducin from bovine retinal rod outer segments. Mechanism and effects of cholera toxin-catalyzed ADP-ribosylation. *Journal of Biological Chemistry*, *259*(10), 6686–6693. https://doi.org/10.1016/s0021-9258(20)82197-8

Gao, Y, Eskici, G., Ramachandran, S., Poitevin, F., Seven, A. B., Panova, O., Skiniotis, G., & Cerione, R. A. (2020). Structure of the visual signaling complex between transducin and phosphodiesterase 6. *Molecular Cell*, *80*(2), 237–245. https://doi.org/10.1016/j.molcel.2020.09.013

Gao, Y, Hu, H., Ramachandran, S., Erickson, J. W., Cerione, R. A., & Skiniotis, G. (2019). Structures of the rhodopsin-transducin complex: insights into G-protein activation. *Mol Cell*, *75*(4), 781–790. https://doi.org/10.1016/j.molcel.2019.06.007

Gao, Yang, Westfield, G., Erickson, J. W., Cerione, R. A., Skiniotis, G., & Ramachandran, S.

(2017). Isolation & structure-function characterization of a signaling-Active rhodopsin-G protein complex. *Journal of Biological Chemistry*, *292*(34), 14280–14289. https://doi.org/10.1074/jbc.M117.797100

Gillespie, P. G., Prusti, R. K., Apel, E. D., & Beavo, J. A. (1989). A soluble form of bovine rod photoreceptor phosphodiesterase has a novel 15-kDa subunit. *Journal of Biological Chemistry*, *264*, 12187–12193.

Granovsky, A. E., & Artemyev, N. O. (2001). A conformational switch in the inhibitory γ-subunit of PDE6 upon enzyme activation by transducin. *Biochemistry*, *40*(44), 13209–13215. https://doi.org/10.1021/bi011127j

Granovsky, A E, Natochin, M., & Artemyev, N. O. (1997). The gamma subunit of rod cGMP-phosphodiesterase blocks the enzyme catalytic site. *Journal of Biological Chemistry*, *272*, 11686–11689.

Granovsky, Alexey E, Natochin, M., & Artemyev, N. O. (1997). Phosphodiesterase Blocks the Enzyme Catalytic Site *. *Biochemistry*, 11686–11689.

Grant, J. E., Guo, L. W., Vestling, M. M., Martemyanov, K. A., Arshavsky, V. Y., & Ruoho, A. E. (2006). The N terminus of GTPγS-activated transducin α-subunit interacts with the C terminus of the cGMP phosphodiesterase γ-subunit. *Journal of Biological Chemistry*, *281*(10), 6194–6202. https://doi.org/10.1074/jbc.M509511200

Granzin, J., Wilden, U., Choe, H. W., Labahn, J., Krafft, B., & Buldt, G. (1998). X-ray crystal structure of arrestin from bovine rod outer segments. *Nature*, *391*, 918–921.

Gray-Keller, M. P., Biernbaum, M. S., & Bownds, M. D. (1990). Transducin activation in

electropermeabilized frog rod outer segments is highly amplified, and a portion equivalent to phosphodiesterase remains membrane-bound. *Journal of Biological Chemistry*, *265*, 15323–15332.

Gulati, S., Palczewski, K., Engel, A., Stahlberg, H., & Kovacik, L. (2019). Cryo-EM structure of phosphodiesterase 6 reveals insights into the allosteric regulation of type I phosphodiesterases. *Science Advances*, *5*(2), eaav4322. https://doi.org/10.1126/sciadv.aav4322

Guo, L.-W. W., & Ruoho, A. E. (2008). The Retinal cGMP Phosphodiesterase γ-Subunit — A Chameleon. *Current Protein & Peptide Science*, *9*(6), 611–625. https://doi.org/10.2174/138920308786733930

Guo, L. W., Grant, J. E., Hajipour, A. R., Muradov, H., Arbabian, M., Artemyev, N. O., & Ruoho, A. E. (2005). Asymmetric interaction between rod cyclic GMP phosphodiesterase gamma subunits and alphabeta subunits. *J Biol Chem*, *280*, 12585–12592.

Guo, L. W., & Ruoho, A. E. (2008). The retinal cGMP phosphodiesterase gamma-subunit - a chameleon. *Curr Protein Pept Sci*, *9*, 611–625.

Gupta, R., Liu, Y., Wang, H., Nordyke, C. T., Puterbaugh, R. Z., Cui, W., Varga, K., Chu, F., Ke, H., Vashisth, H., & Cote, R. H. (2020). Structural analysis of the regulatory GAF domains of cGMP phosphodiesterase elucidates the allosteric communication pathway. *J Mol Biol*, *432*(21), 5765–5783. https://doi.org/10.1016/j.jmb.2020.08.026

Gurevich, V. V, & Benovic, J. L. (1995). Visual arrestin binding to rhodopsin. Diverse functional roles of positively charged residues within the phosphorylation-recognition

region of arrestin. *Journal of Biological Chemistry*, *270*, 6010–6016.
https://doi.org/10.1074/jbc.270.11.6010

Gurevich, V. V, & Benovic, J. L. (1997). Mechanism of phosphorylation-recognition by visual
arrestin and the transition of arrestin into a high affinity binding state. *Mol Pharmacol*, *51*,
161–169.

Hanson, S. M., Cleghorn, W. M., Francis, D. J., Vishnivetskiy, S. A., Raman, D., Song, X., Nair,
K. S., Slepak, V. Z., Klug, C. S., & Gurevich, V. V. (2007). Arrestin mobilizes signaling
proteins to the cytoskeleton and redirects their activity. *Journal of Molecular Biology*, *368*,
375–387. https://doi.org/10.1016/j.jmb.2007.02.053

Hanson, S. M., Gurevich, E. V, Vishnivetskiy, S. A., Ahmed, M. R., Song, X., & Gurevich, V.
V. (2007). Each rhodopsin molecule binds its own arrestin. *Proceedings of the National
Academy of Sciences of the United States of America*, *104*, 3125–3128.
https://doi.org/https://doi.org/10.1073/pnas.0610886104

Hanson, S. M., Van Eps, N., Francis, D. J., Altenbach, C., Vishnivetskiy, S. A., Arshavsky, V.
Y., Klug, C. S., Hubbell, W. L., & Gurevich, V. V. (2007). Structure and function of the
visual arrestin oligomer. *The EMBO Journal*, *26*, 1726–1736.
https://doi.org/10.1038/sj.emboj.7601614

Hirsch, J. A., Schubert, C., Gurevich, V. V, & Sigler, P. B. (1999). The 2.8 A crystal structure of
visual arrestin: a model for arrestin's regulation. *Cell*, *97*, 257–269.
https://doi.org/10.1016/s0092-8674(00)80735-7

Horner, T. J., Osawa, S., Schaller, M. D., & Weiss, E. R. (2005). Phosphorylation of GRK1 and

GRK7 by cAMP-dependent protein kinase attenuates their enzymatic activities. *Journal of Biological Chemistry*, *280*, 28241–28250. https://doi.org/10.1074/jbc.M505117200

Hu, G., & Wensel, T. G. (2002). R9AP, a membrane anchor for the photoreceptor GTPase accelerating protein, RGS9-1. *Proceedings of the National Academy of Sciences of the United States of America*, *99*(15), 9755–9760. https://doi.org/10.1073/pnas.152094799

Hu, G., & Wensel, T. G. (2004). Characterization of R9AP, a membrane anchor for the photoreceptor GTPase-accelerating protein, RGS9-1. *Methods in Enzymology*, *390*, 178–196. https://doi.org/10.1016/S0076-6879(04)90012-2

Humphrey, W., Dalke, A., & Schulten, K. (1996). VMD: Visual molecular dynamics. *Journal of Molecular Graphics*, *14*(1), 33–38. https://doi.org/https://doi.org/10.1016/0263-7855(96)00018-5

Imamoto, Y., Tamura, C., Kamikubo, H., & Kataoka, M. (2003). Concentration-dependent tetramerization of bovine visual arrestin. *Biophysical Journal*, *85*, 1186–1195. https://doi.org/10.1016/S0006-3495(03)74554-8

Irwin, M. J., Gupta, R., Gao, X.-Z., Cahill, K. B., Chu, F., & Cote, R. H. (2019). The molecular architecture of photoreceptor phosphodiesterase 6 (PDE6) with activated G protein elucidates the mechanism of visual excitation. *The Journal of Biological Chemistry*, *6*. https://doi.org/10.1074/jbc.ra119.011002

Kang, Y., Kuybeda, O., de Waal, P. W., Mukherjee, S., Van Eps, N., Dutka, P., Zhou, X. E., Bartesaghi, A., Erramilli, S., Morizumi, T., Gu, X., Yin, Y., Liu, P., Jiang, Y., Meng, X., Zhao, G., Melcher, K., Ernst, O. P., Kossiakoff, A. A., … Xu, H. E. (2018). Erratum to:

Cryo-EM structure of human rhodopsin bound to an inhibitory G protein (Nature, (2018), 558, 7711, (553-558), 10.1038/s41586-018-0215-y). *Nature*, *561*(7724), E44. https://doi.org/10.1038/s41586-018-0302-0

Kawamura, S., & Tachibanaki, S. (2008). Rod and cone photoreceptors: molecular basis of the difference in their physiology. *Comparative Biochemistry and Physiology - Molecular & Integrative Physiology*, *150*, 369–377. https://doi.org/10.1016/j.cbpa.2008.04.600

Keresztes, G., Martemyanov, K. A., Krispel, C. M., Mutai, H., Yoo, P. J., Maison, S. F., Burns, M. E., Arshavsky, V. Y., & Heller, S. (2004). Absence of the RGS9.Gbeta5 GTPase-activating complex in photoreceptors of the R9AP knockout mouse. *Journal of Biological Chemistry*, *279*, 1581–1584. https://doi.org/10.1074/jbc.C300456200

Kiser, P D, Golczak, M., & Palczewski, K. (2014). Chemistry of the retinoid (visual) cycle. *Chemical Reviews*, *114*, 194–232. https://doi.org/https://doi.org/10.1021/cr400107q

Kiser, Philip D., Golczak, M., Maeda, A., & Palczewski, K. (2012). Key enzymes of the retinoid (visual) cycle in vertebrate retina. *Biochimica et Biophysica Acta - Molecular and Cell Biology of Lipids*, *1821*(1), 137–151. https://doi.org/10.1016/j.bbalip.2011.03.005

Klenchin, V. A., Calvert, P. D., & Bownds, M. D. (1995). Inhibition of rhodopsin kinase by recoverin. Further evidence for a negative feedback system in phototransduction. *Journal of Biological Chemistry*, *270*, 16147–16152. https://doi.org/https://doi.org/10.1074/jbc.270.27.16147

Krispel, C. M., Chen, D., Melling, N., Chen, Y. J., Martemyanov, K. A., Quillinan, N., Arshavsky, V. Y., Wensel, T. G., Chen, C. K., & Burns, M. E. (2006). RGS expression rate-

limits recovery of rod photoresponses. *Neuron*, *51*, 409–416.

https://doi.org/10.1016/j.neuron.2006.07.010.

Kroll, S., Phillips, W. J., & Cerione, R. A. (1989). The regulation of the cyclic GMP

phosphodiesterase by the GDP-bound form of the α subunit of transducin. *Journal of*

Biological Chemistry, *264*(8), 4490–4497. https://doi.org/10.1016/s0021-9258(18)83770-x

Kučerka, N., Tristram-Nagle, S., & Nagle, J. F. (2006). Structure of fully hydrated fluid phase

lipid bilayers with monounsaturated chains. *Journal of Membrane Biology*, *208*(3), 193–

202. https://doi.org/10.1007/s00232-005-7006-8

Lamb, T D, & Kraft, T. W. (2020). A quantitative account of mammalian rod phototransduction

with PDE6 dimeric activation: responses to bright flashes. *Open Biology*, *10*, 1.

https://doi.org/10.1098/rsob.190241

Lamb, Trevor D., Heck, M., & Kraft, T. W. (2018). Implications of dimeric activation of PDE6

for rod phototransduction. *Open Biology*, *8*(8). https://doi.org/10.1098/rsob.180076

Lambright, D. G., Noel, J. P., Hamm, H. E., & Sigler, P. B. (1994). Structural determinants for

activation of the a-subunit of a heterotrimeric G protein. *Nature*, *369*, 621–628.

Lambright, D. G., Sondek, J., Bohm, A., Skiba, N. P., Hamm, H. E., & Sigler, P. B. (1996). The

2.0 A crystal structure of a heterotrimeric G protein. *Nature*, *379*(25), 311–317.

https://doi.org/10.1038/379311a0

Lishko, P. V., Martemyanov, K. a., Hopp, J. a., & Arshavsky, V. Y. (2002). Specific binding of

RGS9-Gβ5L to protein anchor in photoreceptor membranes greatly enhances its catalytic

activity. *Journal of Biological Chemistry*, *277*(27), 24376–24381.

https://doi.org/10.1074/jbc.M203237200

Liu, Y., Arshavsky, V. Y., & Ruoho, A. E. (1999). Interaction sites of the C-terminal region of the cGMP phosphodiesterase inhibitory subunit with the GDP-bound transducin α-subunit. *Biochemical Journal*, *337*(2), 281–288. https://doi.org/10.1042/0264-6021:3370281

Liu, Y. T., Matte, S. L., Corbin, J. D., Francis, S. H., & Cote, R. H. (2009). Probing the catalytic sites and activation mechanism of photoreceptor phosphodiesterase using radiolabeled phosphodiesterase inhibitors. *Journal of Biological Chemistry*, *284*, 31541–31547. https://doi.org/https://doi.org/10.1074/jbc.M109.018606

Lyon, A. M., Dutta, S., Boguth, C. A., Skiniotis, G., & Tesmer, J. J. G. (2013). Full-length Gαq-phospholipase C-β3 structure reveals interfaces of the C-terminal coiled-coil domain. *Nature Structural and Molecular Biology*, *20*(3), 355–362. https://doi.org/10.1038/nsmb.2497

Maeda, T., Imanishi, Y., & Palczewski, K. (2003). Rhodopsin phosphorylation: 30 years later. *Progree in Retinal and Eye Research*, *22*, 417–434. https://doi.org/10.1016/s1350-9462(03)00017-x

Malinski, J. A., & Wensel, T. G. (1992). Membrane Stimulation of cGMP Phosphodiesterase Activation by Transducin: Comparison of Phospholipid Bilayers to Rod Outer Segment Membranes. *Biochemistry*, *31*(39), 9502–9512. https://doi.org/10.1021/bi00154a024

Marquardt, D., Heberle, F. A., Greathouse, D. V., Koeppe, R. E., Standaert, R. F., Van Oosten, B. J., Harroun, T. A., Kinnun, J. J., Williams, J. A., Wassall, S. R., & Katsaras, J. (2016). Lipid bilayer thickness determines cholesterols location in model membranes. *Soft Matter*,

12(47), 9417–9428. https://doi.org/10.1039/c6sm01777k

Maryam, A., Vedithi, S. C., Khalid, R. R., Alsulami, A. F., Torres, P. H. M., Siddiqi, A. R., & Blundell, T. L. (2019). The Molecular Organization of Human cGMP Specific Phosphodiesterase 6 (PDE6): Structural Implications of Somatic Mutations in Cancer and Retinitis Pigmentosa. *Computational and Structural Biotechnology Journal*, *17*, 378–389. https://doi.org/10.1016/j.csbj.2019.03.004

Melia, T. J., Malinski, J. A., He, F., & Wensel, T. G. (2000). Enhancement of phototransduction protein interactions by lipid surfaces. *Journal of Biological Chemistry*, *275*(5), 3535–3542. https://doi.org/10.1074/jbc.275.5.3535

Mendez, A., Burns, M. E., Roca, A., Lem, J., Wu, L. W., Simon, M. I., Baylor, D. A., & Chen, J. (2000). Rapid and reproducible deactivation of rhodopsin requires multiple phosphorylation sites. *Neuron*, *28*, 153–164. https://doi.org/10.1016/s0896-6273(00)00093-3

Milano, S. K., Wang, C., Erickson, J. W., Cerione, R. A., & Ramachandran, S. (2018). Gain-of-function screen of -transducin identifies an essential phenylalanine residue necessary for full effector activation. *Journal of Biological Chemistry*, *293*(46), 17941–17952. https://doi.org/10.1074/jbc.RA118.003746

Min, K. C., Gravina, S. A., & Sakmar, T. P. (2000). Reconstitution of the vertebrate visual cascade using recombinant heterotrimeric transducin purified from Sf9 cells. *Protein Expression and Purification*, *20*, 514–526. https://doi.org/10.1006/prep.2000.1326

Molday, R. S., & Moritz, O. L. (2015). Photoreceptors at a glance. *Journal of Cell Science*, *128*(22), 4039–4045. https://doi.org/10.1242/jcs.175687

Mou, H, Grazio, H. J., Cook, T. A., Beavo, J. A., & Cote, R. H. (1999). cGMP binding to

noncatalytic sites on mammalian rod photoreceptor phosphodiesterase is regulated by

binding of its γ and δ subunits. *Journal of Biological Chemistry*, *274*, 18813–18820.

https://doi.org/10.1074/jbc.274.26.18813.

Mou, Hongmei, & Cote, R. H. (2001). The Catalytic and GAF Domains of the Rod cGMP

Phosphodiesterase (PDE6) Heterodimer Are Regulated by Distinct Regions of Its Inhibitory

γ Subunit. *Journal of Biological Chemistry*, *276*(29), 27527–27534.

https://doi.org/10.1074/jbc.M103316200

Muradov, H., Boyd, K. K., & Artemyev, N. O. (2010). Rod phosphodiesterase-6 PDE6A and

PDE6B subunits are enzymatically equivalent. *Journal of Biological Chemistry*, *285*(51),

39828–39834. https://doi.org/10.1074/jbc.M110.170068

Nair, K. S., Hanson, S. M., Mendez, A., Gurevich, E. V, Kennedy, M. J., Shestopalov, V. I.,

Vishnivetskiy, S. A., Chen, J., Hurley, J. B., Gurevich, V. V, & others. (2005). Light-

dependent redistribution of arrestin in vertebrate rods is an energy-independent process

governed by protein-protein interactions. *Neuron*, *46*, 555–567.

https://doi.org/10.1016/j.neuron.2005.03.023.

Natochin, M., Granovsky, A. E., & Artemyev, N. O. (1998). Identification of effector residues

on photoreceptor G protein, transducin. *Journal of Biological Chemistry*, *273*(34), 21808–

21815. https://doi.org/10.1074/jbc.273.34.21808

Neubert, T. A., Johnson, R. S., Hurley, J. B., & Walsh, K. A. (1992). The rod transducin a

subunit amino terminus is heterogeneously fatty acylated. *Journal of Biological Chemistry*,

267, 18274–18277.

Ng, C. C., Cheng, Y. L., & Pennefather, P. S. (2004). Properties of a self-assembled phospholipid membrane supported on lipobeads. *Biophysical Journal*, *87*(1), 323–331. https://doi.org/10.1529/biophysj.103.030627

Nikonov, S. S., Brown, B. M., Davis, J. A., Zuniga, F. I., Bragin, A., Pugh Jr., E. N., & Craft, C. M. (2008). Mouse cones require an arrestin for normal inactivation of phototransduction. *Neuron*, *59*, 462–474. https://doi.org/10.1016/j.neuron.2008.06.011.

Noel, J. P., Hamm, H. E., & Sigler, P. B. (1993). The 2.2 A crystal structure of transducin-alpha complexed with GTP gamma S. *Nature*, *366*, 654–663. https://doi.org/10.1016/j.ccr.2020.213617%0Ahttp://dx.doi.org/10.1016/j.ccr.2014.11.016

Norton, A. W., D'Amours, M. R., Grazio, H. J., Hebert, T. L., & Cote, R. H. (2000). Mechanism of Transducin Activation of Frog Rod Photoreceptor Phosphodiesterase. *Journal of Biological Chemistry*, *275*(49), 38611–38619. https://doi.org/10.1074/jbc.m004606200

Omar, F., Findlay, J. E., Carfray, G., Allcock, R. W., Jiang, Z., Moore, C., Muir, A. L., Lannoy, M., Fertig, B. A., Mai, D., Day, J. P., Bolger, G., Baillie, G. S., Schwiebert, E., Klussmann, E., Pyne, N. J., Ong, A. C. M., Bowers, K., Adam, J. M., … Henderson, D. J. P. (2019). Small-molecule allosteric activators of PDE4 long form cyclic AMP phosphodiesterases. *Proceedings of the National Academy of Sciences of the United States of America*, *116*(27), 13320–13329. https://doi.org/10.1073/pnas.1822113116

Osawa, S., Jo, R., & Weiss, E. R. (2008). Phosphorylation of GRK7 by PKA in cone photoreceptor cells is regulated by light. *Journal of Neurochemistry*, *107*, 1314–1324. https://doi.org/https://doi.org/10.1111/j.1471-4159.2008.05691.x

Palczewski, K. (2006). G protein-coupled receptor rhodopsin. *Annual Review of Biochemistry*, *75*, 743–767. https://doi.org/10.1146/annurev.biochem.75.103004.142743

Patil, D. N., Rangarajan, E. S., Novick, S. J., Pascal, B. D., Kojetin, D. J., Griffin, P. R., Izard, T., & Martemyanov, K. A. (2018). Structural organization of a major neuronal g protein regulator, the RGS7-Gβ5-R7BP complex. *ELife*, *7*, 1–27. https://doi.org/10.7554/eLife.42150

Pentia, D. C., Hosier, S., Collupy, R. A., Valeriani, B. A., & Cote, R. H. (2005). Purification of PDE6 isozymes from mammalian retina. *Phosphodiesterase Methods and Protocols*, *307*, 125–140. https://doi.org/10.1385/1-59259-839-0:125

Power, M., Das, S., Schutze, K., Marigo, V., Ekstrom, P., & Paquet-Durand, F. (2020). Cellular mechanisms of hereditary photoreceptor degeneration -- focus on cGMP. *Prog Retin Eye Res*, *74*, 10077. https://doi.org/10.1016/j.preteyeres.2019.07.005

Pugh Jr., E. ., & Lamb, T. . (2000). Phototransduction in Vertebrate Rods and Cones: Molecular Mechanisms of Amplification, Recovery and Light Adaptation. In: Handbook of Biological Physics. Vol. 3, Molecular Mechanisms of Visual Transduction. *Stavenga, D.G., de Grip, W.J., Pugh Jr., E.N. (Eds.), Handbook of Biological Physics. Vol. 3, Molecular Mechanisms of Visual Transduction. Elsevier, Amsterdam, Pp. 183–255 (Chapter 5).*, *3*, 183-255 (Chapter 5).

Qi, C., Sorrentino, S., Medalia, O., & Korkhov, V. M. (2019). The structure of a membrane adenylyl cyclase bound to an activated stimulatory G protein. *Science*, *364*(6438), 389–394. https://doi.org/10.1126/science.aav0778

Qureshi, B. M., Behrmann, E., Schöneberg, J., Loerke, J., Bürger, J., Mielke, T., Giesebrecht, J., Noé, F., Lamb, T. D., Hofmann, K. P., Spahn, C. M. T., & Heck, M. (2018). It takes two transducins to activate the cGMP-phosphodiesterase 6 in retinal rods. *Open Biology*, *8*(8). https://doi.org/10.1098/rsob.180075

Ross, E. E., Mok, S. W., & Bugni, S. R. (2011). Assembly of lipid bilayers on silica and modified silica colloids by reconstitution of dried lipid films. *Langmuir*, *27*(14), 8634–8644. https://doi.org/10.1021/la200952c

Sali, A., & Blundell, T. L. (1993). Comparative protein modelling by satisfaction of spatial restraints. *Journal of Molecular Biology*, *234*, 779–815. https://doi.org/10.1006/jmbi.1993.1626.

Satoh, A. K., Xia, H., Yan, L., Liu, C. H., Hardie, R. C., & Ready, D. F. (2010). Arrestin translocation is stoichiometric to rhodopsin isomerization and accelerated by phototransduction in Drosophila photoreceptors. *Neuron*, *67*, 997–1008.

Schubert, C., Hirsch, J. A., Gurevich, V. V, Engelman, D. M., Sigler, P. B., & Fleming, K. G. (1999). Visual arrestin activity may be regulated by self-association. *Journal of Biological Chemistry*, *274*, 21186–21190. https://doi.org/10.1074/jbc.274.30.21186.

Seitz, H. R., Heck, M., Hofmann, K. P., Alt, T., Pellaud, J., & Seelig, A. (1999). Molecular determinants of the reversible membrane anchorage of the G-protein transducin. *Biochemistry*, *38*, 7950–7960. https://doi.org/https://doi.org/10.1021/bi990298+

Skiba, N. P., Bae, H., & Hamm, H. E. (1996). Mapping of effector binding sites of transducin alpha-subunit using G alpha t/G alpha i1 chimeras. *J Biol Chem*, *271*(1), 413–424.

https://doi.org/10.1074/jbc.271.1.413

Skiba, N. P., Martemyanov, K. a., Elfenbein, A., Hopp, J. A., Bohm, A., Simonds, W. F., & Arshavsky, V. Y. (2001). RGS9-Gβ5 substrate selectivity in photoreceptors: Opposing effects of constituent domains yield high affinity of RGS interaction with the G protein-effector complex. *Journal of Biological Chemistry*, *276*(40), 37365–37372. https://doi.org/10.1074/jbc.M106431200

Skiba, N. P., Spencer, W. J., Salinas, R. Y., Lieu, E. C., Thompson, J. W., & Arshavsky, V. Y. (2013). Proteomic identification of unique photoreceptor disc components reveals the presence of PRCD, a protein linked to retinal degeneration. *Journal of Proteome Research*, *12*(6), 3010–3018. https://doi.org/10.1021/pr4003678

Slep, K. C., Kercher, M. A., He, W., Cowan, C. W., Wensel, T. G., & Sigler, P. B. (2001). Structural determinants for regulation of phosphodiesterase by a G protein at 2.0 Å. *Nature*, *409*(6823), 1071–1077. https://doi.org/10.1038/35059138

Slepak, V. Z., Artemyev, N. O., Zhu, Y., Dumke, C. L., Sabacan, L., Sondek, J., Hamm, H. E., Bownds, M. D., & Arshavsky, V. Y. (1995). An effector site that stimulates G-protein GTPase in photoreceptors. *Journal of Biological Chemistry*, *270*(24), 14319–14324. https://doi.org/10.1074/jbc.270.24.14319

Smith, P. K., Krohn, R. I., Hermanson, G. T., Mallia, A. K., Gartner, F. H., Provenzano, M. D., Fujimoto, E. K., Goeke, N. M., Olson, B. J., & Klenk, D. C. (1985). Measurement of protein using bicinchoninic acid. *Analytical Biochemistry*, *150*, 76–85. https://doi.org/10.1016/0003-2697(85)90442-7

Smith, R. L., Sivaprasad, S., & Chong, V. (2016). Retinal biochemistry, physiology and cell biology. *Developments in Ophthalmology*, *55*, 18–27. https://doi.org/10.1159/000431118

Sohocki, M. M., Daiger, S. P., Bowne, S. J., Rodriquez, J. A., Northrup, H., Heckenlively, J. R., Birch, D. G., Mintz-Hittner, H., Ruiz, R. S., Lewis, R. A., Saperstein, D. A., & Sullivan, L. S. (2001). Prevalence of mutations causing retinitis pigmentosa and other inherited retinopathies. *Human Mutation*, *17*(1), 42–51. https://doi.org/10.1002/1098-1004(2001)17:1<42::AID-HUMU5>3.0.CO;2-K

Sokolov, M., Lyubarsky, A. L., Strissel, K. J., Savchenko, A. B., Govardovskii, V. I., Pugh Jr., E. N., & Arshavsky, V. Y. (2002). Massive light-driven translocation of transducin between the two major compartments of rod cells: a novel mechanism of light adaptation. *Neuron*, *34*, 95–106. https://doi.org/10.1016/s0896-6273(02)00636-0

Sokolov, M., Strissel, K. J., Leskov, I. B., Michaud, N. A., Govardovskii, V. I., & Arshavsky, V. Y. (2004). Phosducin facilitates light-driven transducin translocation in rod photoreceptors. Evidence from the phosducin knockout mouse. *Journal of Biological Chemistry*, *279*, 19149–19156. https://doi.org/10.1074/jbc.M311058200

Sondek, J., Lambright, D. G., Noel, J. P., Hamm, H. E., & Signler, P. G. (1994). GTPase mechanism of Gproteins from the 1.7-A crystal structure of tranducin a-GDP-ALF4-. *Nature*, *385*, 810–813. https://doi.org/10.1038/372276a0.

Song, J., Guo, L. W., Muradov, H., Artemyev, N. O., Ruoho, A. E., & Markley, J. L. (2008). Intrinsically disordered gamma-subunit of cGMP phosphodiesterase encodes functionally relevant transient secondary and tertiary structure. *Proceedings of the National Academy of Sciences of the United States of America*, *105*, 1505–1510.

https://doi.org/10.1073/pnas.0709558105

Song, X., Vishnivetskiy, S. A., Seo, J., Chen, J., Gurevich, E. V, & Gurevich, V. V. (2011). Arrestin-1 expression level in rods: balancing functional performance and photoreceptor health. *Neuroscience*, *174*, 37–49. https://doi.org/10.1016/j.neuroscience.2010.11.009.

Strissel, K. J., Sokolov, M., Trieu, L. H., & Arshavsky, V. Y. (2006). Arrestin translocation is induced at a critical threshold of visual signaling and is superstoichiometric to bleached rhodopsin. *Journal of Neuroscience*, *26*, 1146–1153. https://doi.org/10.1523/JNEUROSCI.4289-05.2006.

Sutton, R. B., Vishnivetskiy, S. A., Robert, J., Hanson, S. M., Raman, D., Knox, B. E., Kono, M., Navarro, J., & Gurevich, V. V. (2005). Crystal structure of cone arrestin at 2.3A: evolution of receptor specificity. *Journal of Molecular Biology*, *354*, 1069–1080. https://doi.org/https://doi.org/10.1016/j.jmb.2005.10.023

Szabo, V., Kreienkamp, H. J., Rosenberg, T., & Gal, A. (2007). p.Gln200Glu, a putative constitutively active mutant of rod alpha-transducin (GNAT1) in autosomal dominant congenital stationary night blindness. *Human Mutation*, *28*, 741–742. https://doi.org/10.1002/humu.9499.

Tesmer, J. J. (2009). Structure and function of regulator of G protein signaling homology domains. *Progress in Molecular Biology and Translational Science*, *86*, 75–113. https://doi.org/10.1016/S1877-1173(09)86004-3.

Ting, T. D., Lee, R. H., & Ho, Y.-K. (1993). The GTPase Cycle: Transducin. In *GTPases in Biology II* (pp. 99–117).

Troutier, A. L., & Ladavière, C. (2007). An overview of lipid membrane supported by colloidal

    particles. *Advances in Colloid and Interface Science*, *133*(1), 1–21.

    https://doi.org/10.1016/j.cis.2007.02.003

Uversky, V. N., Permyakov, S. E., Zagranichny, V. E., Rodionov, I. L., Fink, A. L., Cherskaya,

    A. M., Wasserman, L. A., & Permyakov, E. A. (2002). Effect of zinc and temperature on

    the conformation of the gamma subunit of retinal phosphodiesterase: a natively unfolded

    protein. *Journal of Proteome Research*, *1*, 149–159. https://doi.org/10.1021/pr0155127.

Vishnivetskiy, S. A., Raman, D., Wei, J., Kennedy, M. J., Hurley, J. B., & Gurevich, V. V.

    (2007). Regulation of arrestin binding by rhodopsin phosphorylation level. *Journal of*

    Biological Chemistry, *282*, 32075–32083. https://doi.org/10.1074/jbc.M706057200

Wada, Y., Sugiyama, J., Okano, T., & Fukada, Y. (2006). GRK1 and GRK7: unique cellular

    distribution and widely different activities of opsin phosphorylation in the zebrafish rods

    and cones. *Journal of Neurochemistry*, *98*, 824–837. https://doi.org/10.1111/j.1471-

    4159.2006.03920.x

Wang, X., Plachetzki, D. C., & Cote, R. H. (2019). The N termini of the inhibitory γ-subunits of

    phosphodiesterase-6 (PDE6) from rod and cone photoreceptors differentially regulate

    transducin-mediated PDE6 activation. *Journal of Biological Chemistry*, *294*(21), 8351–

    8360. https://doi.org/10.1074/jbc.RA119.007520

Webb, B., Viswanath, S., Bonomi, M., Pellarin, R., Greenberg, C. H., Saltzberg, D., & Sali, A.

    (2018). Integrative structure modeling with the Integrative Modeling Platform. *Protein*

    Science, *27*(1), 245–258. https://doi.org/10.1002/pro.3311

Weiss, E. R., Ducceschi, M. H., Horner, T. J., Li, A., Craft, C. M., & Osawa, S. (2001). Species-specific differences in expression of G-protein-coupled receptor kinase (GRK) 7 and GRK1 in mammalian cone photoreceptor cells: implications for cone cell phototransduction. *Journal of Neuroscience*, *21*, 9175–9184. https://doi.org/10.1523/JNEUROSCI.21-23-09175.2001

Wensel, T. G., He, F., & Malinski, J. A. (2005). Purification, reconstitution on lipid vesicles, and assays of PDE6 and its activator G protein, transducin. *Methods in Molecular Biology*, *307*, 289–313. https://doi.org/10.1385/1-59259-839-0:289

Wensel, T. G., & Stryer, L. (1988). Membrane-bound GTP-transducin efficiently activates retinal cGMP phosphodiesterase. In C. Y. Huang, C. L. Tsou, & J. H. Wang (Eds.), *Enzyme Dynamics and Regulation* (pp. 102–112). Enzyme dynamics and regulation. Springer. https://doi.org/10.1007/978-1-4612-3744-0_13

Wensel, T. G., & Stryer, L. (1990). Activation mechanism of retinal rod cyclic GMP phosphodiesterase probed by fluorescein-labeled inhibitory subunit. *Biochemistry*, *29*, 2155–2161. https://doi.org/https://doi.org/10.1021/bi00460a028

Yoshida, T., Willardson, B. M., Wilkins, J. F., Jensen, G. J., Thornton, B. D., & Bitensky, M. W. (1994). The phosphorylation state of phosducin determines its ability to block transducin subunit interactions and inhibit transducin binding to activated rhodopsin. *Journal of Biological Chemistry*, *269*, 24050–24057.

Zeng-Elmore, X., Gao, X. Z., Pellarin, R., Schneidman-Duhovny, D., Zhang, X. J., Kozacka, K. A., Tang, Y., Sali, A., Chalkley, R. J., Cote, R. H., Chu, F., & Zeng-Elmore X., G. X. Z. P. R. S.-D. D. Z. X. J. K. K. A. T. Y. S. A. C. R. J. C. R. H. et al. (2014). Molecular

architecture of photoreceptor phosphodiesterase elucidated by chemical cross-linking and integrative modeling. *J Mol Biol*, *426*(22), 3713–3728. https://doi.org/10.1016/j.jmb.2014.07.033

Zhang, H., Constantine, R., Frederick, J. M., & Baehr, W. (2012). The prenyl-binding protein PrBP/δ: A chaperone participating in intracellular trafficking. *Vision Research*, *75*, 19–25. https://doi.org/10.1016/j.visres.2012.08.013

Zhang, K. Y. J., Card, G. L., Suzuki, Y., Artis, D. R., Fong, D., Gillette, S., Hsieh, D., Neiman, J., West, B. L., Zhang, C., Milburn, M. V., Kim, S. H., Schlessinger, J., & Bollag, G. (2004). cA glutamine switch mechanism for nucleotide selectivity by phosphodiesterases. *Molecular Cell*, *15*(2), 279–286. https://doi.org/10.1016/j.molcel.2004.07.005

Zhang, L. R., Sports, C. D., Osawa, S., & Weiss, E. R. (1997). Rhodopsin phosphorylation sites and their role in arrestin binding. *Journal of Biological Chemistry*, *272*(23), 14762–14768. https://doi.org/10.1074/jbc.272.23.14762

Zhang, X., Feng, Q., & Cote, R. H. (2005). Efficacy and selectivity of phosphodiesterase-targeted drugs in inhibiting photoreceptor phosphodiesterase (PDE6) in retinal photoreceptors. *Investigative Ophthalmology and Visual Science*, *46*(9), 3060–3066. https://doi.org/10.1167/iovs.05-0257

Zhang, X. J., Gao, X. Z., Yao, W., & Cote, R. H. (2012). Functional mapping of interacting regions of the photoreceptor phosphodiesterase (PDE6) γ-subunit with PDE6 catalytic dimer, transducin, and regulator of G-protein signaling9-1 (RGS9-1). *Journal of Biological Chemistry*, *287*(31), 26312–26320. https://doi.org/10.1074/jbc.M112.377333

Zhang, X. J., Skiba, N. P., & Cote, R. H. (2010). Structural requirements of the photoreceptor

    phosphodiesterase gamma-subunit for inhibition of rod PDE6 holoenzyme and for its

    activation by transducin. *Journal of Biological Chemistry*, *285*, 4455–4463.

    https://doi.org/10.1074/jbc.M109.057406.

Zhang, Zhixian, He, F., Constantine, R., Baker, M. L., Baehr, W., Schmid, M. F., Wensel, T. G.,

    & Agosto, M. A. (2015). Domain organization and conformational plasticity of the G

    protein effector, PDE6. *Journal of Biological Chemistry*, *290*(20), 12833–12843.

    https://doi.org/10.1074/jbc.M115.647636

Zhang, Zhongming, & Artemyev, N. O. (2010). Determinants for phosphodiesterase 6 inhibition

    by its γ-subunit. *Biochemistry*, *49*(18), 3862–3867. https://doi.org/10.1021/bi100354a

Zoraghi, R., Corbin, J. D., & Francis, S. H. (2004). Properties and Functions of GAF Domains in

    Cyclic Nucleotide Phosphodiesterases and Other Proteins. *Molecular Pharmacology*, *65*(2),

    267–278. https://doi.org/10.1124/mol.65.2.267

Appendix 1: General workflow for chemical cross-linking/mass spectrometry experiments utilizing Integrative Structural Modeling
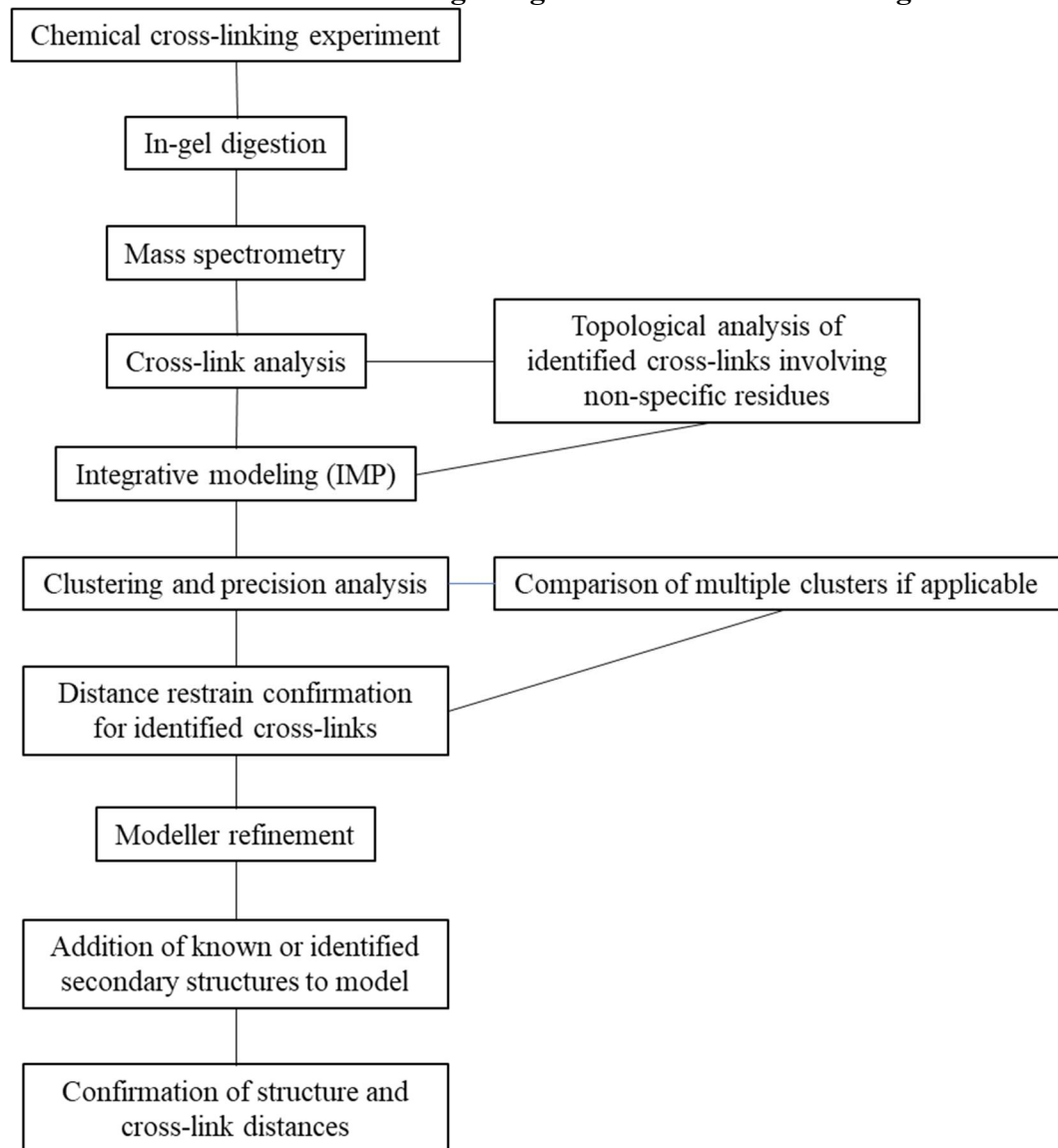
Appendix Figure 1: **Flow chart of cross-linking to homology modeling process**. Mass spectrometry RAW files were converted to MGF files using RawConverter 1.2.0.0 (http://fields.scripps.edu/rawconv/). Protein Prospector (https://prospector.ucsf.edu/prospector/mshome.htm) or xiSEARCH (https://www.rappsilberlab.org/software/xisearch/) was used for cross-link analysis. Pymol was used for topological analysis, confirmation of structures, and distance restraint confirmation. The Integrative Modeling Platform was used for modeling, clustering, and precision analysis, and Modeller was used for structure refinement. Both JPRED and Pymol were used for secondary structure prediction and assignment.

Appendix 2: Workflow for performing Integrative Structural Modeling

A comprehensive tutorial for the Integrative Modeling Platform can be found here: https://integrativemodeling.org/2.5.0/doc/manual/rnapolii_stalk.html. Sample scripts and all output files can be found here: https://github.com/rcotelab/Irwin-et-al-2019. Specific implementations of modeling can be found in the Chapter 3 Materials and Methods section.

The first step in integrative modeling is to identify the rigid bodies that will be involved in the modeling. Rigid bodies are the overall structures that should stay together as a single structure during modeling. You can also identify super rigid bodies and chains of super rigid bodies which can give your model more overall flexibility. These are all added to your topology file.

Within the topology file, you label each molecule in the model with a name, color, fasta file, fasta name, pdb file, chain identifier, residue range, bead size, rigid body, super rigid body, and chain of super rigid body. If including EM structural information, you also include the residues per gaussian (gaussian mixture models are used to speed up approximation of electron density of individual subunits) in the topology file. All of the identified structures and files need to be present in a single data folder.

Once your topology file is formatted correctly, it can be called in the modelling script. All files, including the topology file, should be present in your data directory. Rigid body movement parameters as well as flexible bead movement are the initial parameters to be set which sets the overall flexibility for the modeling. Next, you input a list of your rigid bodies, super rigid bodies, and chains of super rigid bodies as identified in your topology file. Finally,

you set the randomization of your initial conformation before sampling begins. The number of frames is the number of samples run, typically 20,000.

For cross-linking information, files need to be formatted as CSV files. The column titles for cross-linked peptides and residues are input and the relevant CSV is called. The cross-link distance is set as a length. The slope can be set which impacts the scoring function of the cross-link distance. Higher values create a greater score penalty in the event of a cross-link that has a distance violation in the final model.

Monte Carlo temperature is set to 1.0, minimum temperature is set to 0.5, maximum temperature is set to 2.5, and the number of best scoring models is typically set to 100. Following the completion of the script, the standard clustering script is run, analyzing the movement of the chains that are of most interest.

Modeller is then run with the same set of crosslinks present in the IMP run. Modeller will refine the model as well as add missing atoms to the structure, since the output from IMP is an α-carbon only model.